Clathrate Hydrates in Frozen Confections: Formation by Carbon Dioxide Flash Freezing and Behavior During Distribution and Consumption

by

Teresa Baker Peters

B.S. Earth, Atmospheric and Planetary Science
B.S. Mechanical Engineering
Massachusetts Institute of Technology, 2003

M.S. Mechanical Engineering
Massachusetts Institute of Technology, 2006

SUBMITTED TO THE DEPARTMENT OF MECHANICAL ENGINEERING IN PARTIAL FULFILLMENT OF THE REQUIREMENTS FOR THE DEGREE OF

DOCTOR OF PHILOSOPHY IN MECHANICAL ENGINEERING
AT THE
MASSACHUSETTS INSTITUTE OF TECHNOLOGY

SEPTEMBER 2009

Signature of Author……...
Department of Mechanical Engineering
September 11, 2009

Certified by……...
Professor John G Brisson II
Professor of Mechanical Engineering
Thesis Supervisor

Accepted by……...
Professor David E. Hardt
Professor of Mechanical Engineering
Chairperson, Department Committee on Graduate Students

(This page intentionally left blank.)

Clathrate Hydrates in Frozen Confections: Formation by Carbon Dioxide Flash Freezing and Behavior During Distribution and Consumption

by

Teresa Baker Peters

Submitted to the Department of Mechanical Engineering on September 11, 2009 in Partial Fulfillment of the Requirements for the Degree of Doctor of Philosophy in Mechanical Engineering

ABSTRACT

Carbonated frozen foods are not common on the market due to the limited liquid water available to dissolve CO_2. CO_2 clathrate hydrates can change this because CO_2 is trapped in crystalline water. The CO_2 flash-freezing process developed in this thesis forms CO_2 hydrates directly in a confection as it freezes. In this process, the confection mixture is dispersed in liquid CO_2; then the combined fluids are flashed to 10-20 bars. The mixture breaks up into small fragments, which rapidly crystallize into CO_2 hydrate (instead of ice) due to the intimate contact between mixture and evaporating CO_2. This CO_2 hydrate formation results in a frozen, carbonated confection.

CO_2 hydrates have a significant impact on packaging and storage requirements for the confection. This study shows that the minimum storage pressure is determined by the ice-CO_2 hydrate-gas equilibrium (IHG) curve, which does not change with the concentration of solutes in the aqueous phase. The minimum CO_2 content in a storage vessel is determined by the amount of CO_2 needed to avoid ice; in the presence of ice CO_2 can redistribute quickly, leading to an inhomogeneous product. Packaging must therefore be designed considering the significant CO_2 evolution from dissociating CO_2 hydrates during heat shock. Warming of a confection causes CO_2 hydrates to dissociate, even at pressures greater than the IHG pressure due to the requirement of chemical equilibrium between water in aqueous and crystalline phases. In packaging with limited headspace, this CO_2 release increases the pressure significantly.

When CO_2 hydrate confections are consumed CO_2 is strongly perceived both through tingling caused by carbonic acid and through tactile stimulation caused by bubbles. A higher concentration of CO_2 is required in CO_2 hydrate confections than in carbonated beverages for similar fizziness perception because a significant fraction of the CO_2 escapes when a consumer exhales. The CO_2 concentration in the melted confection does not exceed the solubility of CO_2 at atmospheric pressure, but ingredients in the recipe can modulate the growth of bubbles as the confection melts. Consumer testing is needed to define the form and style of CO_2 hydrate confection that should be pursued.

Thesis Supervisor: John G Brisson II
Title: Professor of Mechanical Engineering

Acknowledgements

Funding for this research was provided through Nestlé S.A., the Deshpande Center for Technological Innovation, and the MIT Cryogenics Engineering Lab.

I would like to thank my advisors, Professor Brisson and Professor Smith, for challenging questions, suggestions, guidance and help with equipment design and machining, and encouragement throughout this project. I would like to thank all the PTC Beauvais people who have worked with us on this project, especially Hans Wille, Max Puaud, Bob Mazurek, Joumana Saikali and Anthony Pizzagalli. The opportunity to work with you has been invaluable. I would also like to thank the technicians who have helped in so many ways with equipment development and operation, especially Francis Verdin and Mike Demaree. Finally, I would like to thank my family, lab mates and housemates for participating in and contributing to so many conversations about clathrate hydrates and ice cream. You've been a huge help with sorting out my thoughts, thinking through new ideas, and getting me to look at things from new perspectives. Thanks be to God. Amen.

Contents

(This page intentionally left blank.)

1 Introduction

1.1 Background and objectives

Carbonated foods offer the opportunity for product differentiation, novelty and increased product appeal. For example, bottled water, fruit, flavored beverages, and wine all come in sparkling and non-sparkling varieties. Recently, carbonated foods also include milk (e-Moo from Mac Farms Inc.), yogurt (Fizzix from Yoplait USA Inc) and fruit (The Fizzy Fruit Company). Fizzy Fruit, Fizzix and e-Moo are all marketed with an eye to using carbonation to increase consumption of healthy foods in comparison to candy and soda (Glasner, 2005; Botelho, 2007). Carbonation is often associated with refreshment (i.e. cold soda), excitement (i.e. pop rocks) and celebration (i.e. champagne). The omnipresence of carbonated beverages in stores and recent development of fizzy yogurt and fruit suggest a large market for carbonation.

Carbonating a frozen food is more challenging than carbonating a food that does not contain ice. Beverages, fruit, and yogurt all have significant non-crystalline aqueous phases in which CO_2 can be dissolved and retained. However, in frozen foods a significant portion of the water is ice in which the solubility of CO_2 is extremely low, 10^{-8} g/g ice (Rhode & Price, 2007) compared to 10^{-3} g/g liquid water (Diamond & Akinfiev, 2003). To achieve CO_2 concentrations similar to the CO_2 concentration in soda and sparkling water, CO_2 in frozen foods must be retained by a mechanism other than solution in the aqueous phase. It will be shown in the following section that CO_2 clathrate hydrates are the best option to achieve a high concentration of CO_2 in frozen foods.

The objective of this thesis is to provide a scientific basis for development of a carbonated frozen confection based on CO_2 hydrates (CO_2 hydrate confection). While gas hydrates have been extensively studied for flow assurance in oil and gas pipelines, as an energy storage and transport mechanism, as a naturally occurring element of marine geology, and as a mechanism for CO_2 sequestration or water desalination, this knowledge has not typically been applied to development of food products. To enable development of a CO_2 hydrate confection, this thesis 1) describes a flash-freezing process that forms CO_2 hydrates in a confection as it is frozen; 2) identifies constraints on process parameters, product design and storage conditions based on the characteristics of CO_2 hydrates; 3) provides explanations for CO_2 hydrate behavior in the CO_2 flash freezer, in storage, and during consumption based on thermodynamics, transport processes, and experimental results; and 4) identifies the areas of significant unknowns regarding CO_2 hydrate confections and provides the groundwork for further studies in these areas.

This thesis is divided into eight chapters that follow CO_2 hydrates from formation by flash freezing thru being eaten, and make recommendations for future work. In chapter 1 clathrate hydrates are defined and shown to be the best option for carbonating frozen food products. A flash-freezing process to form CO_2 hydrates in the confection is introduced. A simple experimental apparatus that is used for measurements described in several of the following chapters is presented. Chapter 2 describes CO_2 interaction with the ingredients mixture before flash freezing and CO_2 hydrate formation. Chapter 3 discusses the formation

of CO_2 hydrates during the flash-freezing process. Chapter 4 discusses the storage conditions that are necessary for a stable, homogeneous CO_2 hydrate confection. Chapter 5 discusses the changes in CO_2 hydrate crystals during storage due to recrystallization processes and heat shock. Chapter 6 discusses CO_2 perception in frozen foods and dissociation of CO_2 hydrates as a CO_2 hydrate confection is eaten. The key findings are summarized in Chapter 7 and recommendations for future work are presented in Chapter 8.

1.2 Clathrate hydrates and their importance to carbonated frozen confections

Clathrate hydrates are a crystalline form of water that look like snow or ice, but contain a high concentration of gases such as CO_2, CH_4, O_2, or N_2. The gas molecules stabilize cavities formed by hydrogen-bonded water molecules. CO_2 clathrate hydrates (hereafter CO_2 hydrates) are important to carbonated frozen confections because of their high CO_2 concentration. In CO_2 hydrates the average gas density is 296 kg/m^3, approximately 160 times the density of CO_2 at standard temperature and pressure and 50 times the density of CO_2 in solution in sparkling water. Unfortunately, above 218 K CO_2 hydrates do not exist at atmospheric pressure. Figure 1-1 shows the minimum pressure for CO_2 hydrates as a function of temperature. At 253 K, a typical freezer temperature, the minimum pressure for CO_2 hydrates is 5 bars.

In this section several possible mechanisms for carbonating a frozen confection are compared in order to show that CO_2 hydrates provide the highest CO_2 concentration with the least constraints on the confection. The mechanisms compared are: CO_2 dissolved in the aqueous phase, CO_2 hydrates, CO_2 in gas bubbles, ingredients that react to form CO_2 as a confection is eaten, and solid CO_2. The comparison is made for a confection at 253 K made from 20 wt% sucrose aqueous solution (hereafter referred to as the model solution).

Table 1.1 provides an overview of the discussion below. For reference, the room temperature storage pressure of a carbonated beverage (such as Coca-cola®) is typically 3.8 bars and the CO_2 concentration is about 6 grams of CO_2 per kilogram of soda (Meraj, 2000).

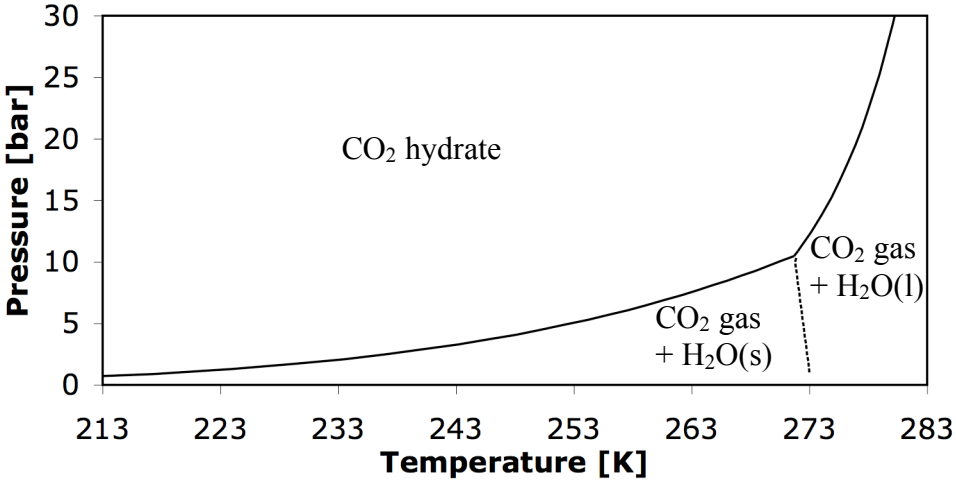

Figure 1-1 Pressure-temperature phase diagram for CO_2 hydrate formation (Data from Sloan & Koh, 2008).

Table 1.1 Comparison of CO_2 storage mechanisms

Mechanism	g CO_2/kg 20 wt% sucrose solution (model solution)	Constraints
Dissolved in aqueous phase	0.75 g	---
CO_2 hydrates	264 g	store at pressure >5 bars
CO_2 gas bubbles (to match concentration in soda)	6 g	gas volume fraction >50%, 0.8 μm bubbles, and brief storage, or store at pressure >2.8 bars
Acid + carbonate reaction (to match concentration in soda)	6 g	large mass fraction of salt by-product, must separate reactants during storage and ensure reaction during eating
Solid CO_2	---	2000 bar minimum pressure at 253 K or need a special low-temperature cold chain

In frozen foods, CO_2 can only be dissolved in the fraction of water that does not crystallize. The amount of water available to dissolve CO_2 depends on the concentration of solutes and the temperature. At 253 K, the aqueous phase of a sucrose solution is concentrated to 70 wt% sucrose (Blond et al., 1997). In one kilogram of the model solution this leaves 0.086 kg of water available in the aqueous phase. The extrapolated solubility of CO_2 in water at 253 K, 1 bar is 8.7 g CO_2/kg H_2O (Diamond & Akinfiev, 2003). Assuming CO_2 solubility is unaffected by the high concentration of sucrose in the aqueous phase, the frozen confection would contain 0.75 grams of CO_2 per kilogram of the model solution. This is less than 15% of the CO_2 content in soda. Further, in section 2.1 it is shown that sucrose decreases the solubility of CO_2 in water, so the actual amount of CO_2 that can be dissolved in the aqueous phase is probably significantly lower. Therefore, even in the most optimistic estimate, the frozen confection cannot match the CO_2 concentration of soda by CO_2 dissolved in the unfrozen aqueous phase.

On the other hand, CO_2 hydrates trap CO_2 in the fraction of water that is crystalline. In one kilogram of the model solution at 253 K, 0.714 kg of H_2O is crystallized. The average concentration of CO_2 in CO_2 hydrates is 0.37 kilograms of CO_2 per kilogram of H_2O. If all of the ice is replaced by CO_2 hydrates, the CO_2 content of the frozen confection could reach 264 grams of CO_2 per kilogram of the model solution, almost fifty times the amount of CO_2 in a kilogram of soda. The CO_2 concentration remains high regardless of the concentration of solutes in the recipe because more than 50% of the water in a frozen confection crystallizes. The only constraint is that a CO_2 partial pressure of 5 bars is required to keep the CO_2 hydrates stable at 253 K, as shown in Figure 1-1.

The amount of CO_2 that can be trapped in bubbles in a frozen confection depends on the total volume of the bubbles, bubble size, storage pressure and the surface tension of the bubbles. An estimate for the amount of CO_2 that can be reasonably stored in bubble form in a frozen confection can be obtained by considering a confection that is 50% vapor by volume (this is the typical gas volume in ice cream). The surface tension of the bubble can reasonably be assumed to have a value of 0.07 J/m^2, the value of a water-CO_2 vapor interface at 3 atm and 284 K (Jho et al., 1978). The surface tension serves to increase the pressure, and hence the density of the CO_2 inside the bubble. As a consequence, the density of the CO_2 is a function of the radius of the bubble, increasing as the size of the bubble decreases.

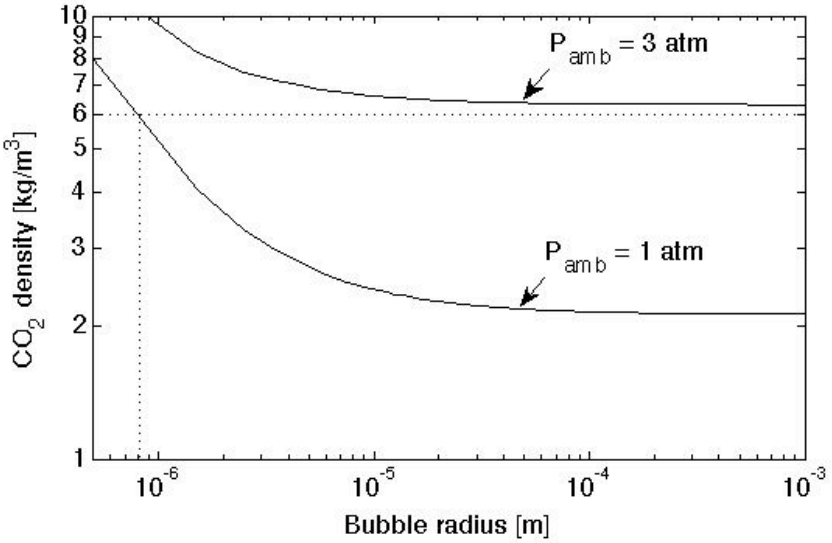

Figure 1-2 A plot of the density of CO_2 as a function of bubble radius at 253 K for two ambient pressures (3 atm and 1 atm).

More specifically the pressure inside the bubble varies as

$$P_{bubble} = P_{amb} + \frac{2\gamma}{r}, \tag{1.1}$$

where P_{bubble} is the pressure inside the bubble, P_{amb} is the ambient pressure, γ is the surface tension and r is the radius of the bubble. If the confection is held at a temperature of 253 K at an ambient pressure of 1 bar, the total CO_2 density inside the bubble can be found as a function of the bubble radius by using Eq. 1.1 and the ideal gas law. The results are shown in Figure 1-2. The density necessary to match the CO_2 concentration in soda is 6 kg/m^3. This density is achieved with a bubble diameter of 0.8 μm (as shown by the dotted lines in the figure), which is significantly smaller than the mean size of bubbles in standard ice cream, 22 μm (Clarke, 2004). To achieve this bubble size (0.8 μm) current ice cream making equipment would have to be modified. However, reducing the initial bubble size in the ice confection may not be enough. Bubbles in ice cream tend to coarsen in storage due to the surface energy reduction associated with the reduction of the radius of curvature of the bubbles. CO_2 bubbles coarsen more rapidly than air bubbles because CO_2 is more soluble than air in the confection matrix. Therefore, CO_2 bubbles in the frozen confection will grow in storage, leading to expansion of the confection and or loss of CO_2 into the headspace (gas phase volume in the package).

Figure 1-2 also shows that if the confection is stored at a pressure of 3 atm, the CO_2 content of the ice confection is above the target density of 6 kg/m^3 regardless of the bubble size. However it is not clear that CO_2 will remain in the confection long enough to provide a sensation of carbonation to the consumer after the storage container is opened and there may be other issues with gas bubble storage in the product at 3 atm. The product could expand when the package is opened. This may be a feature (like in whipped cream) or a detriment (requiring design of a container to accommodate this expansion). If the expansion is undesirable, it may be necessary to add a gelling substance to the mixture recipe to mitigate the change in product volume. In addition, bubbles in a frozen confection contribute to its softness and ease-of-scooping. The requirement to have 50% bubble volume constrains the

texture of the confection, and it is unlikely that a "bubble-storage" confection could be made to an ice-lolly consistency. Based on these considerations it is clear that storage of CO_2 in bubbles in an ice confection can match the CO_2 concentration in a soda, but places constraints on both the product texture and recipe.

Carbon dioxide can also be provided chemically during consumption of a frozen confection by the reaction of a carbonate and an acid. An example would be a confection containing sodium bicarbonate and citric acid. These reactants would be dissolved in the freeze-concentrated aqueous phase in separate regions of the frozen confection. While the confection is frozen low water mobility reduces contact between the carbonate and the acid, but when the confection melts the regions containing carbonate and acid are mixed and CO_2 is released into the consumer's mouth as the reaction proceeds. The reaction for sodium bicarbonate and citric acid is

$$NaHCO_3 + C_6H_8O_7 \rightarrow C_6H_7O_7Na + H_2O + CO_2.$$

To provide the same concentration of CO_2 as found in soda (6 g CO_2/kg mixture), 26.2 g of citric acid and 11.5 g of sodium must react. The reaction produces 29.2 g of a salt byproduct ($C_6H_7O_7Na$) and 2.5 g of water in addition to the desired CO_2. The salt byproduct mass is approximately 3% of the mass of the model solution, which is not insignificant. It may be necessary to reformulate the recipe to compensate for the taste and texture of the salt. In addition, the carbonate and acid must be kept separate while the frozen confection is in storage and must react completely during consumption (or excess reactants must be used).

Finally, solid CO_2 is another possible storage method to consider for carbonating a frozen confection. Unfortunately, solid CO_2 does not exist at 253 K for pressures less than 2000 bars. These pressures preclude the use of solid CO_2 storage at typical ice confection temperatures. Solid CO_2 (dry ice) does exist at atmospheric pressure (it sublimates at 198.4 K (-78.4°C) (Lemmon et al., 2009)), so it could be used to carbonate an ice confection at the time of consumption. For example, very fine dry ice grains could be stirred into a granular or soft-serve ice confection. It would be necessary to ensure that the solid CO_2 particles do not burn the tongue or skin of the consumer. The use of solid CO_2 to carbonate a confection at the time of consumption would require the development of an additional low temperature (-78°C) cold chain for distribution of the dry ice.

In summary, CO_2 hydrates are the best choice for incorporating carbon dioxide into a frozen confection. They provide the highest CO_2 concentration with the greatest flexibility in the product recipe. With CO_2 hydrates it is not necessary to incorporate and stabilize a particular distribution of bubbles. The recipe can be varied freely and does not require management of separate components. There is no need for a new cold chain at dry ice temperatures. It is only necessary to store the confection at the minimum pressure for CO_2 hydrates, which is shown as a function of temperature in Figure 1-1. Assuming a freezer temperature of 253 K, this minimum pressure is 5 bars, which is a couple bars larger than the typical storage pressure of a carbonated beverage. Even this constraint can be avoided if the confection is eaten at the site of production.

1.3 Flash-freezing process overview

Formation of CO_2 hydrates is easily achieved using a CO_2 flash-freezing process developed for this research. The flash-freezing process causes rapid formation of CO_2 hydrates directly

in a confection as it is frozen. The concept is to disperse the ingredients mixture in liquid CO_2 and then rapidly reduce the pressure, causing some CO_2 to evaporate. The heat uptake associated with this CO_2 evaporation causes the ingredients mixture to freeze. Because the ingredients mixture is in intimate contact with CO_2, CO_2 is incorporated as water crystallizes in the mixture, forming CO_2 hydrates instead of ice in the confection. In this section, two batch-implementations of the CO_2 flash-freezing process are described and implementation of a continuous process is discussed.

Figure 1-3 shows a schematic of the first batch-implementation of the CO_2 flash-freezing process. Before production, the mixture tank is filled with the ingredients mixture (mixture), which includes all water, sugars, fats, stabilizers, emulsifiers and flavors in the confection recipe. Pressurized nitrogen gas drives the mixture through a heat exchanger (ice box 1) and then a nozzle (mixture nozzle) into a small chamber filled with liquid CO_2 (emulsion chamber). Liquid CO_2 is supplied through the dip tube of a room temperature bottle of saturated CO_2, pre-cooled in a heat exchanger (ice box 2), and throttled to the desired pressure. The temperature and pressure in the emulsion chamber are typically 283 K and 50 bars respectively. The combined mixture and liquid CO_2 are then sprayed through a second nozzle (flash-freezing nozzle) into a chamber maintained at a characteristic pressure of 10 bar (ice confection tank, hereafter ICT). CO_2 is vented to the atmosphere from the ICT through a backpressure regulator. After a batch is frozen, the ICT is vented to atmospheric pressure and opened to collect the frozen powder. A dewar of liquid N_2 is used to pre-cool the ICT walls before each batch is produced and thus reduce transients in the operation of the flash freezer. The pre-cooling is achieved by spraying cold gas on the outside walls of the ICT.

In the implementation of the CO_2 flash freezer used for this research, the mixture tank and ICT are made of 0.1 m (4") ANSI Schedule 40 stainless steel pipe and 0.01 m (0.5") thick stainless steel end plates. Rubber o-rings in a groove on each endplate form the pressure seal and the plates are bolted together by six 0.01 m (0.5") stainless steel threaded rods. The volume of the ICT is approximately 3.4 L. Due to the low density of the frozen powder a batch process can only be run for 5-8 minutes before the ICT is filled. A stainless steel wire-cloth mesh with a surface area on the order of 0.001 m^2 covers the vent line opening in the ICT to prevent powder from clogging the vent line. The mixture and flash-freezing nozzles are 1.0 and 3.0 solid cone Delavan oil-burner nozzles respectively. The mixture flow rate is typically 1 g/s and the CO_2 flow rate is typically 3 g/s. Ice boxes 1 and 2 are filled with water and ice.

As shown in the enlarged schematic of the ICT and emulsion chamber in Figure 1-3, the CO_2 flash-freezer is equipped with thermocouples in the mixture and in the CO_2 lines just before the emulsion chamber, in the vent line just after the ICT, and in the ICT hanging within 3 cm of the top and within 1 cm of the bottom. There are pressure transducers in the mixture, CO_2, and vent lines and in the top plate of the ICT. The pressure transducer in the top plate of the ICT is redundant unless the entrance to the vent line is plugged, which does not occur with the filter installed. There are no flow meters on this apparatus; flow rates are estimated based on the average CO_2 and mixture flow rates measured in a calibration test carried out when the equipment was first assembled. The estimated flow rates are similar to those measured by flow meters in a second batch apparatus that was built for and operated by the sponsors of this research. The second batch apparatus will be described later in this section. It is not used for experiments in this thesis, but some experience gleaned from its operation is reported here.

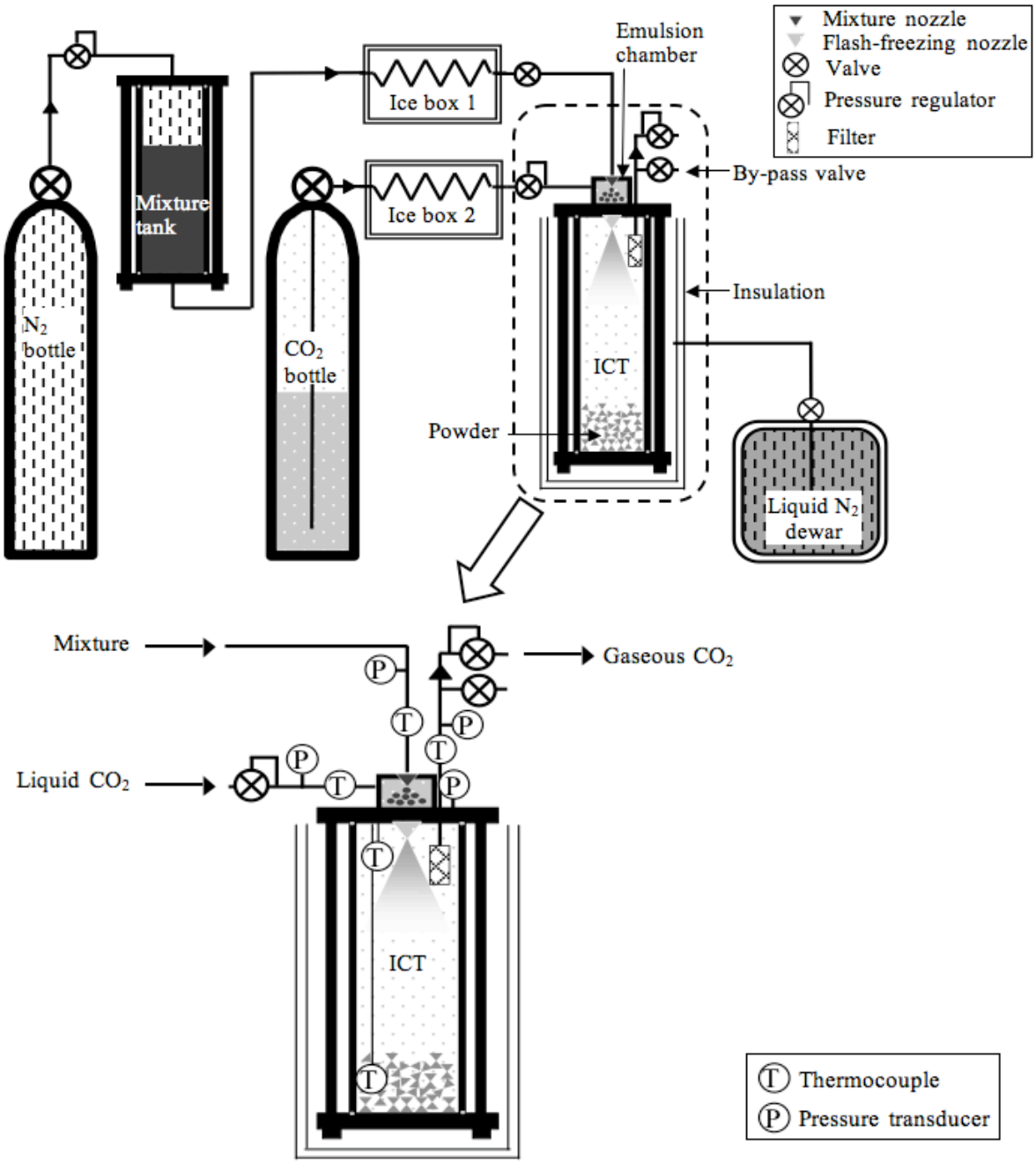

Figure 1-3 Schematic of CO_2 flash freezing batch process (ICT - ice confection tank) with enlarged view of the ICT and emulsion chamber showing pressure and temperature sensor locations.

In Figure 1-4 the pressure and temperature profiles are shown for a typical trial with the batch apparatus used for this thesis. Pre-cooling the ICT takes about 25 minutes. At the start of the trial the ICT temperature is stabilized at a temperature of approximately 230 K (in this particular trial the ICT was slightly overcooled). When the trial begins the vent temperature drops rapidly to 238 K. The mixture and liquid CO_2 temperatures gradually approach 283 K. The process attains steady state operation after about two minutes. When the mixture and CO_2 flows are stopped at the end of the trial the flash-freezing nozzle immediately becomes

blocked, presumably due to CO_2 hydrate growth in the nozzle channels. The equilibration of CO_2 and mixture pressure indicates that the flash-freezing nozzle is blocked while the mixture nozzle remains open. The by-pass valve for venting the ICT is immediately opened and the ICT pressure begins to fall. The ICT pressure and the temperature of the lower ICT thermocouple both fall, but plateau temporarily at approximately minute 38 of the trial. The pressure and temperature of this plateau correspond to the CO_2 triple point, so the plateau is related to solid CO_2 formation. This solid CO_2 is due to excess liquid CO_2 collected in the ICT during the batch process. During venting, the liquid CO_2 that collected in the ICT concurrently evaporates and solidifies. The thermocouple at the top of the ICT does not show a similar temperature decrease, suggesting that the dry ice formation is limited to the bottom of the ICT. The venting process takes approximately six minutes and the ICT is opened and the powder is removed about four minutes later.

Dry ice formation in this equipment is a common occurrence due to the imprecise control of mixture and CO_2 flow rates and in some cases excessive pre-cooling of the ICT. The dry ice typically forms a porous solid ring at the bottom of the ICT that can be easily separated from the powder. The frozen product of the process has a texture similar to fresh fallen snow due to atomization of the mixture by the flash-freezing nozzle.

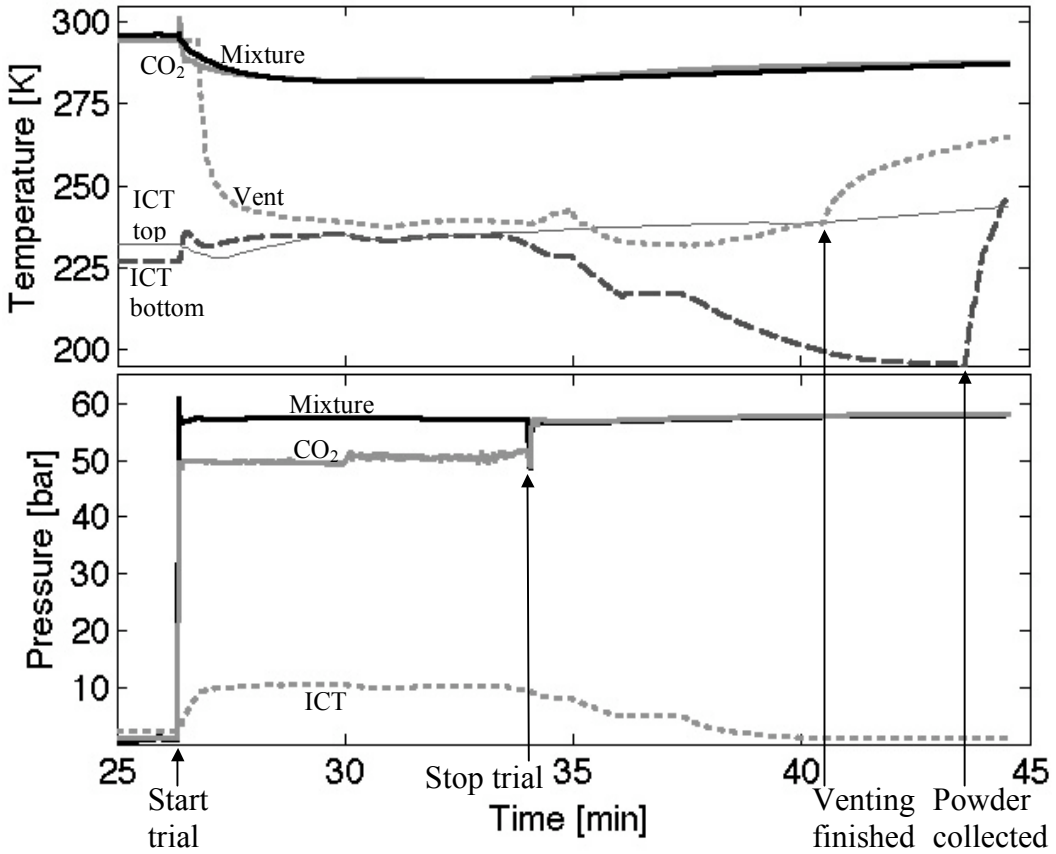

Figure 1-4 Example of temperature and pressure profiles for CO_2 flash-freezer batch process (mixture is 25 wt% sucrose solution). Time refers to minutes since start of pre-cooling.

A second batch-implementation of the CO_2 flash-freezing process was built at the research facilities of the sponsor. There were several improvements in the second implementation. To allow longer trials, the ICT was enlarged from 3.4 L to 10 L and the CO_2 supply was changed from a single bottle to a bank of eight bottles. The ICT was designed with doors sealed by sanitary clamps on both the bottom and the front of the tank. This allows quick access to either the initially formed or most recently formed powder. Flow meters for the mixture and liquid CO_2 lines and computer-controlled pressure regulators were used. The entire process can be monitored and controlled from a single computer console. With the improved control of flow rate enabled by this implementation, dry ice formation during venting is less common. However, the temperature in the ICT typically falls to 213 K during venting and dry ice clumps are observed about 20% of the time even without noticeable variations in the operating parameters.

In the future, the CO_2 flash-freezing process could be implemented in a continuous cycle by re-compressing the vented CO_2 and removing the powder using an airlock or extrusion screw. Instead of pressurizing the mixture with nitrogen gas, a liquid pump would be used to directly compress the mixture to high pressure. In a continuous cycle, the vented CO_2 would need to be carefully filtered before compression. The CO_2 compressor must be food grade and the re-compressed CO_2 would need to be supplemented to replace CO_2 trapped in CO_2 hydrates. Lopez (2009) describes development work on an attachment for continuous extraction of the powder.

The CO_2 flash-freezing process has several attractive features. The process requires minimal moving parts and does not require a scraped-surface heat exchanger. This should reduce maintenance costs and enable a small footprint compared to traditional ice cream freezers. Also, the product of the process has a powder texture not normally seen in frozen confections. This powder can be packed to any desired density or add-ins like chocolate bits can be stirred in easily. Most importantly the process is a rapid, single-step method of producing CO_2 hydrate confections. For comparison, slower, multi-step methods of making a CO_2 hydrate confection involve holding small ice confection particles in a high pressure CO_2 environment or stirring ground-up CO_2 hydrate particles into a partially frozen confection. The holding time necessary to convert small ice confection particles to CO_2 hydrates can range from an hour to more than a day depending on particle size. Ground-up CO_2 hydrate particles could be manufactured from agglomerates formed by agitating liquid water in contact with CO_2 at an appropriate pressure. While CO_2 hydrate agglomerates could be made in tens of minutes, grinding the agglomerates would be energy intensive and CO_2 hydrates would dissociate both during grinding and while the particles are stirred into the partially frozen confection. Due to this CO_2 hydrate dissociation during processing it would be impossible to make an ice-free CO_2 hydrate confection. In contrast, the CO_2 flash-freezing process can cause nearly complete CO_2 hydrate formation in the confection and produce the confection in less than a minute.

1.4 Pressure-temperature-mass storage apparatus

The pressure-temperature-mass storage apparatus (PTM) was developed and then used in several experiments to understand the behavior of CO_2 hydrate confections. The apparatus is introduced in this section, but the specific experiments are described as the results are

presented in the following chapters. The PTM is a small load cell in a stainless steel housing in which the pressure can be controlled by adding or venting gas. The PTM is operated in a standard reach-in chest-style freezer to allow temperature control. Changes in the load cell output and the pressure in the PTM can indicate CO_2 hydrate formation and dissociation in the sample. Increasing mass corresponds to CO_2 hydrate formation and decreasing mass corresponds to CO_2 hydrate dissociation. Using the PTM it is possible to measure: the CO_2 content of fresh flash-frozen powder, the rate of CO_2 loss, the rate of CO_2 absorption, the CO_2 hydrate equilibrium pressure, and the CO_2 hydrate dissociation and reformation rate and extent with temperature cycling.

Figure 1-5 shows a schematic of the PTM. The 300 g capacity aluminum single-point load cell (Vishay Tedea-Huntleigh, Model 1004) is mounted in the base of a 3-piece stainless steel (SS) chamber. The SS upper cap and SS base of the SS chamber are bolted to the SS mid-plate, with eighth-inch silicone o-rings forming the pressure seal. The sample sits in an aluminum can resting on an aluminum tray in the upper section of the chamber. The aluminum tray is bolted to the load cell through a hole in the mid-plate, as shown in the figure. There is no contact between the connecting bolts and the mid-plate. The sample capacity is 250 g or 250 mL. A sixteenth-inch, SS sheathed T-type thermocouple (Omega, TTSS-116U-2, 0.5 K limits of error) is mounted in the upper cap of the chamber. The thermocouple tip is close to the top of the sample, but does not touch the sample so that it does not influence the mass measurement. A sixteenth inch outer diameter capillary tube is connected to the upper section of the chamber. The capillary tube is 0.5 mm (0.02") inner diameter, 1.5 m (60") long and connects to a tee joint outside the freezer. The second port of

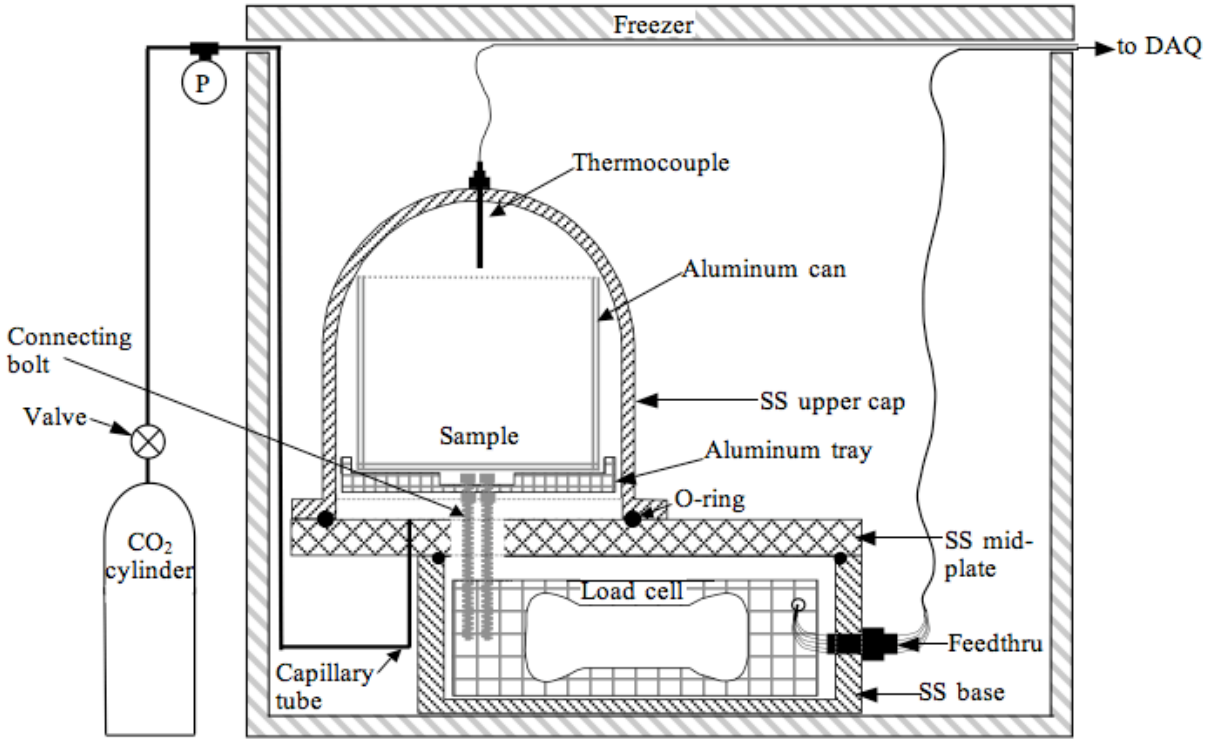

Figure 1-5 Schematic of Pressure-Temperature-Mass (PTM) apparatus used to monitor CO_2 hydrate formation and dissociation during storage.

the tee contains a pressure transducer (Kulite, XTL-123B-190-15bara) and the third connects to a 2.3 kg (5 lb.) CO_2 cylinder. Due to the bolt size and arrangement, the maximum operating pressure in the PTM is 12 bars, which is adequate for measurements up to the typical ICT pressures. The stainless steel chamber containing the load cell is placed at the bottom of a variable temperature chest freezer (Frigor GLE20) with a 228 to 273 K (-45°C to 0°C) range.

Pressure, temperature and mass signals are recorded using a National Instruments Compact FieldPoint system (cFP-1804 Ethernet interface with cFP-SG140 and cFP-TC120). A wire feedthru was made for the electrical connection to the load cell inside the SS chamber. The feedthru consists of copper wires in a short piece of half-inch SS rod. To make the feedthru, the SS rod was drilled with five close-fit holes for the copper wires. The copper wires were then epoxied into the stainless steel rod. The rod containing the copper wires was sealed in a ½" swagelok-½"male NPT union and screwed into a threaded hole in the base section of the chamber. The load cell wiring was soldered to the inside end of the copper wires and additional wiring was soldered to the outside end of the Cu wires for connection to the FieldPoint system.

The internal volume of the PTM is 625 mL, which is at least three times the volume of the sample. Typically the internal volume of the PTM is almost 14 times the volume of the sample due to the high porosity of the powder. Considering the entire internal volume of the PTM (625 mL), 1 g of CO_2 released due to CO_2 hydrate dissociation increases the pressure in the PTM by 0.77 bar at 253 K.

The load cell supplied by Vishay Tedea-Huntleigh comes with an encapsulation material to provide protection against dust and temporary flooding (IP66 environmental protection). Vishay specially provided the load cell for the PTM without encapsulation because the encapsulation causes transients in the load cell response to rapid changes in pressure. The un-encapsulated load cell is calibrated as a function of temperature and pressure using standard masses (10 to 100 g) from Christian Becker Inc., NY. The load cell signal decreases with increasing pressure. Due to corrections for pressure and temperature effects as well as uncertainty due to vibrations in the freezer, the resolution of the load cell in the PTM is 0.1 g. The load cell is calibrated at atmospheric pressure using the standard masses before each experiment to ensure that it has not been affected by moisture and temperature changes in the freezer.

The pressure transducer was calibrated against a 0.25% accuracy test gauge (Ashcroft Inc.) and found to be off by up to 0.1 bar (increasing error with increasing pressure). In addition, the CO_2 partial pressure in the chamber depends on the mixture of CO_2 and air in the chamber at the time it is sealed. When it is desirable to ensure a pure CO_2 environment in the PTM, the chamber is flushed with CO_2 entering through the capillary tube and escaping through the loosened thermocouple connection. As can be seen in the schematic of the PTM, it is difficult to completely flush the lower section of the chamber. The base section of the chamber is approximately 10% of the total volume of the chamber. The CO_2 partial pressure could be up to 0.1 bar lower than the total pressure measured, if the base section of the chamber contains air at atmospheric pressure at the time of sealing. The pressure measurements therefore have an uncertainty +/-0.1 bar. Unfortunately, during any pressurization or venting through the capillary tube the pressure transducer signal does not represent the pressure in the chamber because the transducer is located next to the CO_2 source.

In this thesis CO_2 hydrates in frozen confections are studied with the aid of the PTM and the CO_2 flash-freezer batch implementation. The CO_2 flash-freezer is used to produce CO_2 hydrate powder and the PTM is used to measure CO_2 hydrate formation and dissociation in the powder at varied pressure and temperature. These measurements are used to identify factors affecting CO_2 hydrate formation in the mixture, CO_2 hydrate stability in storage, and CO_2 hydrate dissociation when the confection is eaten, which will enable development of CO_2 hydrate confections.

2 Liquid CO_2-liquid ingredients mixture emulsion

In the flash freezing process, the ingredients mixture first comes into contact with CO_2 in the emulsion chamber, as was shown in Figure 1-3. The characteristics of the emulsion, including interactions between CO_2 and other ingredients, mixture droplet size and inhibition of CO_2 hydrate formation are important for rapid and complete formation of CO_2 hydrates when the emulsion is flash frozen. In this chapter, recipe formulation is discussed, including water content, CO_2 solubility, and interaction of fats and proteins with CO_2. The degree of mixing in the current emulsion chamber and the minimum degree of mixing that must be achieved are estimated. The effect of CO_2 hydrate formation in the emulsion chamber is described and the minimum temperature to avoid CO_2 hydrate formation, as a function of recipe, is presented. Based on these considerations, it is concluded that while emulsion of CO_2 and the mixture before flash freezing is essential to ensure close contact between CO_2 and the mixture during flash freezing, the process is robust to a variety of recipe ingredients and mixture dispersions.

2.1 CO_2-mixture ingredients interaction

The interactions between mixture ingredients and CO_2 during processing are manifold. The ingredients and ingredient proportions in the mixture affect CO_2 solubility. CO_2 in turn can cause some ingredients to precipitate from the mixture due to changes in pH, solubility and surface energy. Ingredients such as fats are soluble in CO_2, which can cause separation of the ingredients mixture and change the CO_2 saturation curve. In this section the ingredients water, sugars, proteins and fats are considered.

Water is the main ingredient (by mass) of any frozen confection. The mass fraction of water in the mixture is the dominant recipe parameter affecting CO_2 use during flash freezing and the CO_2 content of a CO_2 hydrate confection. Increasing the water mass fraction increases the amount of CO_2 necessary for flash freezing and the amount of CO_2 that can be captured in the product (see Section 3.1). Increasing the water mass fraction decreases the amount of CO_2 released during heat shock (see Section 5.3), but increases the total amount of CO_2 necessary in a storage vessel (see Section 4.2), which in turn increases the maximum pressure that can be generated if the product melts in a sealed storage vessel. Overall, a low water fraction (high total solids) recipe will reduce CO_2 use and packaging challenges.

A first estimate of CO_2 solubility in the mixture can be made by considering CO_2 solubility in pure water as a function of pressure and temperature. Figure 2-1 shows the solubility of CO_2 in water as a function of pressure and temperature based on data assembled by Diamond and Akinfiev (2003). The equilibrium mass fraction of CO_2 dissolved in water increases with pressure and decreases with temperature. Above the saturation curve CO_2 solubility is only a weak function of pressure because liquid CO_2 has a lower isothermal compressibility than gaseous CO_2 (Hofland et al., 1999). The equilibrium mass fraction of CO_2 in pure water at the conditions in the emulsion chamber (283 K, 50 bar) is 0.068 g CO_2/g solution. Dissolved CO_2 also lowers the pH of the mixture due to formation of carbonic

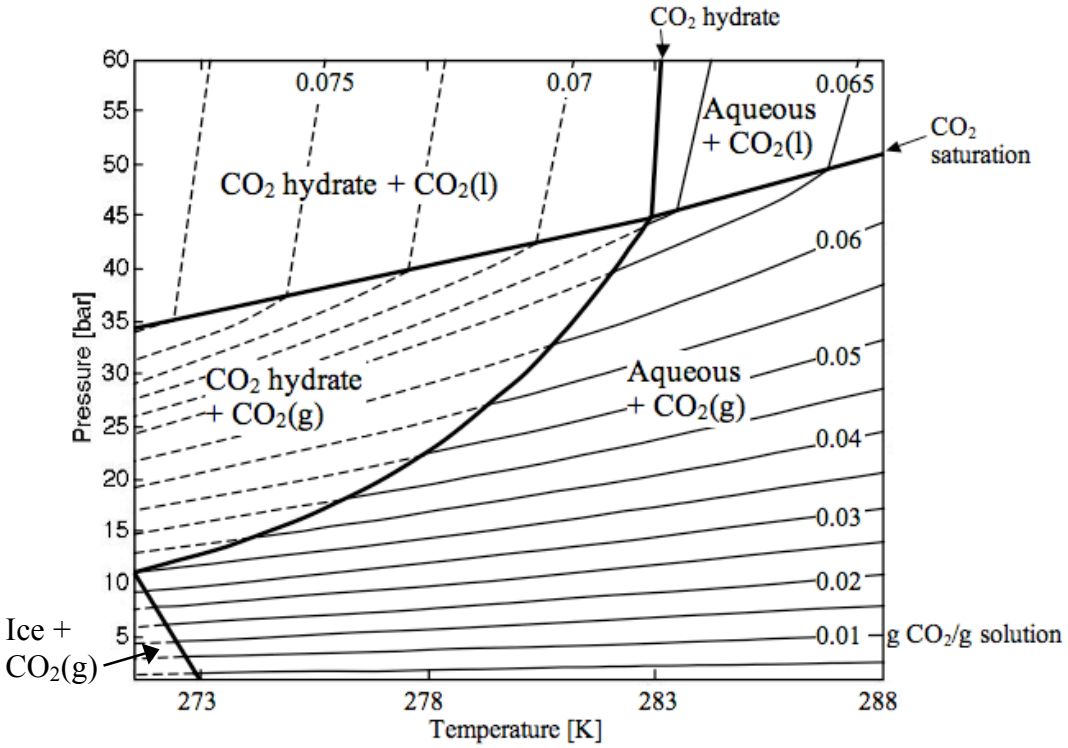

Figure 2-1 Curves of constant CO_2 mass fraction in CO_2-water solution, data from Diamond and Akinfiev (2003). Overlying black curves show phase boundaries. Curves are dashed in regions where aqueous CO_2 is metastable.

acid; in a water mixture without buffers the pH would approach 3 (Meyssami et al., 1992). Solubility in the converse direction is very low; 0.0008 weight fraction water is soluble in liquid CO_2 (King & Bott, 1993).

Sugars decrease the solubility of CO_2 in an aqueous solution. Descoins et al. (2006) compared CO_2 solubility in buffered aqueous solutions at 6 atm, 284 K (11°C), pH 3.1. Beet sugar at concentrations of 10 and 40 g sugar/L decreased both the rate of CO_2 dissolution and the final CO_2 concentration in the aqueous solution (Descoins et al., 2006). The magnitude of the decrease in CO_2 solubility is not reported but may be as high as 8% for 40 g sugar/L (4 wt% sugar) based on the reported decrease in CO_2 partial pressure in equilibrium with the solution and the Henry's Law constant used by Descoins et al. Calix et al. (2008) measured CO_2 solubility above the critical point of CO_2 (304 K, 74 bar) in 10-11 wt% sugar solutions containing D-fructose, sucrose and glucose and less than 0.01 wt% citric or malic acid. At 313 K (40°C) in the pressure range 76 to 159 bar the CO_2 concentration was decreased by at least 11% in the water-acid-sugar solutions compared to pure water. The effect of dissolved sugars on CO_2 solubility decreased with decreasing pressure in Calix's experiments.

The sugar concentration in the ingredients mixture for CO_2 flash freezing is typically 10-30 wt%, which is higher than the sugar concentration in Descoins' and Calix's experiments. Also, the CO_2 flash-freezing process involves liquid CO_2, whereas Descoins' experiments involve gaseous CO_2 and Calix's experiments involve supercritical CO_2. Despite these differences, the experiments of Descoins and Calix demonstrate that sugars decrease CO_2 solubility in the unfrozen mixture. The order of magnitude of this decrease may be 10%.

Solubility in the converse direction does not need to be considered because sugars are not soluble in liquid CO_2 (King & Bott, 1993).

The effect of proteins on CO_2 solubility in aqueous solutions is unclear. CO_2 can cause proteins with ionic groups to precipitate from aqueous solution because CO_2 lowers the pH of the solution. Decreasing pH causes hydrogen ions to associate with some of the ionic groups, changing the net charge on the protein molecule. At the isoelectric point, the net charge on the protein is zero and proteins agglomerate because hydrophobic interactions overcome charge repulsion. Isoelectric precipitations of casein and soy protein (which is often used as an analog for precipitation of other vegetable proteins) have both been demonstrated (Hofland et al., 2000). Soy protein was precipitated at 278-298 K (5-25°C) and less than 50 bars (Hofland et al., 2000). Casein was precipitated at >305 K (32°C) and 27-55.2 bars (Tomasula et al., 1995) and 298-323 K (25-50°C) and 10-60 bars (Hofland et al., 1999). The processes described by Tomasula and Hofland only involve gaseous or supercritical CO_2 because liquid CO_2 does not offer any advantages for increasing CO_2 solubility or decreasing pH. Nevertheless, liquid CO_2 does decrease the pH of aqueous solutions, so protein precipitation could occur in the emulsion chamber. The extent of precipitation will depend on the change in pH of the ingredients mixture. Precipitation may not be significant for casein at emulsion chamber temperature because Tomasula reported that casein did not precipitate from milk exposed to 0 to 69 bars CO_2 pressure at 298 K (25°C) (Tomasula & Boswell, 1999). Protein that precipitates in the emulsion chamber would not be lost from the frozen powder because protein agglomerates would be separated from CO_2 during the flashing process. However, protein agglomerates would not provide surfactant functionality in the frozen product.

There are conflicting results for solubility of CO_2 in aqueous solutions containing proteins. Descoins et al. (2006) found that the proteins bovine serum albumin (BSA) and β-casein increase the solubility of CO_2 in aqueous solution at 6 atm, 284 K (11°C), pH 3.1. Descoins added 50 mg/L of these proteins individually to solutions containing 10 g sugar/L. Both the kinetics of CO_2 dissolution and the solubility of CO_2 in the aqueous solution increased. Again the magnitude of the increase in CO_2 solubility was not reported, but appeared to approach 7% for 50 mg/L BSA or casein (0.005 wt% protein). Surprisingly, this small protein concentration seems to cancel the CO_2 solubility decrease caused by 200 times as much sugar. The CO_2 concentration measurement is based on the partial pressure of CO_2 in the gas phase in equilibrium with the solution, so this measured increase in CO_2 solubility is not due to chemical bonding between CO_2 and proteins. In contrast to the results of Descoins et al., Tomasula and Boswell (1999) measured a 10-23% decrease of CO_2 solubility in skim milk compared to water at 298 K (25°C) in the pressure range 0-69 bars. Skim milk is about 2.5 wt% casein and 6 wt% minerals and lactose, but the casein does not seem to compete with the effect of the sugars (lactose) as in Descoins' experiments. Perhaps the conflicting results are related to protein precipitation and minerals buffering the milk. Combining the solubility effects measured by Descoins, Calix and Tomasula, it is estimated that the solubility of CO_2 in the ingredients mixture is lower than the solubility of CO_2 in pure water by 10-20% due to the sugars and proteins.

CO_2 and fats are mutually soluble because both are non-polar. The effect of fat on CO_2 solubility in the mixture depends on the state of the fat. Ma and Barbano (2003) demonstrated that CO_2 dissolves more readily in liquid fat than in solid fat by measuring the pH of milk as a function of fat content at 273 K and 313 K and constant total CO_2 concentration. They found that the pH decreased with increasing milk fat content at 273 K (0°C), but remained constant

with increasing milk fat content at 313 K (40°C). Milk fat is solid at 273 K and liquid at 313 K (Ma & Barbano, 2003). Ma and Barbano suggested that at 273 K CO_2 concentrates in the aqueous phase and very little dissolves in the fat portion because it is solid, but at 313 K CO_2 dissolves in both the liquid fat and the aqueous phase. Ma and Barbano also demonstrated that at 273 K pH is higher for 15% vegetable oil emulsion than for 15% fat cream or butter oil. Vegetable oil is liquid at 273 K, while butter oil and cream are both solid, so Ma and Barbano again suggest that more CO_2 dissolves in liquid fat than in solid fat. Ma's experiments do not address the total amount of CO_2 dissolved in aqueous-fat emulsions. It may be possible to increase the CO_2 concentration in the mixture in the emulsion chamber using fats that are liquid at 283 K, but fats that are solid at 283 K probably do not affect CO_2 solubility in the mixture significantly.

Near-critical and supercritical CO_2 are commonly used to extract oils and other non-polar and slightly polar materials from natural products. Solubility of oils and fats in CO_2 decreases with increasing molecular weight (King & Bott, 1993). Volatile hydrocarbons are completely miscible, but natural oils are sparingly soluble in CO_2. For example, at 283 K and 50 bars the solubility of soybean oil in CO_2 is less than 0.1 wt%. For a 3:1 CO_2:mixture mass ratio in the emulsion chamber, only up to 0.003 grams of oil per gram of mixture could dissolve in the CO_2. Dissolution of fats from the mixture in CO_2 would change the fat particle distribution created during preparation of the mixture (specifically homogenization), but any oil or fat that dissolves in the emulsion chamber will come out of solution during flashing. The resulting fat particles would probably be small and irregular, as observed in rapid expansion of supercritical solutions of hydrogenated palm oil in CO_2 (Li et al., 2005), but would not be lost from the confection. Conversely, volatile flavoring compounds initially in the mixture may dissolve completely in the liquid CO_2 in the emulsion chamber. It is possible that a significant fraction of these volatiles are lost with the vented CO_2 gas. This could be the reason that higher-than-normal concentrations of flavor are needed in mixtures used for CO_2 flash freezing.

It is likely, based on the above discussion of the effect of sugars, proteins and solid fats on CO_2 solubility that the CO_2 concentration in the mixture in the emulsion chamber is less than, but similar to the concentration of CO_2 in pure water at 283 K and 50 bars (0.068 g/g solution). The amount of CO_2 dissolved in the mixture will be even less if the mixture is under-saturated, which could occur if the residence time in the emulsion chamber is not long enough to reach equilibrium (see section 2.2 for a discussion of residence time). A concentration of 0.068 g/g solution is less than one third the mass fraction of CO_2 in CO_2 hydrates (0.242-0.298 g CO_2/g CO_2 hydrate). Therefore, dissolved CO_2 is not the main source of CO_2 for CO_2 hydrate formation during flash freezing. In section 3.3 it will also be argued that the fraction of CO_2 that can be dissolved in the mixture is probably too small to significantly enhance atomization of the mixture. However, the CO_2 dissolved in the mixture in the emulsion chamber can improve nucleation of CO_2 hydrates during flashing by increasing the supersaturation of CO_2 in the mixture when it is expanded to ICT pressure. The CO_2 dissolved in the mixture before flashing also reduces the amount of CO_2 that must be transported through a droplet surface for CO_2 hydrate formation, potentially improving the ratio of CO_2 hydrate to ice formation.

As discussed in this section, CO_2 and the ingredients in the mixture can interact in a variety of ways and the interactions depend on the specific type of protein and fat and the particular concentration in the mixture. Despite this, the CO_2 flash-freezing process has been

used with a large variety of recipes successfully, demonstrating that the process is robust to different recipes. Further work is required to understand the effect of ingredients and concentrations on the microstructure of the CO_2 hydrate confection. The changes in microstructure may be very important for mitigating recrystallization in the CO_2 hydrate confection during storage and heat shock.

2.2 Dispersion of the ingredients mixture

The emulsion chamber is designed to intimately mix liquid CO_2 and the ingredients mixture, but the actual distribution of fluids in the emulsion chamber is not known because the current apparatus does not have a view window. It is clear that the fluids mix sufficiently in the emulsion chamber because the CO_2 flash-freezer produces a carbonated powdered product. Qualitatively, carbonated powder has successfully been made with a wide range of mixtures, including high viscosity mixtures, high total solids mixtures and mixtures containing fat. The necessary degree of mixing is not clear because further atomization occurs downstream of the emulsion chamber and CO_2 hydrate formation requires more CO_2 than can be provided by saturation of the ingredients mixture in the emulsion chamber. In this section an estimate of the mixture dispersion achieved in the emulsion chamber is presented and then constraints on the maximum droplet size are suggested.

Figure 2-2 shows a schematic of the emulsion chamber in the batch apparatus. It is assumed that mixture is dispersed as droplets in liquid CO_2. The solubility of CO_2 in water at emulsion chamber temperature and pressure is only 6-7 wt% and water is sparingly soluble in CO_2, so the fluids are essentially immiscible. In a quiescent chamber the fluids would separate into a liquid CO_2 layer on top of CO_2-saturated mixture. However, in the emulsion

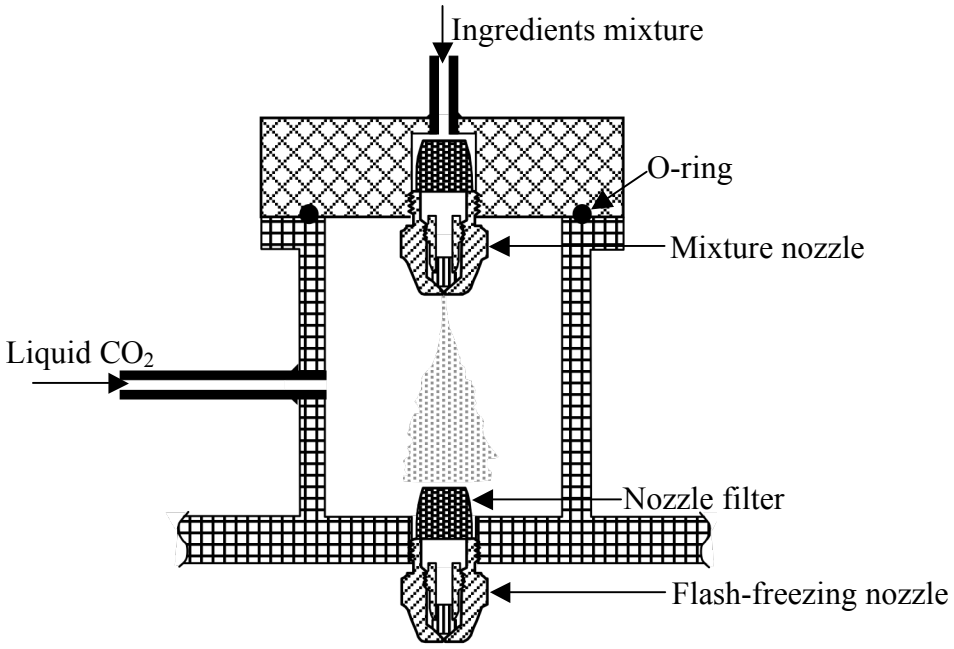

Figure 2-2 Schematic of emulsion chamber.

chamber mixture is continually injected through a 279 μm nozzle orifice at 16.4 m/s while CO_2 enters through a 3.2 mm inner diameter tube at 0.4 m/s. The volume fraction of mixture in the emulsion chamber is approximately 23% and the typical residence time of the fluid in the emulsion chamber is five seconds.

The mixture nozzle is a Delavan solid-cone, oil-burner nozzle. This pressure-swirl nozzle is designed to accelerate fluid into a rotating sheet with a vapor core. After leaving the nozzle orifice the thin fluid annulus spreads into a hollow cone and breaks into droplets. The average droplet diameter for fuel oil (typical viscosity 3.5 cP) sprayed by a 1.0 nozzle operating at 6.89 bars is 50 μm (Olson, 1999). However, some combinations of fluid viscosity, nozzle size and pressure drop cause a solid jet of fluid to form instead of the desired hollow cone. Specifically, for a particular fluid viscosity and nozzle size, the pressure drop must be greater than some minimum value to avoid formation of a jet. For example, with an 18.7 cP fluid and a 1.0 nozzle it was observed that a jet of fluid forms if the pressure drop is less than 19.3 bars. In the emulsion chamber the pressure drop across the 1.0 nozzle is typically less than 6.89 bars. The viscosity of a water-sucrose-glucose solution at 283 K is 2.98 cP for 20% total solids, but 23-25 cP for 50% total solids (Migliori et al., 2007) and viscosity increases significantly (for example 100 cP) with addition of stabilizers such as guar. Thus many ingredients mixtures are too viscous to form a spray cone with the current mixture nozzle and applied pressure drop.

In addition, an annulus of mixture may not form in the nozzle because the oil-burner nozzle is designed to introduce the working fluid into a vapor phase environment, whereas the ingredients mixture enters a liquid CO_2 environment. In standard operation of a pressure-swirl nozzle the rotational velocity of the working fluid causes a radial pressure gradient, with the lowest pressure occurring along the axis of the nozzle. A vapor column forms in the nozzle due to the low-pressure core. In this core, vapor is sucked in along the axis of the nozzle and dragged out with the exiting working fluid. A schematic cross-section of the fluid velocities is shown in Figure 2-3. In order to have no slip at the vapor column-working fluid interface, part of the exiting vapor must be accelerated to the same rotational and axial velocity as the mixture at the interface. When the operating environment of the nozzle is

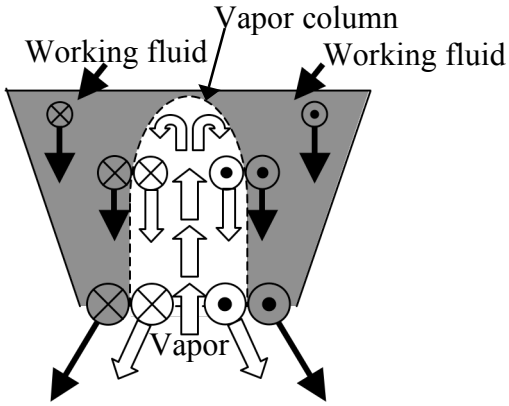

Figure 2-3 Cross-sectional view of vapor and working fluid velocities in a pressure-swirl nozzle under standard operation. White block arrows represent vapor flow, black arrows represent mixture flow. Circles with x's and dot's represent flow into and out of the page, respectively.

liquid CO_2, rather than a vapor at atmospheric pressure, the density of the fluid that would form the central column is increased by a factor of more than 800. Due to the significantly larger inertia of liquid CO_2, one might expect mixture rotation in the nozzle to be slowed, causing the mixture annulus to thicken. In support of this argument, Ibrahim and Jog (2007) found, both computationally and experimentally, that the thickness of the annulus at the exit of a pressure-swirl nozzle increases with increasing gas density in the operating environment of the nozzle. Therefore it is expected that liquid CO_2 at the nozzle exit hinders formation of a fluid column in the nozzle and the exiting mixture approaches a jet formation. In this case even low viscosity ingredients mixtures probably enter the emulsion chamber as a jet.

The ingredients mixture jet is broken up into droplets due to hydrodynamic interaction with CO_2 in the emulsion chamber. Riestenberg et al. (2004) studied the break up of a jet of liquid water entering a column of liquid CO_2 thru a capillary tube in the pressure and temperature ranges 55-62 bars and 283-285 K. Riestenberg et al. identified three different jet break-up patterns: Rayleigh, transitional and spray mode. The break up mode can be predicted by calculating the product of the Ohnesorge and Reynolds numbers of the flow. The Ohnesorge number (Oh) is a non-dimensional ratio of the effective viscous force to the interfacial force, and the Reynolds number (Re) is a non-dimensional ratio of the inertial force to the viscous force. Oh and Re are defined as

$$\mathrm{Oh} = \frac{\mu_d}{\sqrt{\rho_d \sigma d_o}}, \quad \mathrm{Re} = \frac{\rho_d v d_o}{\mu_d},$$

where μ is the dynamic viscosity, ρ is the density, σ is the interfacial tension, d_o is the orifice diameter and v is the velocity of the jet. The subscript d indicates properties of the dispersed fluid (the water or mixture droplets). Riestenberg et al. showed that spray mode jet break up occurs for

$$\mathrm{Oh} \cdot \mathrm{Re} = \sqrt{\frac{\rho_d d_o}{\sigma}} v > 18. \tag{2.1}$$

Spray mode jet break up is characterized by immediate break up of the jet at the nozzle tip into fine droplets that are relatively uniform in size. Riestenberg et al. measured average spray mode droplet diameters and found that they are smaller than the droplet size predicted on the basis of Rayleigh's maximum instability theory,

$$d = d_o \left(\frac{3\pi}{2}\right)^{1/3} \left(1 + \frac{3\mu_d + \mu_c}{\sqrt{d_o \sigma \rho_d}}\right)^{1/6}, \tag{2.2}$$

where the subscripts d and c refer to the dispersed (water or mixture) and continuous (liquid CO_2) phases respectively.

Typical properties of the system are ρ_d=1000 kg/m^3, σ=0.029 N/m based on a liquid CO_2-water interface at 283 K (Uchida & Dawabata, 1997), d_o=279 μm, and v=16.4 m/s based on a 0.001 kg/s flow rate through the nozzle orifice, which means the $\mathrm{Oh} \cdot \mathrm{Re}$ product is 50; it is surmised that the mixture breaks up in spray mode based on Eq. 2.1. The effect of CO_2 entry into the emulsion chamber on jet breakup is neglected; the CO_2 flow may help to disperse the spray, but the CO_2 velocity entering the emulsion chamber is less than the mixture velocity entering the emulsion chamber by almost two orders of magnitude. All droplets should be smaller than the Rayleigh instability theory droplet size calculated according to Eq. 2.2, 540 μm for average viscosity mixture (0.040 Pa-s) or 470 μm for water. The average droplet size should be close to the value Riestenberg measured for spray mode break up of a water jet in liquid CO_2 with a 254 μm nozzle orifice, namely 162 μm.

The ingredients mixture dispersion in the emulsion chamber may affect the CO_2 concentration of the mixture before flash freezing and the characteristic size of the CO_2 flash-freezing powder. Small mixture droplets are desirable because they can pass through the flash-freezing nozzle in direct contact with liquid CO_2, rather than in alternating slugs of mixture and liquid CO_2. Small droplets provide significant interfacial surface area for heat and CO_2 transport. This surface area may cause mixture droplets to stay in thermal equilibrium with CO_2 during expansion, leading to significant super-cooling. High levels of super-cooling are associated with increased nucleation rate. If the mixture droplets are small enough they can become fully saturated with CO_2 before flashing, which could also improve CO_2 hydrate nucleation and growth, leading to more complete CO_2 hydrate formation in the ICT.

CO_2 saturation of the mixture droplets will occur if the mixture droplet radius is smaller than the characteristic diffusion length associated with the residence time of the mixture in the emulsion chamber. The residence time in the emulsion chamber, t_{res}, is the volume of the emulsion chamber, V_{EC}, divided by the mixture, $\dot{Q}_{mixture}$, and CO_2, $\dot{Q}_{CO_2}$, volume flow rates,

$$t_{res} = \frac{V_{EC}}{\dot{Q}_{CO_2} + \dot{Q}_{mixture}}.$$

The distance a CO_2 atom will diffuse in a liquid droplet in this time is given by the characteristic diffusion length, L, which is

$$L = \sqrt{4 D_{CO_2 in H_2O} t_{res}},$$

where $D_{CO_2 in H_2O}$ is the diffusivity of CO_2 in water. The residence time of mixture and CO_2 in the emulsion chamber is about five seconds. $D_{CO_2 in H_2O}$ at 283 K is 1.3 x 10^{-9} m^2/s (Versteeg & van Swaall, 1988), giving a characteristic diffusion length of 171 μm. Therefore CO_2 should dissolve throughout 100 μm radius water droplets in the emulsion chamber (the estimated droplet size based on Riestenberg's work). However, it is not clear that this is true for more complex mixtures because diffusivity of CO_2 in aqueous solutions decreases with increasing viscosity. Versteeg and van Swaall (1988) demonstrate that the relationship between viscosity and diffusivity for aqueous amine solutions is $D_{CO2}*\mu^n$=constant, where n=0.8 for amine solutions. This relationship is a modification of the Stokes-Einstein relation. For a mixture viscosity of 100 cP, CO_2 diffusivity may be decreased to 3.3 x 10^{-11} m^2/s. The characteristic diffusion length in viscous mixture droplets is then only 26 μm, which is smaller than the estimated droplet radius in the emulsion chamber. CO_2 cannot saturate the core of viscous mixture droplets in the emulsion chamber if CO_2 transport is only by static diffusion.

It is possible that CO_2 is advected into the mixture droplets by internal circulation, but Saboni et al. (2007) showed that the mass transfer depends strongly on the ratio of the dispersed and continuous phase viscosities, Reynolds number (Re) and the Peclet number (ratio of advection to diffusion, Pe). Saboni et al. used a numerical solution of the Navier-Stokes equation to calculate the mass transfer coefficient as a function of the viscosity ratio, Re, and Pe for a fluid sphere moving in another fluid. Assuming a typical mixture viscosity of 40 cP, the viscosity ratio is 500, suggesting that the relative velocity between the mixture droplets and liquid CO_2 would need to be extremely large to induce significant fluid circulation in the droplet. Based on Saboni's mass transfer correlation, the amount of CO_2 that can be advected into a viscous mixture droplet during its residence time in the emulsion

chamber is about 10% of the CO_2 needed to saturate the droplet. Further work is needed to understand CO_2 advection into the mixture droplets and whether the mixture is saturated with CO_2 when it enters the flash-freezing nozzle. This work would require measuring CO_2 saturation of the droplets in situ. Based on the above consideration of CO_2 diffusion and advection it is likely that the ingredients mixture is not always saturated with CO_2 in the emulsion chamber. Regardless, CO_2 hydrate confections have been produced successfully with even 100 cP recipes, suggesting that saturation of mixture in the emulsion chamber is not necessary for flash freezing.

Preliminary measurements of CO_2 content in fresh powder indicate that initial CO_2 content decreases slightly with increasing mixture viscosity (A. Pizzagalli 2007, pers. comm., July 27). Mixtures with varying viscosity (1-100 cP) were frozen in the second batch apparatus for CO_2 flash freezing. The mixture and CO_2 flow rates (averaging 1 and 3.2 g/s respectively) were approximately constant for this comparison. Frozen powder was collected from the top of the powder pile in the ICT at the end of each batch. This ensured that the CO_2 content of the freshest powder was measured and avoided any dry ice that formed at the bottom of the pile during venting of the ICT. The collected powder was placed in a small plastic cup on an electronic balance in a freezer at 253 K and the initial mass was measured. The powder was then melted in the plastic cup and the mass was measured again to determine the mass of mixture in the sample. Figure 2-4 shows the measured initial CO_2 content as a function of mixture viscosity. There is a small decrease in initial CO_2 content with increasing mixture viscosity. This trend may be related to an increase in average droplet diameter and decrease in CO_2 saturation of the mixture in the emulsion chamber due to increasing mixture viscosity.

The main constraint on the droplet size in the emulsion chamber may be that it should be similar to the diameter of the flash-freezing nozzle orifice. If the mixture droplets are significantly larger than the orifice of the flash-freezing nozzle, mixture and CO_2 can be sprayed into the ICT in alternating slugs. In this case, CO_2 and the mixture are not in intimate contact during the CO_2 phase change. Freezing of the particle may not occur as rapidly and a high concentration CO_2 source (the liquid) may not be readily available to form CO_2 hydrates

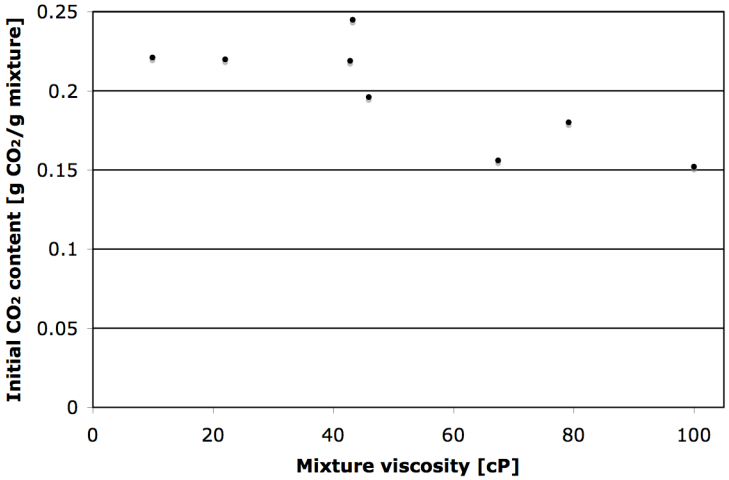

Figure 2-4 Effect of viscosity on CO_2 content in CO_2 flash-freezing powder. CO_2:mixture flow ratio is approximately 3:1 for all tests.

during freezing. Formation of CO_2 hydrates in the flash-freezer is only effective if CO_2 hydrates are formed directly from the mixture, rather than by subsequent conversion of ice particles. In the "high" pressure CO_2 gas environment of the ICT the flash-freezing nozzle orifice diameter is about 500 μm, so 100-200 μm droplets satisfy the criteria suggested here.

Based on Riestenberg's observations the Delavan oil burner nozzle is not necessary in the flash-freezing apparatus; a simple 279 μm capillary tube could be just as effective, with a pressure drop of 5 bars through a 2 mm length tube. If the Delavan oil burner nozzle is replaced by a capillary tube the mixture flow rate for a fixed pressure drop will become much more sensitive to viscosity. The viscosity of the mixture can change dramatically, so good mixture flow rate information and a variety of capillary lengths would be needed.

In conclusion, liquid CO_2 and the ingredients mixture must be well mixed in the emulsion chamber. In the current apparatus, the estimated droplet size is 150-200 μm and the residence time is 5 seconds. These parameters ensure acceptable mixture and CO_2 contact in the flash-freezing nozzle. These parameters are effective for a range of mixture viscosities (0-100 cP); however, there is preliminary evidence that smaller droplets and or longer residence time could be desirable for high viscosity mixtures in order to improve CO_2 saturation before flash freezing. Increasing the emulsion chamber volume or decreasing the CO_2 and mixture flow rates will increase residence time. Mixture droplets should be smaller than the diameter of the flash-freezing nozzle orifice, but beyond this the CO_2 flash-freezing process is not very sensitive to droplet size because the mixture is further atomized in the ICT by multiple mechanisms (hydrodynamic forces due to expansion of CO_2 and design of the flash-freezing nozzle) and the CO_2 supply for filling CO_2 hydrates does not come from saturation of the mixture in the emulsion chamber. CO_2 for CO_2 hydrates is supplied by the liquid CO_2 phase or CO_2 vapor in the ICT.

2.3 CO_2 hydrate formation in the emulsion chamber

CO_2 hydrates can form in the emulsion chamber if the temperature is low enough. CO_2 hydrate formation in the emulsion chamber is not desirable because CO_2 hydrates form on the mixture droplet surfaces and agglomerate. These agglomerations can block the flash-freezing nozzle and inhibit contact between CO_2 and mixture. CO_2 hydrate formation can be avoided by operating the emulsion chamber at a temperature greater than the maximum temperature at which CO_2 hydrates are stable. Figure 2-5 shows the curves of maximum temperature and minimum pressure for CO_2 hydrate formation in water and sucrose or glucose solutions. CO_2 hydrates do not form in the region to the lower right-hand side of the curves and can form in the region to the upper left-hand side of the curves. There is a kink in the curves at the aqueous solution-CO_2 hydrates-CO_2 liquid-CO_2 gas equilibrium point. In the figure, dotted lines indicate the expected trend where data is not available. The curve farthest to the right corresponds to pure water. Sugar and other dissolved components in the ingredients mixture act as thermodynamic inhibitors (above 273 K), decreasing the temperature and increasing the pressure required for CO_2 hydrate to form. As shown in Figure 2-5, the maximum temperature of CO_2 hydrate formation decreases with increasing sucrose and glucose concentration. Clearly then, CO_2 hydrate formation in the emulsion chamber can be avoided by ensuring that the mixture and liquid CO_2 are 283 K or warmer. If there are dissolved ingredients the temperature in the emulsion chamber could be lower. For example, with a

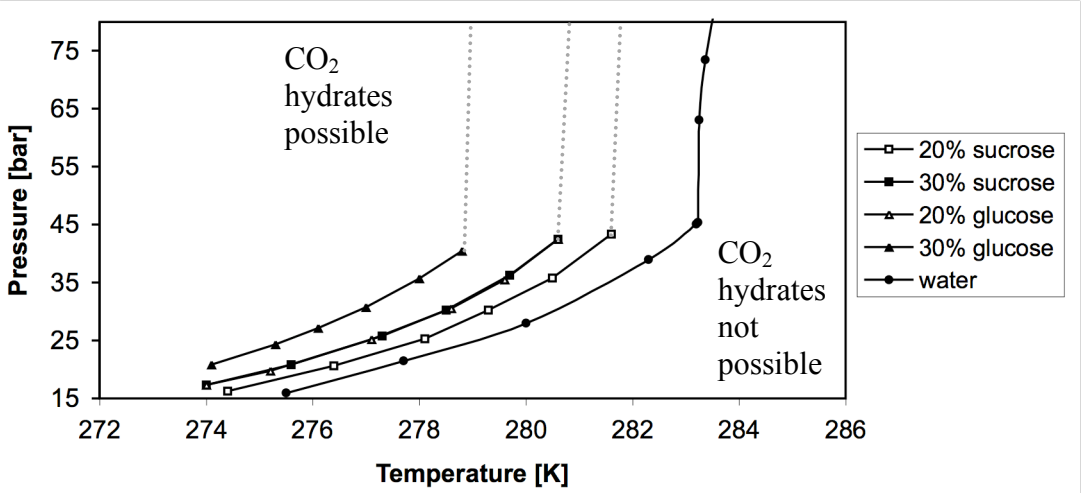

Figure 2-5 CO_2 hydrate phase equilibrium with sucrose and glucose in the pressure-temperature range used in the emulsion chamber. Data from Chun and Lee (1999) and Sloan and Koh (2008).

30% glucose solution, the chamber could be operated at 279 K without CO_2 hydrate formation. In optimizing the flash-freezing process for a given mixture, Figure 2-5 or similar data for the appropriate dissolved ingredients can be used to determine the maximum temperature for CO_2 hydrate formation. This temperature then is the minimum temperature at which the emulsion chamber can be operated with the given mixture.

Experimentally, CO_2 hydrate formation is inferred when the flash-freezing nozzle becomes blocked, stopping both CO_2 and mixture flow. The nozzle does not become blocked when the CO_2 and mixture temperatures entering the emulsion chamber are too warm for CO_2 hydrate formation. The nozzle becomes blocked frequently, but not always, when the mixture and CO_2 are pre-cooled below 283 K, in particular if the mixture is water. This inconsistent blockage may be due to variations in heterogeneous nucleation of CO_2 hydrates or flow patterns. When the nozzle becomes blocked during a trial, flow is re-established by heating the flash-freezing nozzle.

Formation of CO_2-hydrate-covered droplets and agglomeration of these droplets have been observed visually by Riestenberg et al. (2004) and Lee et al. (2003). Riestenberg et al. injected water through a capillary tube into quiescent liquid CO_2 under CO_2 hydrate formation conditions. Jet breakup was similar to the breakup described in section 2.2, but droplets collected into a cohesive mass. Lee et al. formed a CO_2 hydrate-water-liquid CO_2 composite using a co-flow injector. In the co-flow injector, water flows through a 125 μm capillary tube with a 6 mm diameter concentric annulus of liquid CO_2. The fluids mix and form a CO_2 hydrate composite in a 12.5 cm section of the 6 mm diameter tube. The composite is driven out of the 6 mm tube and breaks off in several centimeter sections. The observations reported by Riestenberg and by Lee show that CO_2 hydrate formation and agglomeration can be expected in the emulsion chamber if it is run at CO_2 hydrate formation temperatures.

Formation of a CO_2 hydrate shell reduces CO_2 dissolution in the mixture droplet. Once the shell forms, CO_2 transport into the droplet is limited by the diffusivity of CO_2 in CO_2 hydrate, which is several orders of magnitude slower than the diffusivity of CO_2 in water (Radhakrishnan et al., 2003). Additionally, the shell reduces fluid circulation in the droplet and may provide mechanical stability against break up of the droplet during flashing.

Yamasaki et al. (2000) demonstrated slow dissolution of liquid CO_2 through a CO_2 hydrate shell. Yamasaki et al. filled a clear polycarbonate vessel with water and liquid CO_2 and rotated a stirrer in the vessel to agitate the system. At a stirring rate of 500 rpm, liquid CO_2 is dispersed into the water as droplets covered with CO_2 hydrate shells. Initially these droplets are positively buoyant because CO_2 is less dense than water, but as the CO_2 hydrate shell thickens the bulk density of a droplet increases until the droplet begins to sink. Yamasaki showed that droplets with a diameter of 0.1 mm did not form enough CO_2 hydrate to sink during 10 minutes of rapid stirring, indicating that liquid CO_2 transport through the initially formed CO_2 hydrate shell is impeded. Rapid stirring also did not cause the CO_2 hydrate covered droplets to break up into smaller droplets. This suggests that CO_2 hydrate shells surrounding mixture could hinder further CO_2 hydrate formation during flashing.

If nozzle blockage can be overcome and the powder is not adversely affected, it would be preferable to run the CO_2 flash freezer with liquid CO_2 and mixture entering the emulsion chamber at 277 K (4°C). This would reduce the amount of CO_2 required for freezing, reduce the necessary liquid CO_2 pressure, and conform to the temperature normally maintained between pasteurization and freezing of ice cream mixtures. It is likely that the process can be run with CO_2 hydrate formation in the emulsion chamber by using a flash-freezing nozzle designed to minimize blockage and continually heating the nozzle to dissociate any CO_2 hydrate contacting the nozzle walls. In the past, the CO_2 flash-freezing apparatus has been operated despite CO_2 hydrate formation in the emulsion chamber by heating the flash-freezing nozzle with a heat gun. It is not clear whether this heating completely dissociated the CO_2 hydrate formed in the emulsion chamber or merely dissociated enough of the CO_2 hydrates to re-establish flow. Qualitatively, the resulting powder was not changed. While this experience suggests that operating the emulsion chamber at 277 K is possible, a careful comparison of powder texture and initial CO_2 content with and without CO_2 hydrate formation in the emulsion chamber would be useful to check for any adverse effects on the powder, for example increased particle size or decreased total CO_2 hydrate formation.

3 Flash-freezing

In the CO_2 flash-freezing process, CO_2 hydrates form directly from the liquid mixture during and immediately after expansion to ICT pressure. It is inferred that CO_2 hydrate nucleation and growth occur concurrently with CO_2 flashing. CO_2 hydrates are present in the freshly frozen powder, but the emulsion chamber is too warm for CO_2 hydrate formation and conversion of ice to CO_2 hydrate is too slow to proceed during the residence time of the powder in the ICT. It is known that CO_2 hydrates are present in the powder when it is removed from the ICT because the CO_2 concentration is typically 12-25% CO_2 by mass, which is in the range of partial to nearly complete crystallization of water into CO_2 hydrates. Additionally, pellets formed from fresh powder collapse if the pellets are stored at atmospheric pressure, indicating that CO_2 hydrates were initially present and subsequently dissociated. Although dry ice can form if the process parameters are not correct (i.e. high CO_2 flow rate, over-cooled ICT, or poor atomization of a viscous mixture), dry ice is easily recognized by abnormally fast loss of CO_2 from the powder or by porous dry ice blocks that can be separated from the powder.

In this chapter, several elements of CO_2 hydrate formation by the CO_2 flash-freezing process are explained. The key elements of CO_2 hydrate formation are the CO_2:mixture flow ratio, atomization of the mixture to maximize surface area, and the competition between crystallization of ice and CO_2 hydrates. Flashing of CO_2 enables such rapid cooling of the mixture that any mixture with insufficient CO_2 exposure will freeze as ice. It will be shown in section 3.2 that it is unlikely that this ice can be converted to CO_2 hydrate during the residence time of the powder in the ICT. In the current batch implementation of the CO_2 flash freezer it is not possible to investigate the atomization and freezing of the mixture directly. The powder is only accessible at the end of each batch production, at which point the powder must be exposed to atmospheric pressure before it can be observed.

3.1 CO_2:mixture flow ratio

The appropriate CO_2:mixture mass flow ratio is predicted by considering a control volume including the ICT and the flash-freezing nozzle. The inputs to this control volume are liquid CO_2 and mixture and the outputs are gaseous CO_2 and frozen powder, which is comprised of CO_2 hydrates and a concentrated, non-crystalline aqueous phase. The flow ratio is calculated by balancing the cooling required to freeze and carbonate the mixture with the cooling provided by the CO_2 that flashes from liquid to vapor. The overall CO_2:mixture ratio is the sum of the ratio required for freezing the mixture and the additional CO_2 that is trapped in CO_2 hydrates. This calculation provides a first estimate of the optimum flow ratio. The necessary flow ratio may be larger due to heat losses to the surroundings, but excess CO_2 can result in dry ice when the ICT is vented, so the flow ratio should not be increased without reason.

The cooling provided by the CO_2 that flashes is the difference between the specific enthalpy of liquid CO_2 at the emulsion chamber pressure and temperature and the specific enthalpy of gaseous CO_2 at the vent pressure and temperature. For the batch flash-freezing

apparatus described in section 1.3, the pressure and temperature in the emulsion chamber are 283 K and 50 bars and at the vent are 233 K and 10 bars. For these values, the change in specific enthalpy of CO_2 is $\Delta H_{CO2} = 211.1$ kJ/kg CO_2.

The cooling required to freeze the mixture can be calculated by determining the difference between the enthalpy of the mixture entering the emulsion chamber and the enthalpy of the frozen powder. The change from liquid mixture to carbonated frozen powder can be expressed in the overall reaction,

$$(u+n)H_2O(aq) + CO_2(l) \Leftrightarrow CO_2 \cdot nH_2O(s) + uH_2O(aq) \quad \Delta H_{tot}\text{=-79.9 kJ/(u+n)mol } H_2O$$

where H_2O(aq) represents the ingredients mixture, *u* represents the water that ultimately remains unfrozen, *n* represents the water that ultimately becomes CO_2 hydrates and ΔH_{tot} is the change in enthalpy per mole of water in the mixture. Calculation of ΔH_{tot} will be discussed in detail shortly. The temperature and pressure of the reactants correspond to the temperature and pressure in the emulsion chamber, 283 K and 50 bars. The temperature and pressure of the products correspond to the ICT conditions, 233 K and 10 bars. The overall reaction above gives the enthalpy change per mole of H_2O in the mixture. The heat release on a mixture mass basis, ΔH_{mix}, can be calculated from this value according to

$$\Delta H_{mix} = \frac{\Delta H_{tot}}{(u+n) * M_{H_2O}} * (1 - TS),$$

where M_{H_2O} is the molecular weight of water, 0.018 kg/mol, and TS is the total solids fraction of the mixture on a mass basis, which can range from 0 to 0.5. Using the above equation for ΔH_{mix}, the heat release on a mixture mass basis is 445.6 kJ/kg mixture for a 15% total solids mixture. This is more than double the specific heat absorbed by CO_2 evaporation.

While the exact process of CO_2 hydrate formation and concentration of the aqueous solution is not known, the change in enthalpy of the overall reaction, ΔH_{tot} is calculated by considering the reactions:

(i) separation of the mixture into pure water and a concentrated aqueous solution

$$(u+n)H_2O(aq, T_{EC}, P_{EC}) \Leftrightarrow nH_2O(l) + uH_2O(aq) \qquad \Delta H = \sim 0 \text{ kJ/(u+n)mol}_{H2O}$$

(ii) cooling and depressurizing pure water to the freezing temperature and pressure

$$nH_2O(l, T_{EC}, P_{EC}) \Leftrightarrow nH_2O(l, T_f, P_f) \qquad \Delta H = -7.04 \text{ kJ/(n)mol}$$

(iii) cooling and depressurizing CO_2 to the freezing temperature and pressure

$$CO_2(l, T_{EC}, P_{EC}) \Leftrightarrow CO_2(g, T_f, P_f) \qquad \Delta H = 10.9 \text{ kJ/mol}_{CO2}$$

(iv) crystallization of water as CO_2 hydrate

$$nH_2O(l, T_f, P_f) + CO_2(g) \Leftrightarrow CO_2 \cdot nH_2O(s) \qquad \Delta H = -64.5 \text{ kJ/mol}_{hydrate}$$

(v) cooling the CO_2 hydrate to the ICT temperature

$$CO_2 \cdot nH_2O(s, T_f, P_f) \Leftrightarrow CO_2 \cdot nH_2O(s, T_P, P_P) \qquad \Delta H = -12.84 \text{ kJ/mol}_{hydrate}$$

(vi) cooling the concentrated aqueous solution to the ICT temperature

$$uH_2O(aq, T_{EC}, P_{EC}) \Leftrightarrow uH_2O(aq, T_P, P_P) \qquad \Delta H = -5.9 \text{ kJ/(u)mol}_{H2O}.$$

The subscripts EC, f, and P refer to conditions in the emulsion chamber, at CO_2 hydrate formation, and in the final product respectively. In the set of reactions above, the temperature

and pressure indicated for the first reactant apply to the entire reaction unless otherwise indicated. The number of moles of water per CO_2 molecule in the CO_2 hydrates, n, can vary between 5.75 and 7.67 because CO_2 hydrates are non-stoichiometric. For these calculations, it is assumed that n=6.8, T_f=270.2 K and P_f=10 bar based on correlations by Anderson (2003).

The change in enthalpy is shown to the right of each reaction listed above. The enthalpy of separating the mixture into pure water and concentrated unfrozen solution is set to zero, the value for an ideal solution. The actual enthalpy of (un)mixing is not known, but should be small relative to the latent heat of CO_2 and water phase changes. The enthalpy to cool n moles of water to the CO_2 hydrate formation conditions is found in the National Institute of Standards and Technologies (NIST) Standard Reference Database (Lemmon et al., 2009). The enthalpy to convert CO_2 from a liquid at the emulsion chamber conditions to a gas at the hydrate formation temperature is also found in the NIST Database. The enthalpy of CO_2 hydrate formation is found in Anderson (2003). Anderson calculated the enthalpy of CO_2 hydrate formation along the CO_2 hydrate-aqueous solution and CO_2 hydrate-ice equilibrium curves. The enthalpy change to cool CO_2 hydrate from the formation temperature to the product temperature is calculated based on the specific heat capacity of structure I hydrates given by Sloan and Koh (2008), 2.08 kJ/kgK (0.324 kJ/molK). The effect of change in pressure is neglected. The concentration of the aqueous solution containing u moles of H_2O varies with the product temperature and the mixture recipe. When aqueous solutions of sugar water are cooled, water freezes out as pure ice, leaving behind an increasingly concentrated aqueous phase. To reach the theoretical limit of maximum freeze concentration, careful annealing processes are typically required (Roos & Karel, 1991). For simplicity in the flow ratio calculation, it is estimated that 80% of the water content in the mixture can come out of solution to freeze. In this case u can be calculated as $u = n\frac{1-f}{f} = 0.25n$, where f represents the fraction of water in the mixture that crystallizes. The change in enthalpy to cool this highly concentrated mixture from the emulsion chamber temperature to the product temperature is not known, but is again estimated using the specific heat capacity of water, neglecting the effect of pressure. The specific heat capacity of water at 273 K is 0.076 kJ/mol (Lemmon et al., 2009).

The additional CO_2 required to fill the cages in CO_2 hydrates is calculated by again considering the fraction of water in the mixture that ultimately freezes. The mass of CO_2 required per kilogram of mixture, A, is given by

$$\mathrm{A} = \frac{(1-\mathrm{TS})*f}{M_{H_2O}*n} * M_{CO_2},$$

where M_{CO_2} represents the molecular weight of CO_2, 0.044 kg/mol. This is the fraction of CO_2 that would need to be replenished in a continuous cycle implementation of the CO_2 flash-freezing process.

The total CO_2:mixture mass flow ratio can then be calculated as the sum of the CO_2:mixture ratio for freezing, which is given by the ratio of ΔH_{mix} to ΔH_{CO2} and the mass of CO_2 trapped per kilogram of mixture, A. Thus the total mass flow ratio is

$$\frac{\dot{m}_{CO_2}}{\dot{m}_{mixture}} = \frac{\Delta H_{mix}}{\Delta H_{CO_2}} + A.$$

Using the above parameters the mass flow ratio for a 15% total solids mixture is 2.35; the ratio for balancing the latent and sensible heat exchange is 2.1 and the ratio for filling CO_2

hydrates is 0.25. In the batch implementation of the CO_2 flash-freezing process the flow ratio is typically 3.0-3.6. The ratio implemented in the batch apparatus is larger than the calculated ratio due to some combination of heat losses in the system, underestimation of the heat capacity of the concentrated aqueous solution and underestimation of the fraction of water that crystallizes.

The energy required to generate the surface area of the powder is not included in the flow ratio balance. While the surface area of the powder product is much greater than the surface area of the mixture entering the emulsion chamber, the energy required to generate that surface is not significant relative to the flow ratio calculated above. The energy to form the powder surface is estimated using the particle size and an appropriate surface tension. Based on microscopy, the powder particles have a size distribution that varies over a range from 10 μm to 100 μm. Considering a kilogram of mixture with a density 1000 kg/m^3, the surface area of the mixture if broken into 10 μm spherical droplets is 600 m^2. The surface energy of an ice-air interface is 0.106 J/m^2 (Pruppacher & Klett, 1997). The energy required for formation of the particle surface is 0.063 kJ/kg mixture, which is much less than the 445.6 kJ/kg mixture cooling required for the 15% total solid mixture considered above. The volume increase of CO_2 hydrate relative to liquid water is less than 25% so it is not included in this estimate. The surface energy of CO_2 hydrate interfacing with gas is not known, but should be similar to the surface energy of ice. The actual surface area of the powder could be much larger due to many crystalline facets, but the equivalent droplet size would have to decrease to 0.01 μm for the surface energy to exceed one-tenth the latent heat exchanged assuming bulk phases.

The above flow ratio calculations assume that the powder product temperature is equal to the vapor-liquid CO_2 saturation temperature at ICT pressure and that CO_2 hydrate is the only crystalline phase formed. Decreasing the flow ratio decreases the cooling provided by evaporating CO_2. This reduction in available cooling can result in a warmer product and or ice forming in place of CO_2 hydrate. For small decreases in flow ratio, it is likely that the product temperature increases and ice does not replace CO_2 hydrate because crystallization occurs before the powder is cooled to its final temperature. As an example, product at 253 K (-20°C) could be desirable to parallel conventional ice cream processes. The decreased ratio is calculated by changing the product temperature (T_P) from 233 K to 253 K in reactions (v) and (vi) above. The ratio required for 253 K powder decreases from 2.35 to 2.1 for the assumptions and mixture parameters applied in the original calculation. Achieving this change would require very fine control of the flow ratio.

Increasing the flow ratio will not produce a colder powder because the minimum temperature is tied to the vapor-liquid saturation temperature of CO_2 at the ICT pressure. Extra CO_2 may increase break up of the mixture, but excess CO_2 is undesirable because it will collect as liquid CO_2 in the ICT. In a continuous process the liquid CO_2 would need to be separated from the powder, re-pressurized to the emulsion chamber pressure and returned to the CO_2 supply line. In a batch process when the ICT is vented to atmospheric pressure, some of the liquid CO_2 would evaporate, causing some of the remaining liquid CO_2 to solidify. Dry ice in the powder can result in an excessive CO_2 content, which can be unpleasant to eat and dangerous if allowed to sublimate in a sealed container without adequate pressure relief.

It is also possible for liquid CO_2 to collect in the ICT if some of the mixture freezes as ice instead of CO_2 hydrates despite a sufficient CO_2 flow ratio for CO_2 hydrate formation. For example, this could happen when a large droplet of mixture freezes from the surface inward.

Due to the high concentration of CO_2 surrounding the droplet, the water at the surface would crystallize as CO_2 hydrate. As the thickness of the frozen shell increases, CO_2 must be transported through the CO_2 hydrate shell to reach the inner volume of the droplet. If the droplet is cooled more rapidly than CO_2 reaches the inner volume, ice will form instead of CO_2 hydrate in the inner volume. The latent heat of CO_2 hydrate crystallization from water is about 60% larger than the latent heat of ice crystallization from water. Therefore less heat would be released in crystallization of water to ice than to CO_2 hydrate, so more CO_2 would remain liquid until the ICT is vented.

In summary, the optimum CO_2:mixture flow ratio depends on the specific CO_2 flash freezing equipment. The flow ratio can be calculated by matching the change in enthalpy of CO_2 to the latent heat of CO_2 hydrate formation and sensible heat of cooling the mixture to ICT temperature. The water content of the mixture has the largest effect on the flow ratio because the latent heat of crystallization of water is large and the additional CO_2 needed to fill CO_2 hydrate cages is proportional to the amount of water that crystallizes. The flow ratio is typically between two and three because the latent heat of CO_2 hydrate crystallization is approximately double the latent heat of CO_2 evaporation. The optimum flow ratio can be found empirically during operation of CO_2 flash-freezing equipment by increasing the flow ratio from two until the temperature in the ICT just reaches a steady state value equal to the CO_2 vapor-liquid saturation temperature at ICT pressure.

3.2 Quiescent CO_2 hydrate formation

Quiescent formation of CO_2 hydrate refers to formation of CO_2 hydrate from ice particles in a pressurized CO_2 environment without agitation or high flow rates. In this environment convective heat and mass transfer are negligible. It was thought that quiescent formation of CO_2 hydrates might be relevant to the CO_2 flash-freezing process because during batch processing the mixture particles reside in the ICT for three to eight minutes. However it will be shown in this section that this residence time is too short for significant quiescent formation of CO_2 hydrates in the ICT. Therefore CO_2 hydrates must be formed directly from mixture during flash freezing, rather than in a two-step process of flash freezing to an intermediate ice phase and then forming CO_2 hydrates quiescently while the powder sits in the ICT. Quiescent conversion of ice to CO_2 hydrate is also relevant to formation of CO_2 hydrates during storage of flash-freezing powder. For example, if CO_2 hydrates are not present in the frozen confection at the time of packaging (due to either insufficient operating parameters or dissociation during the packaging process), they can be formed during storage, but the time required to carbonate the frozen confection depends on the quiescent conversion rate. Finally, studying quiescent formation of CO_2 hydrates emphasizes the importance of specific surface area and mass transport in CO_2 hydrate formation, as well as the thermodynamic driving force for formation.

Quiescent conversion of ice to CO_2 hydrate proceeds in several steps. CO_2 hydrates initially nucleate at cracks and defects in the ice at the surface of a particle (Genov et al., 2004). A thin CO_2 hydrate layer, about 2 μm thick, spreads across the exposed ice surface (Genov et al., 2004). This surface-covering step takes several hours on 40-60 μm particles at 253-263 K and 10 bars (Genov et al., 2004), and should be slower at the cooler temperature in the ICT. The CO_2 hydrate shell then thickens and the ice core of the particle shrinks as H_2O

migrates to the particle surface and CO_2 reaches the ice-CO_2 hydrate interface. The microstructure of CO_2 hydrates commonly includes patches of 10-20% porosity with 20-100 nm pores (Genov et al., 2004). In CO_2 hydrate layers more than a few micrometers thick, the pores are closed and filled with CO_2 gas (Kuhs et al., 2006). In a non-porous hydrate, the water density is 796 kg/m^3 (Sloan & Koh, 2008), about 13% lower than the density of ice. Because the density of H_2O in CO_2 hydrates is lower than in ice the particles expand with CO_2 hydrate formation. In packed beds of particles this expansion progressively increases particle-particle contact and fills in the void space between particles, reducing the surface area exposed to CO_2 gas. The conversion rate slows significantly after surface coverage due to the reduction of surface area and the increasingly thick CO_2 hydrate layer through which CO_2 and H_2O must pass to reach the growing interfaces.

Several researchers have measured ice to CO_2 hydrate conversion rates. Their methods and models will be described briefly here and roughly compared at 238 K, 10 bar, near ICT conditions. Henning et al. (2000) pressurized crushed ice particles smaller than 250 μm in liquid CO_2 at 900 psi (62 bar) and 230, 243, 253 or 263 K. Henning et al. showed that a model for diffusion controlled conversion provided a good fit to the data at conversion fractions greater than 20%, with the diffusion coefficient having Arrhenius-type temperature dependence. Henning's model did not incorporate the experimental pressure because it is significantly higher than the CO_2 hydrate dissociation pressure at 230-263 K (2-7 bars). Based on Henning's measurements and model, at 238 K the fraction of ice converted after 20 hours at 62 bars would approach 48% in the <250 μm crushed ice particles. The conversion rate would surely be slower at ICT pressure, with vapor rather than liquid phase CO_2.

Takeya et al. (2000) measured CO_2 hydrate formation in ice spheres with an average diameter of 150 μm at 9.8 bars and 238, 244, 255, 262.5 and 269 K. Takeya et al. developed a model for the conversion rate with two stages, a surface nucleation and coverage stage, which lasts several hours, followed by a diffusion-limited stage. The rate in each stage decreased with Arrhenius-type temperature dependence and increased with the difference between experimental pressure and CO_2 hydrate dissociation pressure at the experimental temperature, which is related to the thermodynamic driving force for CO_2 hydrate formation. Unfortunately Takeya's conversion rate model involves a combination of CO_2 hydrate volume and integrated intensity of x-ray diffraction units, so it is difficult to apply their results to ICT conditions. As the integrated intensity count is proportional to the volume of CO_2 hydrate crystal present, their data indicate that at conditions of 238 to 255 K and 9.8 bars pressure about 18% conversion has occurred after 20 hours. The fraction converted at 238 K and 10 bars should be similar.

Finally, Genov et al. (2004) measured CO_2 hydrate formation in ice spheres with a mean diameter of 54 μm at several temperature and pressure combinations including 253 and 263 K and 10 bars. Genov et al. developed a model for the rate of conversion of ice to CO_2 hydrate based on the particle size, CO_2 fugacity, CO_2 fugacity at the CO_2 hydrate dissociation pressure, and fitted rate parameters for three stages of the conversion reaction – surface covering, reaction-limited and diffusion-limited CO_2 hydrate growth. Surprisingly, in Genov's experiments, slightly more ice is converted to CO_2 hydrate at 253 K and 10 bars than at 263 K and 10 bars after 20 hrs (35% and 33% respectively). Genov et al. suggest that this is due to the increased thermodynamic driving force having a stronger effect than the decreased diffusion rate at 253 K. However, in this case, CO_2 hydrate formation at 253 K should slow relative to CO_2 hydrate formation at 263 K as the conversion process progresses

into the diffusion-limited regime, which does not appear to be the case in Genov's data (see Genov, figure 6). The model for conversion rate is sensitive to the parameter δ_0, the thickness of the initial layer of ice converted to CO_2 hydrate. This suggests that Genov's model is able to fit the measured data well through the flexibility of multiple fitted parameters. Genov's model predicts, with an average value for δ_0 of 2 μm, that the estimated fraction of ice converted after 20 hours in 54 μm spheres at 238 K and 10 bars is 25%.

As can be seen in the models presented above, thermodynamic driving force and diffusion rate are important parameters in the ice to CO_2 hydrate conversion rate. The higher the thermodynamic driving force the higher the CO_2 hydrate nucleation rate, and growth rate if mass transfer or heat transfer at the site of the phase growth are not limiting. The thermodynamic driving force for formation of CO_2 hydrate is the difference in chemical potential between CO_2 and H_2O in their initial phases (aqueous solution or ice with CO_2 liquid or vapor) and the chemical potential of the CO_2 hydrate. Kashchiev and Firoozabadi (2002) developed expressions for the driving force as a function of the difference between operating pressure and dissociation pressure at a fixed temperature or the difference between operating temperature and dissociation temperature at a fixed pressure. The driving force increases with increases in either of these pressure or temperature differences. The thermodynamic driving force in the experiment by Genov et al. (2004) at 253 K and 10 bars is approximately half the driving force in the ICT because the temperature difference is half as large.

The diffusion rates of CO_2 and H_2O in CO_2 hydrate are strong functions of temperature. Demurov et al. (2002) showed in molecular dynamics simulations that CO_2 molecules only move into an adjacent empty cage if there is also a water vacancy in the CO_2 hydrate lattice between the cages. Thus the CO_2 diffusion rate is a function of the concentration of water vacancies, the concentration of CO_2 vacancies, and the free energy barrier, which determines the CO_2 molecule hopping-rate. Demurov et al. calculated 10^{-12} m^2/s for the diffusivity of CO_2 in CO_2 hydrates at 273 K. This diffusivity model is supported experimentally in the work of Radhakrishnan et al. (2003). Based on Demurov's model for the decrease in hopping rate and water vacancy concentration with temperature, the estimated CO_2 diffusivity at 238 K is 10^{-16} m^2/s. Using this value, the characteristic diffusion length in 20 hours is 6 μm. The fraction of ice converted to CO_2 hydrate in 54 μm spheres would approach 47% in 20 hours. This is larger than predicted based on the model of Genov et al.

In most cases growth of a CO_2 hydrate phase is mass transfer limited rather than heat transfer limited because heat can be conducted away from the site of CO_2 hydrate formation more rapidly than heat can be evolved by CO_2 hydrate formation with the available CO_2. A dimensionless ratio of the rate of heat evolved due to incorporation of CO_2 into the growing CO_2 hydrate phase and heat flow through the CO_2 hydrate layer by conduction is developed here to support the argument that CO_2 hydrate formation from ice particles is typically mass transfer limited. Figure 3-1 shows a 1-D geometry for a CO_2 hydrate layer growing at the interface between ice and CO_2 gas. As shown in the figure, there is a CO_2 concentration gradient and a temperature gradient in the CO_2 hydrate layer. These gradients provide the driving forces for heat and mass transfer between the gas phase and the CO_2 hydrate-ice interface. CO_2 hydrate formation occurs at a temperature T_{HI}, which is the ice-CO_2 hydrate equilibrium temperature at the pressure of the system. For the sake of simplicity, it is assumed that the temperature of the ice is equal to T_{HI} throughout the conversion. It is also assumed that the concentration of CO_2 in ice in equilibrium with CO_2 hydrate is negligibly

small. These uniform temperatures and concentrations in the ice guarantee that there is essentially no heat or CO_2 flux through the ice phase.

The heat flow caused by CO_2 diffusion and incorporation at the CO_2 hydrate-ice interface is given by the product of the CO_2 flow rate through the CO_2 hydrate layer and the latent heat released by conversion of ice to CO_2 hydrate per mole of CO_2. The CO_2 flow rate at the CO_2 hydrate-ice interface is equal to the product of the CO_2 diffusivity in CO_2 hydrate, D, and the concentration gradient at the ice-CO_2 hydrate interface. The concentration gradient is estimated as the change in molar density of CO_2 across the CO_2 hydrate layer divided by the thickness of the layer, l. The latent heat released by conversion of ice to CO_2 hydrate is ΔH_{HI}, in Joules per mole CO_2. The heat generation in a given cross-sectional area associated with CO_2 arriving at the CO_2 hydrate-ice interface, $\dot{Q}_{CO_2}$, is then

$$\dot{Q}_{CO_2} = \Delta H_{HI} D \frac{(c_{HI} - c_{HG})}{l} A_c, \tag{3.1}$$

where c_{HI} is the molar density of CO_2 in CO_2 hydrate at the CO_2 hydrate-ice interface, c_{HG} is the molar density of CO_2 in CO_2 hydrate at the CO_2 hydrate-gas interface, and A_c is the cross-sectional area.

Heat flows through the CO_2 hydrate layer according to

$$\dot{Q}_{thermal} = h_{eff} A_c (T_{HI} - T_G), \tag{3.2}$$

where h_{eff} is the effective heat transfer coefficient, A_c is the cross-sectional area, T_{HI} is the temperature at the CO_2 hydrate-ice interface and T_G is the temperature in the gas phase. The effective heat transfer coefficient is found by considering conduction through the CO_2 hydrate layer and natural convection to the gas at the CO_2 hydrate-gas interface. Thus, h_{eff} is given by

$$h_{eff} = \left(\frac{1}{h_c} + \frac{l}{k_H} \right)^{-1},$$

where k_H is the thermal conductivity of CO_2 hydrate, l is the thickness of the CO_2 hydrate layer, and h_c is the convective heat transfer coefficient.

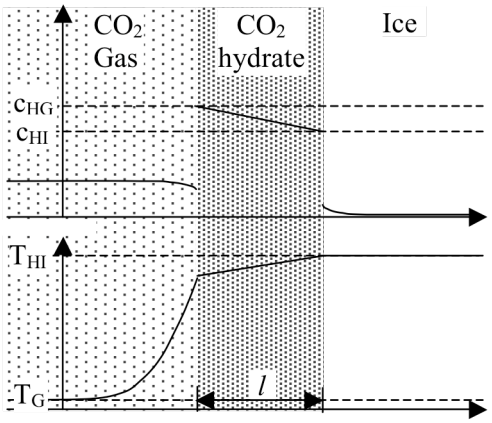

Figure 3-1 Geometry and temperature and concentration profiles for heat and mass flux comparison in conversion of ice to CO_2 hydrate. c_{HG}-CO_2 concentration in CO_2 hydrate at gas interface, c_{HI}-CO_2 concentration in CO_2 hydrate at ice interface, l-thickness of CO_2 hydrate layer, T_{HI}-temperature of CO_2 hydrate formation, T_G-temperature of ambient gas.

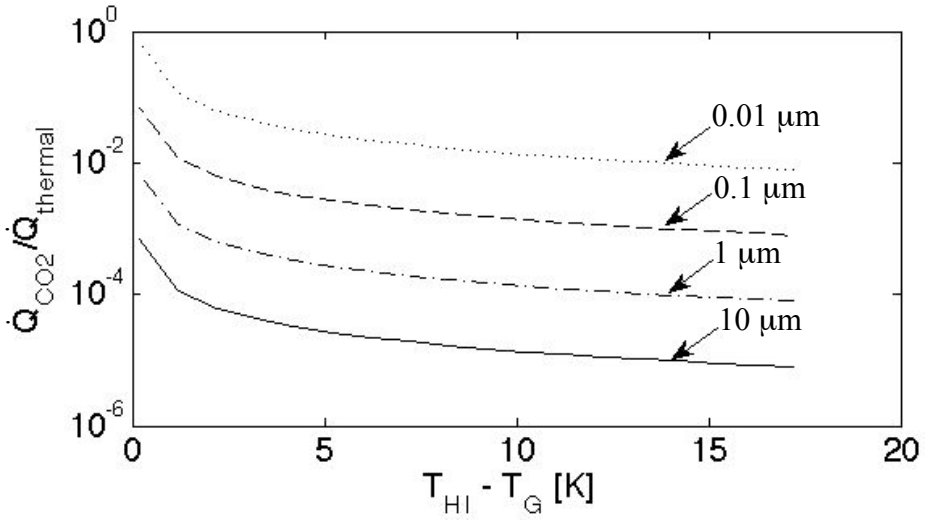

Figure 3-2 Ratio of heat flow rate due to CO_2 flow rate to heat flow rate by conduction through the growing CO_2 hydrate layer for a simple 1-D model of ice to CO_2 hydrate conversion

The ratio of heat generation to heat flow out of the CO_2 hydrate layer in equations 3.1 and 3.2 is then

$$\frac{\dot{Q}_{CO_2}}{\dot{Q}_{thermal}} = \frac{\Delta H_{HI} D(c_{HI} - c_{HG})}{h_{eff}(T_{HI} - T_G)l} . \tag{3.3}$$

The value of this ratio is plotted in Figure 3-2 for a range of temperature differences, (T_{HI}-T_G), and for several CO_2 hydrate layer thicknesses, l. It can be seen in the figure that for the dimensions of physical systems typically encountered, the ratio is less than one, and decreases rapidly with increasing CO_2 hydrate layer thickness. The ratio also decreases as the difference between the CO_2 hydrate formation temperature and the gas temperature increases (i.e. in a system at a fixed pressure, the ratio decreases as the gas temperature decreases). The parameters used in Eq. 3.3 are: ΔH_{HI} = -23.77 kJ/mol CO_2 (Anderson, 2003); D =10^{-16} m^2/s (Demurov et al., 2002); and T_{HI} = 270.2 K, which corresponds to CO_2 hydrate formation at 10 bars. For each layer thickness, h_{eff} is calculated using k_H = 0.5 W/m-K for the thermal conductivity of CO_2 hydrate (Sloan & Koh, 2008) and a low convection coefficient of h_c = 5 W/m^2K. The molar density of CO_2 in CO_2 hydrate cannot be greater than the concentration of filling all of the CO_2 hydrate cage sites (7687 mol/m^3) and cannot be smaller than the concentration of filling on average 5 of the cage sites per unit cell (4805 mol/m^3), which is the critical concentration below which the structure will collapse (Teng et al., 1996). For this calculation it is assumed that c_{HI} is 4805 mol/m^3 and c_{HG} is 7687 mol/m^3. The typical concentration in CO_2 hydrates is smaller (6727 mol/m^3) because the small cages in CO_2 hydrates are only filled at high pressure, so the heat flow ratio may be even smaller than calculated here. As can be seen in the figure, even for a 1 μm thick CO_2 hydrate layer the ratio in Eq. 3.3 is several orders of magnitude less than one, so the conversion process becomes strongly mass transfer limited after only a thin layer of CO_2 hydrate is formed.

In real systems, the heat conducted from the CO_2 hydrate-ice interface into the solid (both the CO_2 hydrate layer and the unconverted ice) is equal to the heat evolved at the interface by CO_2 hydrate formation. Thus, in reality the ratio of $\dot{Q}_{CO_2}$ and $\dot{Q}_{thermal}$ is 1.

Because the conversion process is strongly mass transfer limited, the ice initially at T_{HI} will cool toward T_G with temperature profiles similar to the transient temperature profiles in a semi-infinite body cooled by convection at its surface. The growth of the CO_2 hydrate layer will provide a small heat source at the moving ice-CO_2 hydrate interface, but this heat evolution will not disturb the temperature profile significantly. The CO_2 hydrate layer will grow at a rate controlled by the diffusion of CO_2 regardless of the cooling of the ice.

The PTM apparatus, described in chapter 1 of this thesis, was used to measure the quiescent rate of CO_2 hydrate formation in CO_2 flash-freezing powder and frozen spheres (average diameter 75 μm) at 238 K and 10 bars. These experiments provide information about CO_2 hydrate formation from ice that is specific to the ICT and flash-freezing powder geometry. The experiments with frozen spheres provide a useful comparison between flash-freezing powder and powder with a controlled, known geometry. The frozen spheres also enable comparison of CO_2 hydrate formation rates in ice and samples with a highly viscous, but non-crystalline aqueous phase.

For the powder experiments, powder was formed from water or 20% sucrose mixture using the CO_2 flash-freezer. The powder was placed in the PTM sample can with the storage freezer set to 238 K (-35°C). The bulk density of the powder varied between experiments. The density of the powder produced from water was 90 kg/m^3, while the density of the 20% sucrose powder was 150 kg/m^3. The sample can was loosely covered and the mass was monitored at atmospheric pressure for 3-5 hours while the CO_2 originally in the powder escaped. The mass of the sample asymptotically approached a constant value at which point most of the CO_2 originally in the sample had escaped. Then the PTM apparatus was sealed, flushed with CO_2 and pressurized to 10 bars. The mass of the sample was monitored as CO_2 hydrates re-formed in the powder.

For the frozen sphere experiments, frozen spheres were produced by spraying water or 20% sucrose mixture into liquid N_2 using the mixture nozzle from the CO_2 flash-freezer. The liquid nitrogen and frozen spheres were then poured through a stack of sieves and the spheres in the smallest fraction were collected in the PTM sample can. Twenty-one grams of frozen spheres were used for each experiment to ensure that the length scales for bulk heat and mass transfer were equal. The diameter of the frozen spheres was estimated by comparing some of the frozen spheres to wires of known diameter on a liquid N_2-cooled surface using an optical microscope. The PTM apparatus was sealed and pressurized to a CO_2 pressure of 10 bars. The mass of the sample was monitored as ice was converted to CO_2 hydrate.

Figure 3-3 shows the relative mass of the water and 20% sucrose powder during the experiment. Here, the relative mass is defined as the mass of water and CO_2 in the sample divided the by the mass of water in the sample. The mass of sucrose is not included in the normalization. At the start of the measurement the relative mass of the water powder (Figure 3-3a) is 1.2. Over a period of 3.5 hours the relative mass of the powder decreases because the sample is at atmospheric pressure in the freezer and CO_2 hydrates are dissociating. The large spikes at hour three indicate the time when the SS upper cap of the PTM is placed over the sample, but not sealed. Just before hour four the PTM is sealed and pressurized to 10 bars, which causes the relative mass of the sample to increase as CO_2 hydrates form. After six more hours the relative mass of the sample has almost returned to its initial mass. The plot for the sucrose-solution powder (Figure 3-3b) is similar. The initial relative mass of the sample is 1.25, and the mass decreases due to CO_2 hydrate dissociation over a period of 5 hours. The SS upper cap of the PTM is placed over the sample just after hour three and the sample is

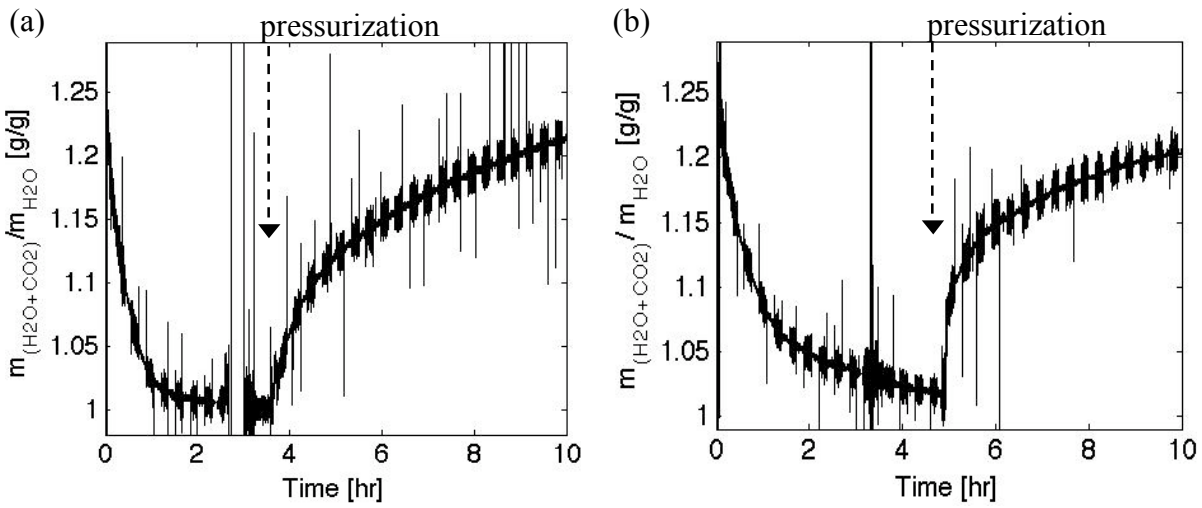

Figure 3-3 CO_2 release and absorption in CO_2 flash-freezing powder as a function of time, (a) pure water "mixture", (b) 20% sucrose mixture. Absorption is plotted as mass of CO_2 and water relative to the water content of the sample.

pressurized at hour five. After five hours, the relative mass of the sample has not reached its initial value.

In Figure 3-3a and b, the high frequency oscillations are due to the freezer compressor. The data is noisier while the compressor is on due to increased vibrations. The large, individual spikes in the data correspond to the compressor turning on and off. There is a gap in Figure 3-3a at hour three because the data acquisition system was accidentally turned off.

As can be seen in the figure, it takes at least three hours for the powder to lose its initial CO_2 content and even longer to reabsorb the same amount of CO_2 (by CO_2 hydrate formation) in the 10 bar CO_2 atmosphere. In Figure 3-3b it can be seen that the relative mass in the 20% sucrose powder did not decrease to a constant value before it was pressurized; this means that not all of the initial CO_2 hydrates were dissociated. The pre-existing CO_2 hydrates may explain the faster initial relative mass increase in the sucrose sample compared to the water sample. Overall, both CO_2 release and absorption appear to be slower in the 20% sucrose mixture compared to the water mixture. The slower kinetics may be associated with the higher bulk density of the sucrose-solution powder, and sintering of the powder due to increased contact between particles and increased water mobility in the aqueous phase. These effects would slow CO_2 transport through the void space between the particles. The powder geometry should not differ significantly between the samples because the mixture viscosities and densities are similar and therefore the hydrodynamics during flash freezing should be similar.

Figure 3-4 shows the absorption of CO_2 in ice spheres and sucrose mixture spheres that were made using the process involving liquid N_2 described above. The PTM is pressurized with CO_2 at time t=0 and the relative mass of each sample begins to increase immediately. The rates of mass increase in the ice and sucrose-solution spheres are essentially equivalent to each other, but significantly slower than the rates of mass increase in the flash-freezing powder. Figure 3-5 shows the comparison of mass increase rate in powder and spherical particles. In Figure 3-4 and Figure 3-5 the individual spikes and apparent large scatter are again due to vibrations when the freezer compressor turns on or off.

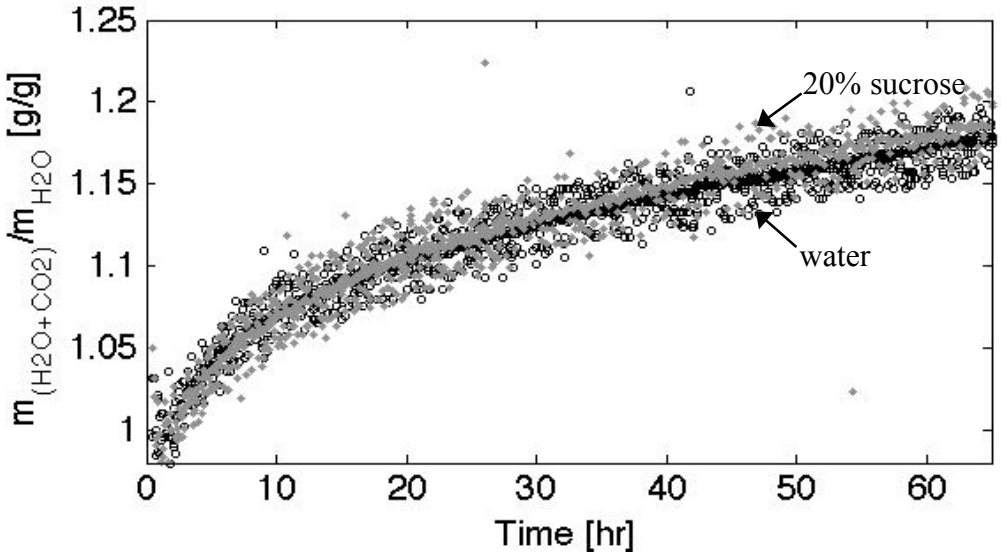

Figure 3-4 CO_2 absorption in 75 μm spheres of ice and sucrose solution at 238 K, 10 bar.

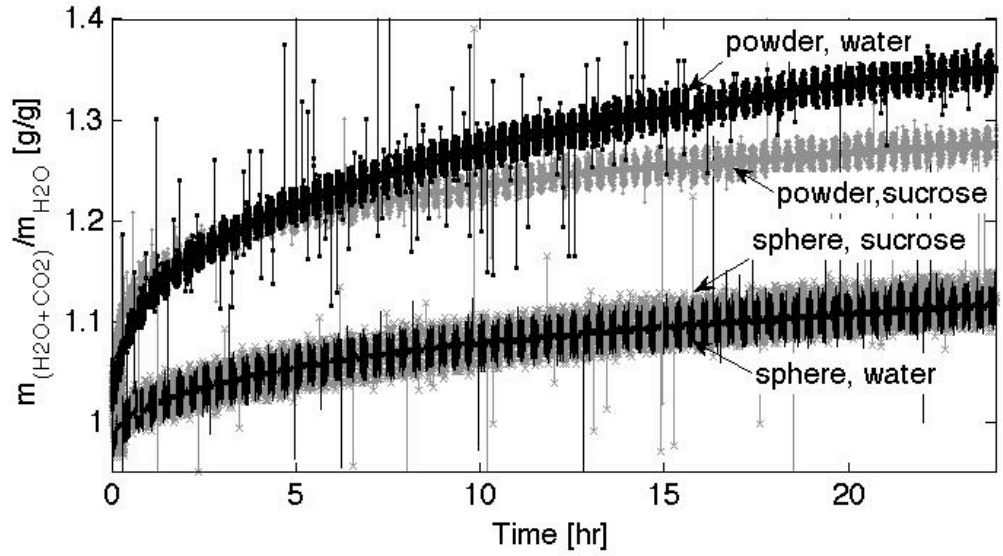

Figure 3-5 Comparison of CO_2 absorption in flash-freezing powder and 75 μm spheres.

The time scale shown in Figure 3-5, 24 hours, is much longer than shown in Figure 3-3 and shorter than shown in Figure 3-4. On this time scale the powder samples approach full CO_2 saturation. The maximum relative mass the water powder can reach is 1.37 to 1.42 (assuming 7 to 8 cages are filled per unit cell). The maximum relative mass for the 20% sucrose mixture powder is 1.35 to 1.4 (for 7 to 8 cages filled per unit cell) because at 238 K the concentrated aqueous phase should approach 80% solids, so in every gram of water, 0.0625 g of water must be in the aqueous phase with 0.25 grams of sucrose. The relative mass increase in the first several hours in the powder is significantly faster than in the spheres. The rate of mass increase in the water powder continues to be faster than in the other samples.

Based on the experiments with flash-freezing powder, CO_2 hydrates must be formed during CO_2 flashing rather than during the subsequent residence time in the ICT. In Figure 3-3, the initial relative mass of the powder (1.2 in Figure 3-3a and 1.25 in Figure 3-3b)

indicates the minimum CO_2 hydrate fraction present at the end of the batch process (54% of the water is CO_2 hydrate in the ice powder and 67% of the water is CO_2 hydrate in the sucrose-solution powder). The actual initial CO_2 hydrate fraction is probably higher because some CO_2 hydrates dissociate while the powder is transferred from the batch freezer to the PTM sample can. Nevertheless, the residence time in the ICT is less than one-eighth the time required for CO_2 hydrate dissociation in Figure 3-3. The batch process lasts three to eight minutes; only a very small fraction of CO_2 hydrate could be formed from icy powder in the ICT. The slow CO_2 hydrate re-formation is striking because there is no nucleation delay and the powder is likely to be porous as a result of prior CO_2 hydrate dissociation.

Based on the equivalent rate of CO_2 absorption in frozen water and 20% sucrose spheres, the presence of sucrose does not affect the rate of CO_2 hydrate formation. The rapid freezing of the particles in liquid N_2 prevents formation of a sucrose rich layer on the particle surface (Hindmarsh et al., 2007). Therefore the concentrated aqueous phase is intermingled with ice crystals, but does not provide a rapid transport route for CO_2. CO_2 diffusion through the glassy concentrated aqueous phase or along the phase boundary must not be significantly faster than CO_2 diffusion through CO_2 hydrates. Assuming that all dissolved sugars behave similarly and do not affect the rate of CO_2 hydrate formation, the fraction of CO_2 hydrate formed in flash-freezing powder should not vary significantly with recipe. This conjecture may not be true for higher total solids mixtures because the concentrated aqueous phase is likely to be non-equilibrium, containing excess water and therefore having greater mobility.

The rate of CO_2 absorption in the flash-freezing powder is significantly faster than in 75 μm spheres. This indicates that the specific surface area of the flash-freezing powder must be much larger than the specific surface area of the spheres. In addition, the fact that CO_2 saturation is approached in the powder suggests that the powder has at least one characteristic dimension that is very thin. This thin dimension limits the thickness of the CO_2 hydrate layer that CO_2 must diffuse through to complete the conversion process.

The relative mass of the frozen water spheres approaches 1.18 after 20 hours. This corresponds at least 42% of the initial ice converted to CO_2 hydrate. This extent of CO_2 hydrate formation is high compared to Genov's measurement for smaller particles (25% for 54 μm particles), an estimate based on Genov's model (20% for 75 μm particles), an estimate based on Takeya's measurements (36% for 75 μm particles) and an estimate of the extent of formation based on Demurov's model for diffusivity (33% for 75 μm particles based on a 5 μm CO_2 hydrate layer). It is not clear why this is true. It is likely that the particles were smaller than estimated using the microscope or there was a significant fines fraction. It is unlikely that cracks or pores changed the results because the spheres in Genov's and Takeya's experiments were also created by freezing droplets in liquid N_2.

The conclusion that quiescent CO_2 hydrate formation is not fast enough to occur in the ICT is not changed even if the particle core is in a metastable liquid state. Slow mass transport through the CO_2 hydrate shell would still hinder the CO_2 hydrate formation process. This conclusion is supported by the work of Moudrakovski et al. (2004). Moudrakovski et al. used H^1 NMR imaging at 275 K, 58 bars to observe the conversion rate of 180-210 μm water particles. CO_2 hydrate shells were formed on liquid water droplets by holding ice particles in a CO_2 atmosphere below 273 K and then raising the temperature to melt the ice in the core. The average conversion rate over all of the particles was slow; only 50% conversion in 14 hrs estimated from figure 5 of Moudrakovski's paper. Moudrakovski et al. observed significant variation in formation rate between particles, with some particles converting completely and

others showing no conversion over the same time frame. Surprisingly, Moudrakovski also observed CO_2 hydrate formation in the bulk of the particle, rather than growth propagating from the hydrate shell. The conversion rate of mixture droplets with CO_2 hydrate shells residing in the ICT after flashing could be even slower because mobility is reduced at the cooler temperature, the thermodynamic driving force is lower and the CO_2 density surrounding the particles is lower.

The quiescent CO_2 hydrate formation rates indicated in Figure 3-3 thru Figure 3-5 demonstrate that it would be possible to make a carbonated frozen confection without using the CO_2 flash freezing process. It would be necessary to produce frozen particles with a large specific surface area and store these particles in a high pressure CO_2 environment for almost a day to achieve large conversion fractions. At an industrial scale, this method is likely to be expensive due to the large volume, high-pressure chamber required.

The rate of quiescent CO_2 hydrate formation from frozen solution may be higher if the freeze-concentrated aqueous phase does not become glassy. This liquid phase would provide channels for faster CO_2 transport into the frozen particle. Gas diffusion in liquids is several orders of magnitude faster than in solids. An example of this possibility comes from experimental work by Bobev and Tait (2004) with up to 20 volume percent aqueous methanol solutions. Frozen deuterated water-methanol particles less than 300 μm in diameter were almost completely converted to CO_2 hydrate in several minutes at 250 K, 170 bar. The eutectic point of the water-methanol system is only reached at 156 K (-117°C) (Takaizumi & Wakabayashi, 1997), so the concentrated aqueous phase should still provide high mobility at 250 K. Ethanol-water solutions reach a eutectic point as well, 149 K, (-124°C) (Takaizumi & Wakabayashi, 1997), rather than becoming glassy. It would be interesting to test CO_2 absorption in spheres made from frozen aqueous ethanol solution, to see if there is a similar increase in conversion rate and confirm that the increased conversion rate is not specific to molecules involving deuterium.

The study of quiescent CO_2 hydrate formation presented in this section has an implication for the design of CO_2 flash-freezing apparatus. In a continuous process, the volume of the expansion chamber that replaces the ICT is not constrained by a required powder residence time in a 10 bar CO_2 atmosphere. The expansion chamber probably only needs to be designed to accommodate the spray cone formed at the flash-freezing nozzle orifice.

In this section it has been shown that the quiescent conversion rate of ice to CO_2 hydrate is a strong function of particle size, temperature and pressure. Based on the conversion rate of ice to CO_2 hydrates at the pressure and temperature in the ICT, it has been confirmed that quiescent conversion is not the CO_2 hydrate formation mechanism dominant in the CO_2 flash freezing process. Also, the presence of a glassy, non-crystalline aqueous phase in a frozen mixture does not significantly improve the rate of conversion of ice to CO_2 hydrate. During flash freezing, processes including droplet break-up, convective mass transfer, boiling heat transfer, and CO_2 hydrate nucleation due to CO_2 supersaturation and mixture sub-cooling assist in CO_2 hydrate formation.

3.3 CO_2 hydrate formation by flash-freezing

In section 3.2 it was demonstrated that conversion of ice particles to CO_2 hydrate is too slow to carbonate the frozen confection during residence in the ICT. Therefore, CO_2 hydrates must form directly from the liquid mixture during the flashing process. CO_2 transport to crystallization sites must keep up with heat removal from the mixture in order to avoid ice formation. In this section it will be shown that nearly complete CO_2 hydrate formation can be achieved during flash freezing because CO_2 hydrate crystallizes from liquid phase sub-cooled mixture and the atomization process generates significant mixture surface area. Most importantly, the ICT pressure is high enough to cause CO_2 hydrate nucleation and growth in the mixture before it is cooled to ICT temperature.

The liquid CO_2-mixture emulsion is atomized by the combined actions of the nozzle and flashing CO_2. The flash-freezing nozzle is a pressure-swirl type oil burner nozzle (Delavan Spray Technologies), shown schematically in Figure 3-6. In the nozzle the working fluid is accelerated into a swirling flow through four tangential slots (only two are shown in the figure). The radial pressure decrease due to the angular velocity of the fluid causes a vapor column to form along the axis of the nozzle. The fluid is further accelerated as it progresses through the swirl chamber due to the decreasing cross-sectional area and radius. At the orifice, the high velocity annulus of liquid spreads into a hollow cone and droplets break off. For an inviscid, incompressible fluid, the thickness of the liquid annulus at the nozzle exit can be estimated based on the correlation for the vapor core area as a function of mass flow rate, $\frac{dm}{dt}$, and over all pressure drop, ΔP,

$$\frac{dm}{dt} = \left[\frac{(1-X)^3}{1+X}\right]^{0.5} A_o\sqrt{2\rho\Delta P}\,, \tag{3.4}$$

where X is the ratio of the vapor core area to the orifice area, A_o is the orifice area, and ρ is the liquid density (Fritsching, 2006). The corresponding thickness of the liquid annulus, t, is

$$t = \frac{d_o}{2}(1-\sqrt{X})\,, \tag{3.5}$$

where d_o is the diameter of the orifice.

In the CO_2 flash-freezing process, the cross-sectional area of the vapor column is affected by the elevated pressure at the nozzle exit and vaporization of a portion of the emulsion. Moon et al. (2007) showed that a flash-boiling fluid does not destroy the vapor core in a pressure-swirl nozzle, but the thickness of the liquid annulus decreases and the pressure in the vapor core increases. Some of the saturated liquid evaporates at the vapor core interface. There should be no metastability at the interface because the saturated liquid is in direct contact with vapor, but evaporation at the vapor column interface cools and therefore stabilizes the surrounding liquid. Ibrahim and Jog (2007) showed that the thickness of the liquid annulus increases with increasing pressure at the nozzle outlet because the vapor density increases, which increases the inertia of the vapor core, slowing the fluid rotation. The effects of partial evaporation of CO_2 and elevated pressure in the ICT are in opposition. Since these effects may cancel each other and the continuous phase of the emulsion (liquid CO_2) has a very low viscosity, the correlation for inviscid, incompressible fluids given above may provide a reasonable estimate of the vapor core area at the nozzle orifice.

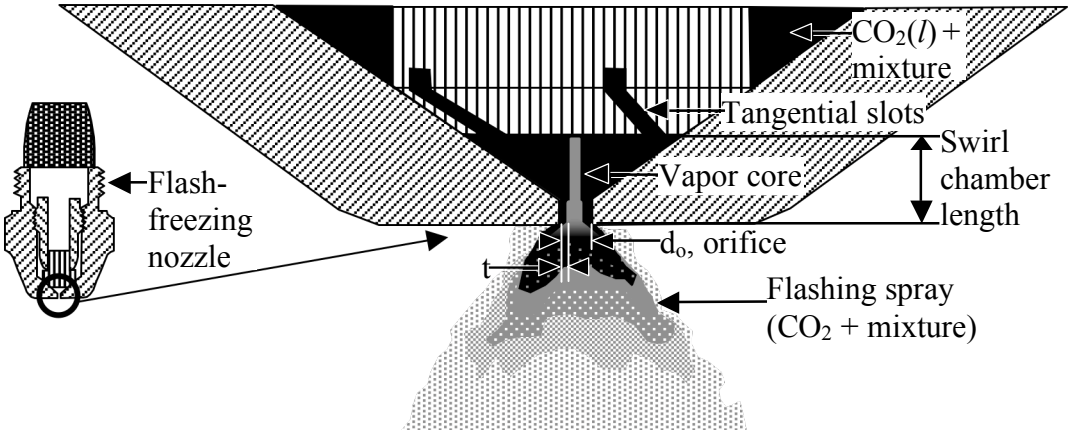

Figure 3-6 Schematic detail of nozzle swirl chamber in flash-freezing nozzle.

Flashing of superheated fluids also causes atomization. When imaging flashing fuel atomization, Vanderwege and Hochgreb (1998) and Vieira and Simões-Moreira (2007) observed metastable liquid fuel at the nozzle followed immediately by breakup into a spray cone. At the nozzle orifice the refrigerant temperature drops immediately to the saturation temperature (Vu et al., 2008) as a fraction of the refrigerant flashes and cools the remaining liquid to the saturation temperature. Increasing the superheat of the flashing fluid decreases the final droplet size (Vu et al., 2008). The superheat is the difference between the temperature of the refrigerant or fuel in the nozzle and the saturation temperature at ambient pressure. The critical superheat or expansion pressure ratio for vigorous flashing depends on the properties of the refrigerant and the jet velocity (Kitamura et al., 1986). Vieira and Simões-Moreira correlated break up of a flashing iso-octane jet to the expansion pressure ratio. For expansion pressure ratios of 5 to 10 the jets were partially shattered by vigorous evaporation, leading to a cloud of liquid droplets. At higher pressure ratios compressible flow phenomena including choking and shock waves were observed. Vu et al. measured a droplet diameter on the order of 10 μm for R-134a flashing with a pressure ratio of 6 and inlet velocity of 50 m/s. Both the elevated ICT pressure and the flashing fluid cause the metastable liquid hollow cone to break up close to the nozzle orifice. As expected, Moon et al. (2007) and Chang and Lee (2005) found that the droplet size in flashing pressure-swirl spray is smaller than in non-flashing pressure-swirl spray.

In work on a process called Carbon-dioxide Assisted Nebulization with a Bubble Dryer (CAN-BD) (Huang et al. 2003), Huang et al. demonstrated that flashing an emulsion of CO_2 and aqueous solution does lead to small aqueous solution particles as well as small CO_2 droplets. Huang et al. mixed supercritical CO_2 and an aqueous solution in a low dead volume tee and then expanded the fluid into an atmospheric pressure dryer through a 100 μm diameter, 9.5 cm long capillary tube. The residence time of the combined fluids in the tee and capillary tube is approximately 0.01s, which is not enough time for significant CO_2 dissolution, but during flashing the aqueous solution is still effectively nebulized into particles less than 3 μm in diameter. Huang et al. showed that increasing the CO_2:aqueous solution ratio decreases the particle size. In CAN-BD the CO_2:aqueous solution volume flow ratio is about ten and the pressure drop is 80 bars. The flow ratio and pressure drop are significantly higher than in the CO_2 flash freezer, and the capillary tube orifice is smaller, but CAN-BD demonstrates that aqueous solutions can be atomized by CO_2 expansion and the atomization does not require saturating an aqueous solution with dissolved CO_2 before flashing.

Bubble formation can also atomize a fluid when a dissolved gas becomes supersaturated due a rapid pressure drop, but this mechanism requires a significant fraction of dissolved gas. Zhang et al. (2005) and Huang et al. (1994) studied atomization of fuels with dissolved methane and CO_2 in simple tube-shaped nozzles with length/diameter ratios of 5-50. Zhang observed spray formation at methane concentrations greater than 21.3 mL_{STP}/mL fuel, and reduced atomization with increasing fuel viscosity. Huang observed that larger length/diameter ratios improved spray atomization because the gas could separate from the fuel in the length of the simple nozzle.

There are correlations to estimate the droplet size generated by pressure-swirl nozzles based on the fluid viscosity, density, flow rate, pressure drop and gas density. It is not clear that these correlations are applicable in the case of the CO_2-mixture emulsion because CO_2 is evaporating, the viscosity of liquid CO_2 is significantly lower than the viscosity of the mixture, and the surface tension of liquid CO_2 is significantly lower than the mixture surface tension. Nonetheless, the following correlation can be used to estimate the order of magnitude of the mixture droplet size and the liquid CO_2 droplet size

$$SMD = 4.52\left(\frac{\sigma\mu_l^2}{\rho_g \Delta P^2}\right)^{0.25}\left(t\cos\theta\right)^{0.25} + 0.39\left(\frac{\sigma\rho_l}{\rho_g \Delta P}\right)^{0.25}\left(t\cos\theta\right)^{0.75}, \quad (3.6)$$

where *SMD* is the diameter corresponding to the average surface area to volume ratio of the droplets (Sauter mean diameter), σ is the fluid surface tension, μ is the viscosity, ρ is the density, t is the thickness of the annulus at the orifice, θ is the cone angle at the orifice and ΔP is the pressure drop across the nozzle (Lefebvre, 1989).

Freezing of aqueous solution droplets proceeds through several steps: liquid cooling, nucleation, recalescence, completion of freezing, and tempering (Hindmarsh et al., 2007, 2004, 2003). During liquid cooling, droplets are super-cooled to a temperature lower than the freezing temperature of water without nucleation occurring. The nucleation temperature is typically 253 K for sucrose concentrations 0-40% and freezing rates 1-20 K/min (Hindmarsh et al., 2003 and Zasypkin & Lee, 1999) unless a nucleating agent such as silver iodide is added. Even when a 20% sucrose solution droplet is frozen by submersion in liquid nitrogen the estimated nucleation temperature is still near 253 K (Hindmarsh et al., 2007). After nucleation, the temperature rises rapidly to the ice crystallization temperature during recalescence. The fraction of water crystallized can be estimated by the heat capacity of the subcooled liquid relative to the latent heat released by ice crystallization. Approximately 25% of a pure water droplet supercooled to 253 K crystallizes during recalescence. Sucrose decreases the rate of recalescence and the temperature reached during recalescence (Hindmarsh et al., 2004). After recalescence the remainder of the water is crystallized. In a pure water droplet, the remainder of the water is crystallized at the water freezing temperature (273 K) and after all crystallization is completed the droplet is cooled to the ambient temperature. In a droplet with sucrose the freezing point continually decreases due to freeze concentration of the aqueous phase, so the recalescence period, the freezing period and the subsequent tempering to the ambient temperature overlap.

Both gas hydrate and ice can nucleate if a droplet is frozen under pressure. Davies et al. (2009) studied gas hydrate and ice nucleation in 40 mg water drops (approximately 4 mm in diameter) using differential scanning calorimetry. Depending on the pressure while the droplet is cooled, either gas hydrate or ice can nucleate first with the other crystalline structure nucleating at a colder temperature. In the experiments of Davies et al., ice

nucleation occurred between 257 and 259 K regardless of gas pressure. Methane and xenon hydrate nucleation occurred at approximately 30 K super-cooling if gas hydrate nucleated before ice (i.e. 30 K super-cooling was reached before reaching the ice nucleation point at 259 K). At lower pressures ice nucleated first and then gas hydrate nucleated with less than 30 K super-cooling. Regardless of gas pressure the majority of the droplet crystallized as ice; only the surface crystallized as gas hydrate. While nucleation is system dependent, the work of Davies et al. indicates that nucleation of one crystalline structure does not preclude nucleation of the other structure and the fraction of gas hydrate formed depends strongly on availability of the gas at the site of crystallization.

In the CO_2 flash-freezing process the flow velocity, droplet size and freezing temperature can be estimated using the above information. Figure 3-7 shows the progress of a mixture particle during flash freezing. The CO_2-mixture emulsion enters the flash-freezing nozzle as a slightly sub-cooled liquid at 283 K and 50 bars. It is assumed that the mixture droplets are dispersed in a continuous liquid CO_2 phase. The volume ratio is approximately 3 volumes CO_2 to 1 volume mixture. The estimated initial mixture droplet diameter is 150 μm (see section 2.1 for an estimate of this dimension) and may decrease when the emulsion passes through the 125 μm mesh filter as it enters the flash-freezing nozzle.

The CO_2-mixture emulsion then passes through the tangential slots of the pressure-swirl nozzle (see Figure 3-6). Both the width (approximately 300 μm) and the depth (approximately 900 μm) of the tangential slots are more than double the estimated droplet diameter (125 μm). Since the tangential slots are larger than the mixture droplets and the pressure drop along the slots is small, the emulsion is expected to remain essentially unaltered as it passes through the slots. To estimate the pressure drop along the slots, the fluid velocity is needed. Using mass

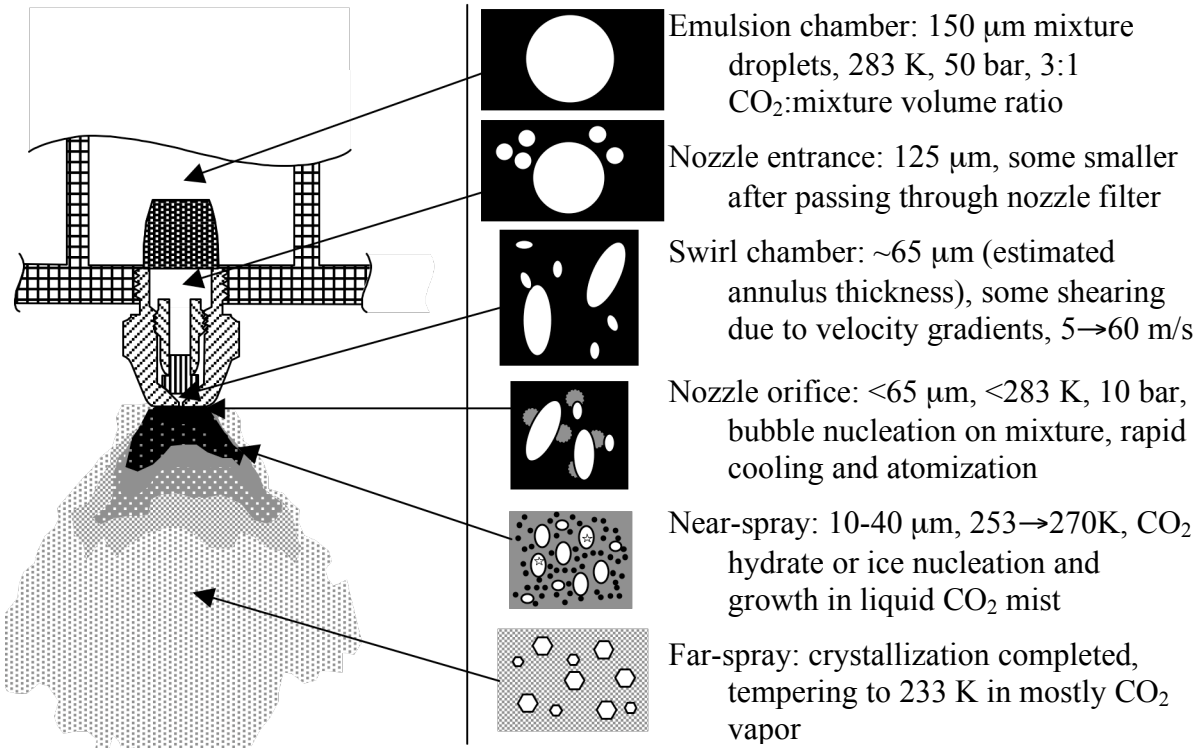

Figure 3-7 Schematic history of mixture particle during flash freezing. Mixture-white, liquid CO_2-black, gaseous CO_2-gray.

conservation, the average fluid velocity in the slots, v_{avg}, can be estimated using the cross-sectional area of the slots and the mass flow rates of CO_2, $\dot{m}_{CO2}$, and mixture, $\dot{m}_{mixture}$, using standard pipe flow methods,

$$v_{avg} = \frac{1}{4w \cdot d}\left(\frac{\dot{m}_{CO_2}}{\rho_{CO_2}} + \frac{\dot{m}_{mixture}}{\rho_{mixture}}\right),$$

where w is the slot width, d is the slot depth, and ρ_{CO_2} and $\rho_{mixture}$ are the density of liquid CO_2 and the mixture at the emulsion chamber temperature and pressure (283 K and 50 bars). The factor of 4 in the denominator accounts for the four tangential slots in the nozzle. The typical flow rates in the batch flash-freezing apparatus are 1 g mixture/s and 3 g CO_2/s. With a CO_2 density of 832 kg/m^3 and mixture density of 1100 kg/m^3, the resulting average velocity in the tangential slots is then 4.2 m/s. The pressure drop, ΔP, is calculated according to

$$\Delta P = K\frac{1}{2}\rho_{avg} v_{avg}^2 + f\frac{L}{d_h}\frac{1}{2}\rho_{avg} v_{avg}^2,$$

where K is the loss coefficient associated with a sharp pipe entrance (K=0.5 (White, 1999)), ρ_{avg} is the mass averaged density of the emulsion (899 kg/m^3), f is the friction coefficient, L is the length of the slot (2.5 mm), and d_h is the hydraulic diameter of the slot (450 μm). The friction coefficient is estimated using the Reynolds number of the flow based on the viscosity of liquid CO_2, giving f = 0.025. The resulting pressure drop is 0.05 bar. With this small pressure drop, liquid CO_2 is not expected to evaporate in the nozzle channels.

In the swirl chamber of the nozzle the mixture droplets may experience further shearing. The pressure drop across the flash-freezing nozzle is 40 bars. Based on the correlation for an inviscid, incompressible fluid (Eq. 3.4) the vapor core should take up 55% of the 500 μm diameter nozzle orifice. The corresponding thickness of the liquid emulsion annulus at the pressure-swirl nozzle orifice (Eq. 3.5) is then 65 μm. Thus the estimated thickness of the emulsion annulus is slightly more than half the estimated mixture droplet size entering the swirl chamber and it is likely that the droplets are sheared into elongated shapes and or broken apart. The estimated thickness of the emulsion annulus at the nozzle orifice also provides a rough indication of the largest particle size expected in the powder.

The majority of mixture atomization occurs immediately after the fluids pass through the nozzle orifice. Mixture droplet surfaces are likely bubble nucleation sites for CO_2 gas. After nucleating, the bubbles should expand rapidly, breaking apart the mixture. Based on the work of Vieira et al. and Vu et al. the annulus of mixture-liquid CO_2 emulsion should shatter into fine droplets at the nozzle orifice. The order of magnitude of the droplets due to CO_2 flashing is estimated to be 10 μm because Vu et al. observed 10 μm droplets formed by R-134a flashing at a pressure ratio of 6; the pressure ratio used across the flash-freezing nozzle in this work is 5. In addition to breakup due to flashing, mixture is broken up due to the pressure-swirl nozzle. The estimated average droplet size based on the (*SMD)* correlation for pressure-swirl nozzles is 3 μm for CO_2 and 15 μm for the mixture, using the density, viscosity and surface tension of each fluid respectively. Atomization by bubble formation in the mixture droplets is not likely to be significant because the maximum volume of gas in the mixture before flashing is too small. The maximum concentration of CO_2 that could be dissolved in the emulsion (0.068 g CO_2/g solution, as presented in section 2.1) corresponds to a volume fraction of 2.7 mL/mL mixture (the volume of CO_2 bubbles is calculated at 10 bar, 233 K) when the mixture reaches the ICT. This volume fraction is only 10% of the minimum volume fraction required in Zhang's experiments. In summary for atomization of the emulsion, the

mixture and CO_2 are broken up into tens of micrometers droplets by the combined action of aerodynamic forces and CO_2 flashing.

The mixture droplets initially cool concurrently with the flashing CO_2 because the heat capacity of the mixture relative to the enthalpy of vaporization of CO_2 is very small and CO_2 evaporation occurs in direct contact with the mixture droplets. The specific enthalpy of the saturated CO_2 increases due to heat transfer from the mixture, increasing the fraction of CO_2 that flashes compared to an ideal constant enthalpy expansion of pure CO_2. In an isenthalpic expansion 38% of the CO_2 would flash when the pressure falls from 50 to 10 bars with no mixture present. If 1 g of mixture is present for every 3 g of CO_2 and the mixture is super-cooled to 253 K during flashing, but does not crystallize, 50% of the CO_2 would be vapor at the end of flashing. At the start of crystallization it is likely that the 10-40 μm mixture droplets are falling in CO_2 mist.

The mixture temperature should diverge from the vapor-liquid CO_2 saturation curve by the time nucleation of crystallized water begins, therefore all of the crystallization occurs at the ICT pressure. The nucleation temperature is not known. Based on the work of Davies et al. and Hindmarsh et al. it could be 253-259 K, however, if the mixture has been saturated with CO_2 in the emulsion chamber, CO_2 hydrate nucleation could be induced with a smaller super-cooling. Once nucleation occurs, the rapid formation of the CO_2 hydrate and the rejection of the large heat of formation to the remaining liquid should quickly warm the droplet to the equilibrium crystallization temperature at which the remaining liquid crystallizes. If the mixture is super-cooled to 253 K and then CO_2 hydrate nucleates, the droplet would warm towards the CO_2 hydrate dissociation temperature at 10 bars, which is 270.5 K. In a pure water droplet, only 13% of the water would be crystallized as CO_2 hydrate during recalescence (compared to 25% for ice formation), due to the higher latent heat of CO_2 hydrate formation compared to ice.

The maximum droplet freezing time can be estimated by considering a droplet of mixture falling at terminal velocity through a CO_2 gas environment at 10 bars and 233 K. The droplet reaches terminal velocity when the drag force balances the action of gravity on the droplet (accounting for the buoyancy force due to CO_2 gas displaced by the droplet). The terminal velocity of the droplet, v_{term}, is given by

$$v_{term} = \sqrt{\frac{\left(\rho_d - \rho_{CO_2}\right)Vg}{C_D A_c \frac{1}{2}\rho_{CO_2}}},$$

where ρ_d is the density of the droplet, ρ_{CO_2} is the density of the CO_2 gas environment, V is the volume of the droplet, g is gravitational acceleration, C_D is the drag coefficient, and A_c is the cross-sectional area of the droplet. For this estimate, C_D is calculated according to the Stoke's flow drag coefficient, namely 24/Re, where Re is the Reynolds number involving the droplet diameter, the gas properties and v_{term}. The heat transfer coefficient is then calculated according to the correlation for the Nusselt number, Nu, of a falling liquid droplet,

$$Nu = \frac{h \cdot d}{k_{CO_2}} = 2 + 0.6\,\mathrm{Pr}^{1/3}\,\mathrm{Re}^{1/2},$$

where h is the heat transfer coefficient, d is the diameter of the droplet, k_{CO2} is the thermal conductivity of the gas, and Pr is the Prandtl number of the gas (Incropera & DeWitt, 1999). Using this heat transfer coefficient, the rate of heat removal from the droplet, $\dot{Q}_{conv}$, is

$$\dot{Q}_{conv} = hA_s(T_d - T_{CO_2}), \tag{3.7}$$

where A_s is the surface area of the droplet, T_d is the freezing temperature, and T_{CO2} is the temperature of the gas. The amount of heat that must be removed from the droplet to freeze all of the water, Q_{freeze}, is

$$Q_{freeze} = \rho_d V \Delta H_{HW}, \tag{3.8}$$

where ΔH_{HW} is the latent heat of formation of CO_2 hydrate from liquid water per kilogram of water. The maximum time to freeze is then given by dividing equation 3.8 by equation 3.7,

$$t = \frac{Q_{freeze}}{\dot{Q}_{conv}}. \tag{3.9}$$

Typical properties for this calculation are ρ_d=1000 kg/m^3, ρ_{CO_2}=26 kg/m^3, k_{CO2}=0.013 W/mK, Pr=9.8x10^{-4}, T_d=270 K, T_{CO2}=233 K, and ΔH_{HW}=529 kJ/kg. For droplet diameters in the range 10 μm to 65 μm the maximum freezing time varies from 0.01 s to 0.35 s. The actual droplet freezing time should be shorter because boiling heat transfer occurs for part of the flashing process and the initial velocity is higher than the terminal velocity of the droplet. Thus the freezing process is very rapid, leaving little time for CO_2 diffusion or convection into the mixture droplets.

With the current CO_2 flash-freezing apparatus it is not possible to measure the instantaneous CO_2 content of frozen powder or observe the particle size distribution during atomization and freezing. However, the CO_2 content of the powder at the end of a batch production has been measured and the final powder has been observed with an optical microscope. To measure the CO_2 content of the powder, the ICT is depressurized and opened, powder is transferred into the PTM sample can and the mass is monitored while CO_2 evolves. Once the mass reaches a steady value, the sample can is removed from the freezer in a plastic bag and allowed to melt at room temperature. The mass is again measured. The initial mass is the mass of CO_2 and mixture at the start of monitoring, while the final mass is the mass of only the mixture in the sample. The fraction of CO_2 hydrates formed in the powder is calculated assuming that all of the mass change is due to CO_2 release from CO_2 hydrates initially in the sample.

To observe the powder using an optical microscope, powder was transferred from the ICT into a chest-style freezer and then sprinkled onto a pre-cooled glass surface that forms the bottom of an optical view cell. A schematic of the view cell is shown in Figure 3-8. The view cell consists of two glass plates sandwiched in scaffolding made of aluminum plates that are held together and aligned by four bolts. After bolting the view cell together in the freezer, the view cell is mounted under the microscope. A fiber-optic light is used to illuminate the sample from below the view cell. The scaffolding rests on four cups of liquid nitrogen (approximately 200 mL each). The liquid nitrogen and the gas produced by its evaporation cool the view cell. A stream of dry nitrogen gas is used periodically to clear condensation from the glass surfaces. While the view cell is under the microscope, it warms slowly due to exposure to the ambient temperature environment. However, as long as the liquid nitrogen is replenished the powder sample can be kept from melting for at least an hour. Even without replenishing the liquid nitrogen there is typically frost on the top aluminum plate (which is the warmest because it is farthest from the cups of liquid nitrogen) for 15 minutes.

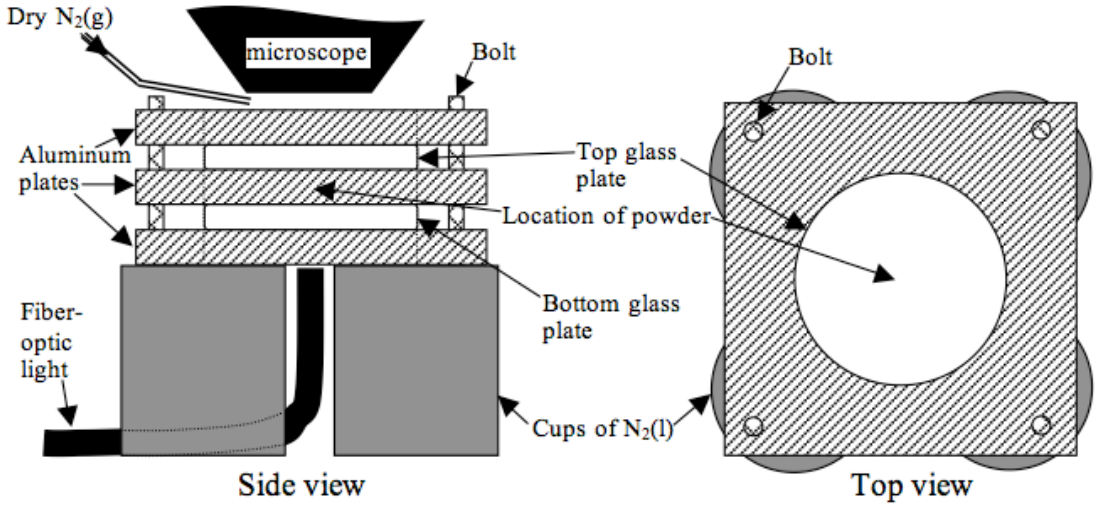

Figure 3-8 Schematic of optical view cell used to observe powder with a stereo-microscope. Powder is placed between two glass plates, which are held together by a bolted aluminum plates. A fiber-optic lamp illuminates the sample from below.

The measured CO_2 content in each trial varies from 12 to 25 % by weight, averaging about 18%. The maximum CO_2 content possible in a water sample is 29% by weight (8 cages filled per unit cell); it is more likely that on average 7 cages are filled per unit call, in which case the maximum CO_2 mass fraction of the sample would be 27%. The large variation in CO_2 concentration may be due to variations in production and transferring of the sample. In particular the powder is removed from the ICT and spooned into the sample can manually for each measurement. The time elapsed between depressurization and the start of mass monitoring can be 4 to 10 minutes. The measured CO_2 content of the sample powder is a lower bound on the initial CO_2 content because CO_2 hydrate dissociation proceeds exponentially with time; the most rapid CO_2 evolution occurs during the time that the powder is transferred to the PTM sample can. Despite the wide range of CO_2 content, these measurements indicate that greater than 80% of CO_2 hydrate formation can be achieved with the CO_2 flash-freezing process, and in most trials at least 37% percent of the maximum possible CO_2 hydrate formation is reached. This CO_2 hydrate content should be representative of the formation during flashing because further CO_2 hydrate formation during residence of the batch in the ICT is relatively small.

Images of the powder in the optical view cell described above are shown in Figure 3-9. The powder is non-spherical. There are individual polygonal particles with a characteristic breadth of 40 μm and large agglomerations with smaller polygonal crystals at the edges. The polygonal particles appear to be thinner in height than breadth. Water and 20% sucrose mixture powder look similar but the water mixture seems to produce more individual particles and slightly smaller particles. The temperature in the view cell is not known, but it is most likely between 243 K (the pre-cooled temperature of the glass) and 273 K, because the powder remains crystalline and a layer of condensation covers even the top of the aluminum scaffolding during the period of observation. However, this temperature is too warm for stable CO_2 hydrates at atmospheric pressure, so these particles may be CO_2 hydrates or more likely ice formed after dissociation of CO_2 hydrates.

The extremely angular powder particles, with some crystals approaching hexagons are surprising. This kind of well-formed morphology is typically seen in slow crystallization processes, whereas spray freezing typically leads to spherical particles. In some supercritical extraction processes particles are elongated or needle-shaped due to rapid freezing, but the edges are still rounded. Perhaps in Figure 3-9 the powder has already recrystallized to ice in a relatively slow process following the dissociation of the initial CO_2 hydrates. In this case the initial particle shape is unknown, but the particle dimensions may still reflect the particle size during crystallization. It would be helpful to collect powder immediately after flashing and plunge it into liquid nitrogen in order to observe powder that cannot have recrystallized.

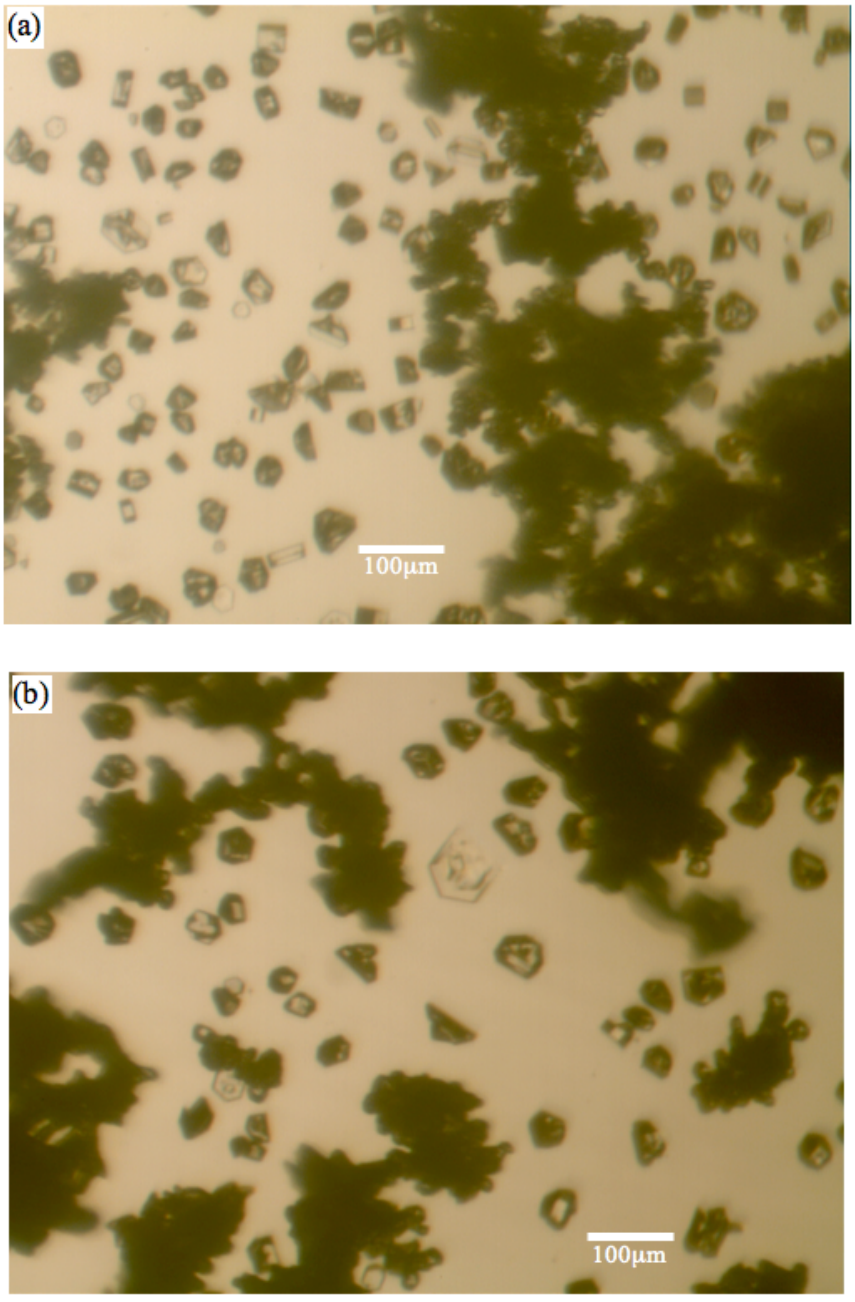

Figure 3-9 CO_2 flash-freezing powder. Mixture is a) water; b) 20wt% sucrose.

As reported above, the initial CO_2 concentration of the powder indicates that nearly complete CO_2 hydrate formation can occur during flash freezing. Thus, the atomization processes decrease the size of the mixture particles sufficiently for CO_2 hydrate formation throughout. If CO_2 hydrate only nucleates at one point on a mixture droplet, CO_2 can diffuse through the liquid droplet to the site of the growing CO_2 hydrate crystal. For CO_2 to diffuse through the droplet to the growing CO_2 hydrate crystal, the characteristic CO_2 diffusion length must be greater than the particle dimension. The characteristic diffusion length considered here is the length associated with the maximum freezing time calculated according to Eq. 3.9. The typical dimension of the mixture particles in Figure 3-9 is 10 to 40 μm. The maximum freezing times for 10 μm and 40 μm particles are 0.01 and 0.14 s respectively. The diffusivity of CO_2 in liquid water at 270 K is 9.2×10^{-10} m^2/s (Versteeg & van Swaall, 1988), giving a characteristic diffusion length of 6 μm for the 10 μm particles and 23 μm for the 40 μm particles. These characteristic diffusion lengths are smaller than the associated particle dimensions, however not all of the CO_2 diffusing through the liquid droplet has to travel the whole diameter of the droplet, so it should be possible for at least some CO_2 to reach a growing CO_2 hydrate crystal through the liquid body of the droplet.

It is also possible that CO_2 hydrate formation is enhanced by shedding of CO_2 hydrate crystals from the surface of liquid mixture particles while the particle velocities are highest (near the flash-freezing nozzle orifice). Yamasaki et al. (2000) studied the effect of hydrodynamics on CO_2 hydrate formation for liquid CO_2 injected against a flowing column of water. Yamasaki observed continuous shedding of a hydrate layer from large droplets, but formation of a stable spherical hydrate shell around small droplets. In two-fluid systems, the mode of droplet fragmentation can be correlated to the Weber number, a comparison of dynamic forces to the surface tension force, which is defined as $\rho_c(v_c-v_d)^2 d_d/\sigma_d$. The subscript c represents the continuous phase (gaseous CO_2) and d represents the dispersed phase (mixture-liquid CO_2 emulsion), ρ is density, v is velocity, d is diameter and σ is surface tension. Stripping of material from the periphery of the drop occurs for Weber number values between 50 and 100 (Kolev, 2007). An estimate of the Weber number of the flow at the flash-freezing nozzle orifice can be made using the estimated velocity and thickness of the fluid annulus at the orifice. The estimated thickness of the annulus is 65 μm according to equations 5.4 and 5.5. Neglecting CO_2 evaporation in the swirl chamber, the axial velocity of the emulsion in the annulus at the nozzle orifice is 51 m/s by conservation of mass. The rotational velocity of the emulsion in the annulus at the nozzle orifice can be estimated using conservation of angular momentum. The emulsion enters the swirl chamber at a radius of 2 mm with a velocity in the circumferential direction of 3.0 m/s and exits at a radius of 200 μm, giving a rotational velocity of 30 m/s at the orifice. Thus the estimated velocity of the emulsion at the flash-freezing nozzle orifice is 59 m/s. Using a CO_2 gas density of 26 kg/m^3, a surface tension of 0.109 N/m (corresponding to an ice-vapor interface) and the estimated velocity and sheet thickness, the Weber number is 54, so stripping fragmentation can occur close to the nozzle orifice.

If a CO_2 hydrate shell forms, CO_2 must be transported through the shell into the core of the droplet. The initial CO_2 hydrate surface layer is probably on the order of 1 μm thick (Peng, 2007), which is less than the 10-40 μm dimension of the mixture particles, but the shell may be porous. Porosity could assist in CO_2 transport into the droplet and may be enhanced by growth of CO_2 bubbles during freezing. Porosity has been observed both in gas hydrates produced in a laboratory and in gas hydrates found in nature, and seems to occur when there

is excess free gas present during formation (Kuhs et al., 2004). At steady state the CO_2 hydrate layer thickness between liquid CO_2 and water can approach tens of micrometers (Radhakrishnan et al., 2003; Ogasawara et al., 2001), which is similar to the size of the mixture particles.

It is unlikely that CO_2 is brought into the mixture droplet by internal convection. Despite the external gas velocity and boiling turbulence, internal convection is damped by partial crystallization and the high viscosity ratio between the mixture droplet and the CO_2 gas, as discussed in section 2.2.

It is possible that the large range of initial CO_2 contents in the flash-freezing powder reflects the competition between ice and CO_2 hydrate crystallization during flash freezing, rather than errors imposed by the measurement method. The ratio of ice to CO_2 hydrate formation could be sensitive to the specific ice and CO_2 hydrate nucleation details and the shape of the fluid mixture particle at the time of crystallization. Gas hydrate nucleation requires the random structuring of guest gas molecules in the water phase (Radhakrishnan & Trout, 2002). Many researchers have seen large variations in gas hydrate nucleation times without varying the experimental apparatus (Davies et al., 2009). In future work the initial CO_2 content of the powder should be measured for multiple repeated trials with fixed process parameters, possibly using in situ collection containers to reduce the exposure of the powder to the ambient environment. This would help confirm the cause of variation in measured initial CO_2 content.

Ice and CO_2 hydrate growth depend strongly on the ICT pressure. Figure 3-10 shows a hypothetical temperature and pressure history for a water droplet during freezing at two different ICT pressures. The zero on the time scale corresponds to the start of flashing and the end of the time scale is set at 1 second, which is longer than the estimated maximum time required to freeze droplets similar in size to the particles in Figure 3-9. As shown in the figure, at the nozzle orifice the pressure falls immediately to ICT pressure. The mixture is cooled rapidly until nucleation, which is assumed to occur at 259 K. After nucleation the droplet rapidly warms to the crystallization temperature due to the latent heat release throughout the droplet. In the 12 bar case CO_2 hydrates nucleate and then grow at 272 K, whereas in the 4.5 bar case ice nucleates and then grows at 273 K. In the case at 4.5 bars, CO_2 hydrates do not form because nucleation and crystallization occur outside of CO_2 hydrate stability range. While the actual nucleation temperature is not known, it is hypothesized that if the CO_2 hydrate formation temperature associated with the ICT pressure is colder than the sub-cooling at which ice nucleates, ice will nucleate before CO_2 hydrate and crystallization will proceed out of CO_2 hydrate stability range.

Figure 3-11 shows a 2D projection onto the P-T plane of the phase diagram for the CO_2-H_2O system; the CO_2 concentration axis has been collapsed. The phase diagram shows the vapor-liquid CO_2 saturation curve, the CO_2 hydrate equilibrium curve, and the ice and dry ice equilibrium curves. Both the ICT pressure and temperature and the CO_2 hydrate dissociation temperature at ICT pressure can be located on this diagram. The ICT pressure and temperature are located on the curve between the CO_2(l)+CO_2 hydrate region and the CO_2(g)+CO_2 hydrate region. The CO_2 hydrate dissociation temperature is located on the curve between the CO_2(g)+CO_2 hydrate region and the CO_2(g)+ice or aqueous region. It can be seen that the distance between these two curves changes with pressure and temperature. As discussed in section 3.2 the difference in pressure at a fixed temperature and the difference in temperature at a fixed pressure are related to the driving force for CO_2 hydrate formation.

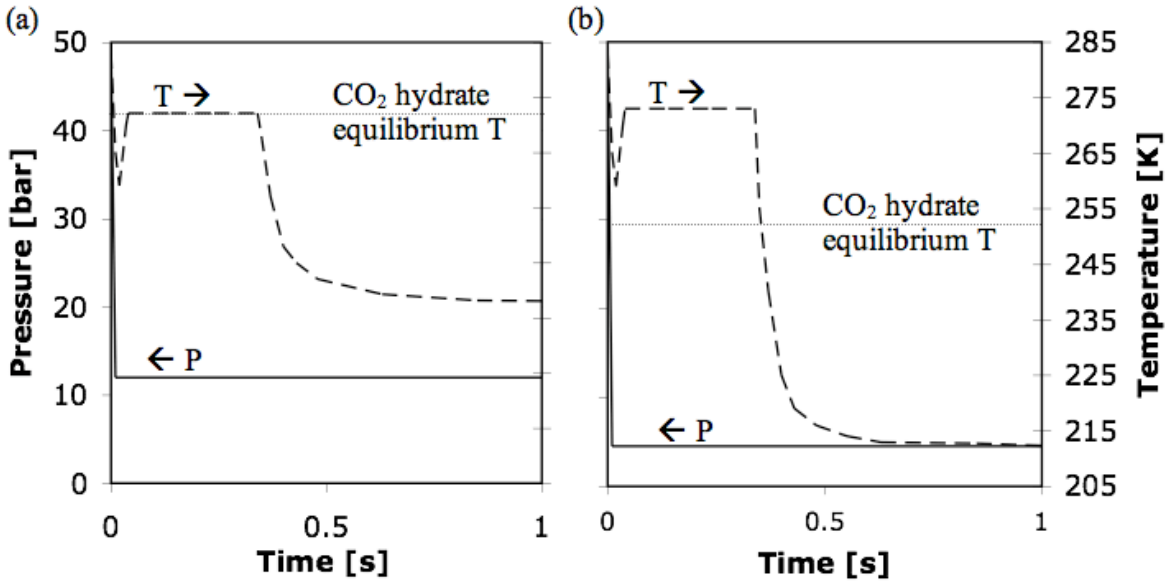

Figure 3-10 Hypothetical pressure (solid lines) and temperature (dashed lines) history in a water droplet during freezing, (a) 12 bars and (b) 4.5 bars ICT pressure. Dotted line represents maximum CO_2 hydrate formation temperature at ICT pressure.

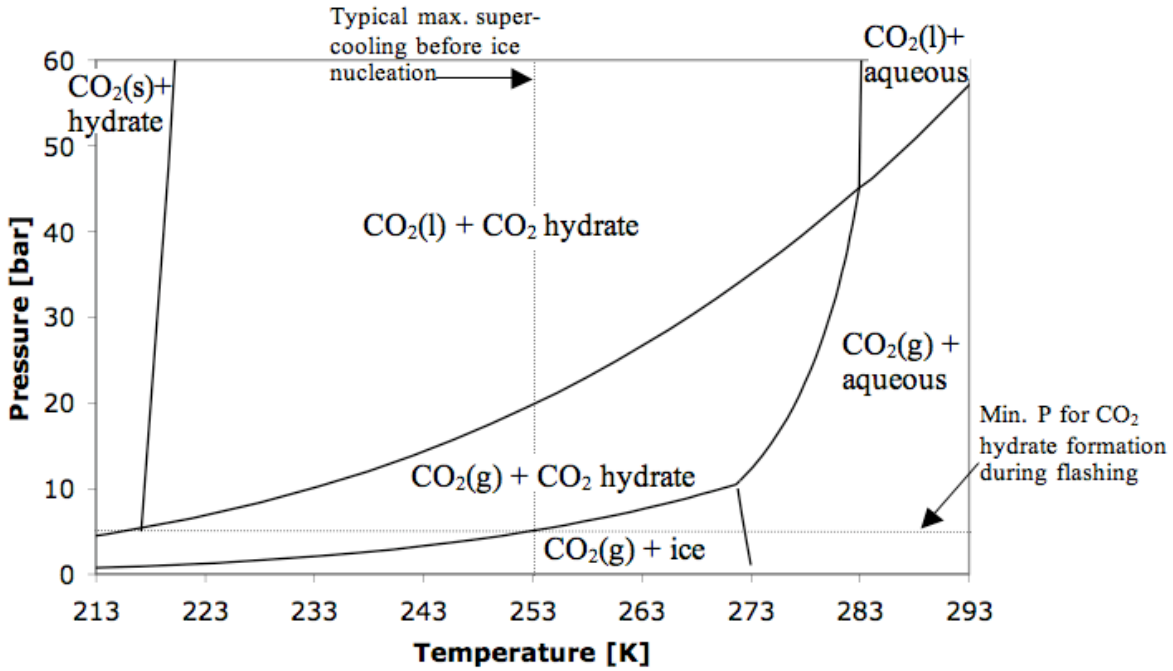

Figure 3-11 CO_2-H_2O pressure-temperature phase diagram. (Data from Sloan and Koh, 2008)

The pressure and temperature at nucleation in the hypothetical freezing histories presented in Figure 3-10 can also be located in Figure 3-11. It can be seen that nucleation in the 12 bar ICT case occurs in the CO_2(g)+CO_2 hydrate region, whereas the nucleation in the 4.5 bar ICT case occurs in the CO_2(g)+ice region. Based on the work of Hindmarsh et al. and Davies et al. ice would be expected to nucleate by the time that the mixture is cooled to 253 or

259 K. At 253 K, the minimum pressure for CO_2 hydrates is 4.7 bars. Therefore the ICT pressure must be greater than 4.7 bars to form CO_2 hydrates during flash freezing. For ICT pressures of 4.7-10 bars it is not clear whether ice nucleation or CO_2 hydrate nucleation will occur first. In the work of Davies et al. a supercooling of 30 K was necessary for gas hydrate nucleation; however CO_2 supersaturation of the mixture due to the CO_2 that was dissolved while the mixture was in the emulsion chamber may induce CO_2 hydrate nucleation with much less super-cooling. Also, in a mixture droplet, in contrast to a water droplet, the freezing point is continually depressed as crystallization proceeds. This would bring the mixture droplet back into the CO_2 hydrate stability range during freezing. Above 10 bars, CO_2 hydrate formation is favored because the mixture does not enter the CO_2 (g)+ice pressure and temperature region.

Currently, the ICT is unintentionally operated at the pressure where CO_2 hydrate and ice crystallization occur at almost the same temperature (10 bars). This could provide an explanation for the variability in the initial CO_2 content of the powder, because CO_2 hydrate and ice nucleation and growth could occur concurrently among the mixture droplets. In several trials, the sponsors of this research operated the second batch apparatus with the ICT at 11-12 bars. They found that the initial CO_2 content of the powder was more consistently 20% or higher (A. Pizzagalli 2008, pers. comm. February 8). This result supports the hypothesis that CO_2 hydrate formation is favored over ice formation above 10 bars. In a few trials, the original batch apparatus was operated with the ICT at atmospheric pressure. The resulting frozen powder was not carbonated. This result also supports the hypothesis that CO_2 hydrate formation is precluded by ice crystallization when the ICT pressure is less than 4.7 bars. Future work could include a systematic investigation of powder CO_2 content as a function of ICT pressure. In the mean time, operating the ICT at a pressure greater than 10 bars is desirable for consistent complete CO_2 hydrate formation.

Increasing the ICT pressure, with a fixed pressure in the emulsion chamber, decreases the pressure drop across the pressure-swirl nozzle and the superheat of the flashing CO_2. This should increase the powder particle size, making transport of CO_2 to the crystallizing water more difficult. At high ICT pressure (i.e. 20 bars) if CO_2 hydrate nucleates first, the particle temperature should approach 277 K after recalescence. However, if there is not enough CO_2 for further growth of CO_2 hydrates, the particle will be cooled by the 253 K CO_2 environment. By 259 K ice will nucleate and any water not in contact with CO_2 will crystallize as ice. Increasing the ICT pressure also increases the temperature in the ICT, which will reduce the rate of freezing of the mixture droplets. This could result in agglomeration of the powder. While an ICT pressure greater than 25 bars may completely preclude ice nucleation because the ICT temperature is greater than 259 K, the powder texture is likely to be changed significantly. The best practice is probably to increase the ICT pressure by a few bars.

In summary, CO_2 hydrate formation during flash freezing occurs due to the combination of fine particles and close contact with CO_2 during freezing and by ensuring that the ICT pressure is high enough for CO_2 hydrate nucleation. The competition between crystallization of water into CO_2 hydrate or ice requires more careful investigation. This investigation could involve: 1) developing a method to measure CO_2 content in the powder immediately after flashing in a controlled and exactly repeatable manner; 2) testing for variation in CO_2 content at 10 bar ICT pressure with all parameters fixed; and 3) testing for low CO_2 content at low ICT pressure and consistent complete CO_2 saturation at high ICT pressure. The particle size distribution and morphology should be monitored concurrently, handling the powder in a

manner that does not allow CO_2 hydrates to dissociate before observation. It may be necessary to increase the pressure in the emulsion chamber or the flash-freezing nozzle size to ensure a similar particle size at higher ICT pressure.

4 Storage

The product of the flash-freezing process can be distributed in several forms, such as a low-density, free-flowing powder; a compacted bulk; granules or pellets with or without a coating; or powder combined with other ingredients. The choice of the form of the confection depends on the target market. The CO_2 hydrate confection could be consumed at the site of production (such as at a flash-freezing cart or walk-in shop) or produced in a central factory and packaged for storage and distribution. Production at a central factory can take advantage of economies of scale and make it possible to reach a large market rapidly, but packaging would need to be specifically designed for the CO_2 hydrate confection. This chapter and the next present CO_2 hydrate characteristics that should be considered in development of a packaged product.

If a central production and distribution model is adopted, the flash-freezing product will need to be transported and stored under conditions that maintain the stability of the CO_2 hydrates. The range of pressures and temperatures at which CO_2 hydrates are stable (hereafter referred to as the stability field) in pure CO_2-H_2O systems is available in the literature. The CO_2-air mixed gas hydrate stability field has not been investigated experimentally, but Sloan and Koh (2008) calculated it using statistical thermodynamics. The CO_2 hydrate stability field in the presence of solutes in addition to H_2O and CO_2 has typically only been studied above the temperature of ice formation, where solutes in the water are used as thermodynamic inhibitors to prevent plugging of gas pipelines. Bobev and Tait (2004) commented in a study of the kinetics of CO_2 hydrate formation from frozen H_2O-methanol solutions that little is known about thermodynamic inhibition in systems containing ice and gas hydrate. In this chapter it will be shown that the ice-CO_2 hydrate equilibrium is independent of the concentration of compounds such as sugars and alcohols that remain in aqueous solution.

The total CO_2 in the confection package, compression of the powder and coating of the compressed powder may also affect CO_2 hydrate stability in storage. To maintain a homogeneous CO_2 concentration in the product, the CO_2 content in any storage vessel must be large enough to convert all freezable water to CO_2 hydrate because CO_2 can redistribute in the presence of ice. Compressing the powder reduces the rate of CO_2 loss due to hydrodynamic effects when the product is not in equilibrium with the gas phase, but without significant sintering the reduction is small because the compressed powder retains a high specific surface area and permeability. Finally, a pellet coating to prevent CO_2 escape must withstand the ice-CO_2 hydrate equilibrium pressure and minimize CO_2 flux through the coating. It is shown that ice can provide the necessary mechanical stability but CO_2 diffusion along grain boundaries makes an ice shell ineffective at retaining CO_2.

4.1 Required pressure for CO_2 hydrate stability

The phase equilibrium of CO_2 hydrates in a pure H_2O-CO_2 system, as shown in Figure 3-11, is available in the literature (Sloan & Koh, 2008). The minimum pressure for CO_2 hydrates at typical freezer temperatures is given by the equilibrium between ice, CO_2 hydrate, and gas. In the temperature range of interest for factory or home freezers a logarithmic curve can be fit to

the ice-CO_2 hydrate-gas equilibrium data, with a maximum error of 1.6%. Alternatively, Sloan and Koh (2008) developed a program called CSMGem that uses statistical thermodynamics to predict hydrate phase equilibria as well as cage filling with an average error of 3.5% in the pressure prediction. Figure 4-1 shows the logarithmic fit plotted with tabulated experimental data (Sloan & Koh, 2008) and the curve calculated by CSMGem (Sloan & Koh, 2008). At the temperature of a typical home freezer, 258 K, the CO_2 pressure required for stable CO_2 hydrates is 5.9 bars. Typical PET multi-serving carbonated beverage bottles are designed for a maximum pressure of 10-14 bars (Nitchman et al., 1985).

Mixed clathrate hydrates involving N_2, O_2 and CO_2 form if air is present in the vapor phase. The ice-gas hydrate-gas equilibrium pressure increases with increasing air concentration in the vapor phase. The fraction of N_2 or O_2 in the gas hydrate phase is less than 0.1% for CO_2 vapor phase mole fractions greater than 0.5. At the air concentration applicable for a container initially filled with air and then pressurized with CO_2 to stabilize the gas hydrates, the effect can be ignored as long as the CO_2 partial pressure is equal to the pressure required for a pure CO_2-H_2O system. Various researchers have measured the equilibrium hydrate formation pressure for N_2-CO_2 hydrates at temperatures above 273 K (Sloan & Koh, 2008), but little data exists at lower temperatures. The pressure for ice-binary gas hydrate-gas equilibrium can be predicted within 7% using CSMGem (Sloan & Koh, 2008). Figure 4-2 shows the incipient gas hydrate formation pressure as a function of CO_2 mole fraction at 258 K, as well as the CO_2 partial pressure. For reference, a vapor phase N_2 mole fraction of 0.15 would be found in a container that is pressurized from atmospheric pressure to 7.2 bars at 258 K, where the initial gas composition is pure N_2 and the container is pressurized by addition of CO_2. The predicted equilibrium pressure for gas hydrate formation with 15 mol% N_2 is about 1 bar higher than for pure CO_2. The partial pressure of CO_2 required for CO_2-N_2 hydrate stability decreases with increasing N_2 fraction, but can be treated as a constant in the range applicable for filling containers initially at atmospheric pressure.

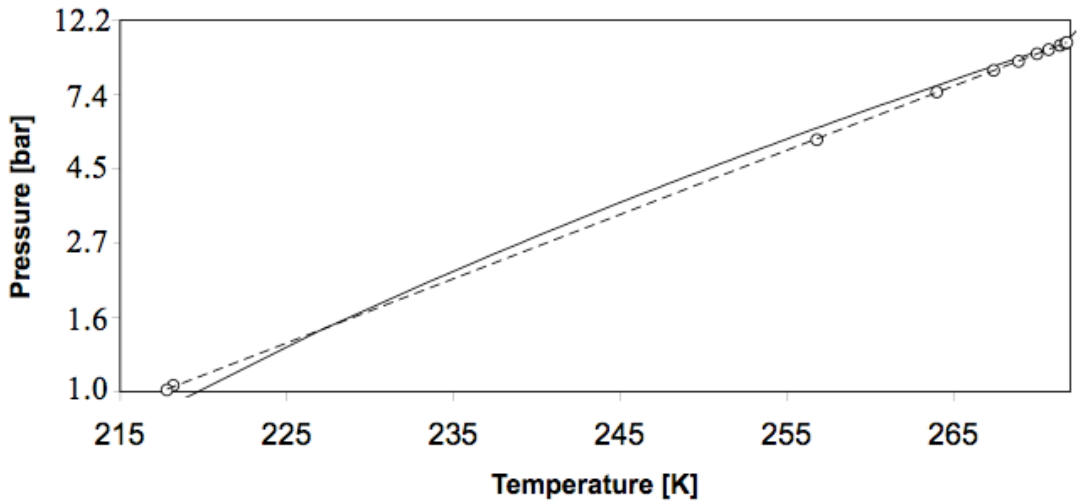

Figure 4-1 Ice-CO_2 Hydrate-Gas equilibrium. circles: tabulated data (Sloan & Koh, 2008); dashed line: fit to data, ln(P)=0.0432*T-9.3826; black curve: statistical thermodynamics calculation from CSMGem (Sloan & Koh, 2008).

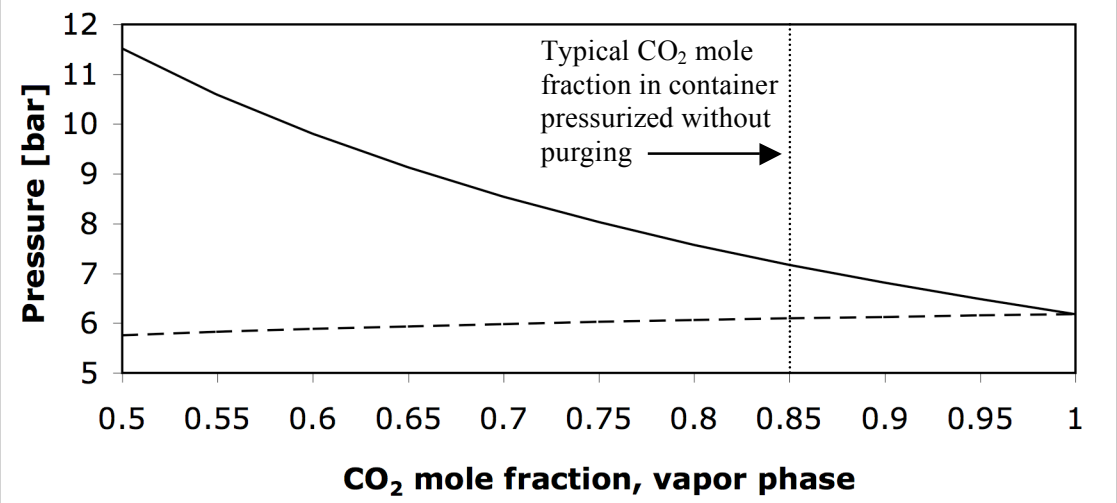

Figure 4-2 N_2-CO_2 mixed gas hydrate formation pressure at 258 K (black curve). CO_2 partial pressure (dashed curve). Calculated using CSMGem (Sloan & Koh, 2008).

CO_2 can form mixed gas hydrates with other gases as well. It would be desirable to find a gas that forms clathrate hydrates at a lower pressure than CO_2 does, such as tetrahydrofuran or Xenon, which could be mixed with CO_2 to reduce the required storage pressure of the product. However, this gas must be edible, which excludes tetrahydrofuran, and economically practical, which excludes Xenon, so that no candidates have been identified at this point. The gas concentration in the mixed gas hydrate favors the gas with the lower clathrate hydrate-forming pressure, so the mixed gas hydrate would still have to be stored at an intermediate total pressure in order to ensure a large enough CO_2 fraction in the product.

Additional sugars in the mixture do not change the minimum pressure for CO_2 hydrates at temperatures where ice is present. To see this, consider freezing a solution of water and sucrose. Sucrose dissolved in water depresses the initial freezing point of the solution by an amount related to the molar concentration of the solute. As a sucrose solution is cooled below its freezing point depression, water begins to freeze out of the solution as pure ice, increasing the concentration of sucrose in the remaining aqueous solution, which in turn further depresses the freezing point. At low temperatures when 80% or more of the water has frozen to ice, the sucrose solution becomes super-saturated. The high viscosity of the concentrated aqueous phase inhibits sucrose crystallization and the super-saturated phase behaves like a glass. The ice and concentrated aqueous solution are in equilibrium at each temperature if freezing occurs slowly enough. Similarly, in the flash-freezing product there is equilibrium between ice, aqueous solution, CO_2 hydrate and CO_2-rich vapor.

The conditions for equilibrium can be found starting with an equation for the change in entropy of an isolated system of water, sucrose and CO_2 as a function of internal energy, volume and number of moles of each component (Tester & Modell, 1996)

$$\delta \underline{S} = \sum_{i=v,l,s} \left[\frac{1}{T^i} \delta \underline{U}^i + \left(\frac{P^i}{T^i} \right) \delta \underline{V}^i - \frac{\mu_w^i}{T^i} \delta N_w^i \right] - \sum_{i=v,l} \frac{\mu_{CO_2}^i}{T^i} \delta N_{CO_2}^i - \frac{\mu_{hyd}^s}{T^s} \delta N_{hyd}^s - \frac{\mu_{suc}^l}{T^l} \delta N_{suc}^l , \qquad (4.1)$$

where the superscripts v, l, and s represent the phases vapor, liquid and solid, the subscripts w, CO_2, hyd and suc represent the components water, CO_2, CO_2 hydrate and sucrose, and S, T, U, P, V, μ, and N represent entropy, temperature, energy, pressure, volume, chemical potential and number of moles, respectively. It is assumed that sucrose is present only in the

aqueous phase, CO_2 is present in the vapor phase, the gas hydrate and the aqueous phase, and H_2O is present in all phases. For an isolated system, there are additional constraints of constant energy, constant volume and constant mass:

$$0 = \delta \underline{U}^v + \delta \underline{U}^l + \delta \underline{U}^s$$

$$0 = \delta \underline{V}^v + \delta \underline{V}^l + \delta \underline{V}^s$$

$$0 = \delta N_{suc}^l$$

For water, CO_2, and CO_2 hydrate, the constraint of conservation of mass is applied by defining the extent of reaction, ξ,

$$6.8H_2O + CO_2 \leftrightarrow CO_2 \cdot 6.8H_2O \Rightarrow \delta\xi = \frac{\delta N_w}{-6.8} = \frac{\delta N_{CO_2}}{-1} = \frac{\delta N_{hyd}}{1},$$

which gives the constraint equations

$$-6.8\delta\xi = \delta N_w^v + \delta N_w^l + \delta N_w^s$$

$$-\delta\xi = \delta N_{CO_2}^v + \delta N_{CO_2}^l$$

$$\delta\xi = \delta N_{hyd}^s$$

The above constraint equations can be multiplied by the Lagrange multipliers $1/T^v$, P^v/T^v, $-\mu_{suc}^l/T^v$, $-\mu_w^v/T^v$, $-\mu_{CO_2}^v/T^v$, $-\mu_{hyd}^s/T^v$ and subtracted from Eq. 4.1. At equilibrium the entropy in the isolated system is at a maximum; the partial derivatives, $\partial S/\partial U$, $\partial S/\partial V$ and $\partial S/\partial N_i$ should be 0, thus dS=0. Finally, the equilibrium criteria are

$$T^v = T^l = T^s$$

$$P^v = P^l = P^s$$

$$\mu_w^v = \mu_w^l = \mu_w^s$$

$$\mu_{CO_2}^v = \mu_{CO_2}^l$$

$$6.8\mu_w^v + \mu_{CO_2}^v = \mu_{hyd}^s$$

The chemical potential of a pure substance is only a function of temperature and pressure. Ice and CO_2 hydrate contain very small concentrations of impurities, and will approach the behavior of pure phases. In this case, at a particular temperature and pressure, the chemical potential of water in ice is unchanged by the concentration of sucrose in the aqueous phase. According to the conditions of equilibrium, the chemical potential of the water in the liquid and vapor phase are then also unchanged. Similarly the chemical potential of the gas hydrate phase is unchanged by the presence of sucrose in the aqueous phase. In this case the chemical potential of CO_2 in the vapor phase, and hence the required CO_2 pressure is also unchanged compared to the system without sucrose. Because the sucrose does not crystallize and has a very low vapor pressure, there is no constraint at equilibrium on the chemical potential of the sucrose dissolved in the aqueous phase. This argument is applicable for any ingredients that remain in solution in the aqueous phase, as long as no additional reactions occur, and the presence of the additional ingredients in the vapor and solid phases is negligible.

The assumption that CO_2 is present in the aqueous phase may not always be true. If CO_2 is not dissolved in the aqueous phase before it reaches a glassy state, high viscosity will hinder diffusion of CO_2 into the supersaturated solution. However, CO_2 will be present at the interfaces of the aqueous phase, so the thermodynamic equilibrium arguments presented

above are unchanged. Also, ingredients in the mixture may affect CO_2 solubility. Proteins or bases may shift the ionic equilibrium in the aqueous phase, increasing the dissociation of CO_2 to carbonic acid and carbonate ions. Some components in solution may precipitate out, leaving a saturated concentration of the component in the aqueous phase. The CO_2 content of the CO_2 flash-freezing product is not significantly affected by the CO_2 concentration in the aqueous phase because the CO_2 concentration in CO_2 hydrates is so high. The CO_2 in the gas hydrates is more than enough for the consumer to perceive that the product is fizzy (see section 6.3).

The foregoing consideration of equilibrium in an isolated water-sucrose-CO_2 system demonstrates that the minimum pressure for CO_2 hydrate formation does not depend on additives when ice is present. The invariance of the ice-CO_2 hydrate-gas (I-H-G) equilibrium pressure can also be predicted by considering Gibb's Phase Rule. Four phases are present in the three-component system of water, CO_2 and sucrose. According to Gibb's Phase Rule, there is only one degree of freedom. For a given temperature along the four-phase equilibrium curve, the pressure for ice-CO_2 hydrate equilibrium is specified, and is not a function of solute concentration. Thus the equilibrium pressure should be the same as the pressure in the limit of a dilute solution, corresponding to the I-H-G curve in Figure 4-1. Even with more than one solute, the ice-aqueous solution-CO_2 hydrate-gas equilibrium is not expected to shift because the water activity as a function of temperature is fixed by the vapor pressure of water in equilibrium with ice. The CO_2 chemical potential is given by the reaction equilibrium between CO_2, H_2O and CO_2 hydrate, which determines the CO_2 activity and thus the CO_2 partial pressure. Note that above the temperature for ice formation, as described in section 2.3, the pressure required for aqueous phase-CO_2 hydrate equilibrium increases with sucrose concentration; this dependence on the sucrose concentration occurs because there is one less phase present.

Measurements using the PTM apparatus (introduced in section 1.4) corroborate the results of the above thermodynamic argument. The I-H-G equilibrium pressure is measured using powder from the CO_2 flash freezer because the high specific surface area of the powder provides a fast response to changes in pressure and temperature. Figure 4-3 shows a sample pressure and temperature profile during measurement of several points along the I-H-G equilibrium curve. Powder is placed in the PTM sample can and CO_2 hydrates are allowed to dissociate for a few hours. The PTM is then flushed with CO_2 gas, pressurized to a pressure a few bar greater than the predicted I-H-G equilibrium pressure and sealed. Due to the formation of CO_2 hydrates the pressure then falls. After the pressure approaches a stable value the pressure is perturbed slightly by adding or venting CO_2 in order to confirm that the equilibrium pressure has been obtained. Due to the perturbation, CO_2 hydrates dissociate or form until the equilibrium pressure is re-established. This procedure is repeated at multiple temperatures between 230 and 260 K with powder formed from several different solutions.

In the sample pressure and temperature profile in Figure 4-3, the temperature spikes near hours two and three are due to handling of the thermocouple, the temperature of the sample stays near 235 K. The high-frequency oscillation in the temperature data is due to the freezer compressor cycling on and off. There is no data between hour 30 and hour 40 because the data acquisition system quit and had to be re-started. Note that the 7 bar pressure recorded during flushing is the pressure near the CO_2 cylinder; the pressure near the sample is less by several bar. During the rest of the trial the pressure data is representative of the pressure near the sample. The discrepancy occurs due to flow resistance in the capillary tube between the

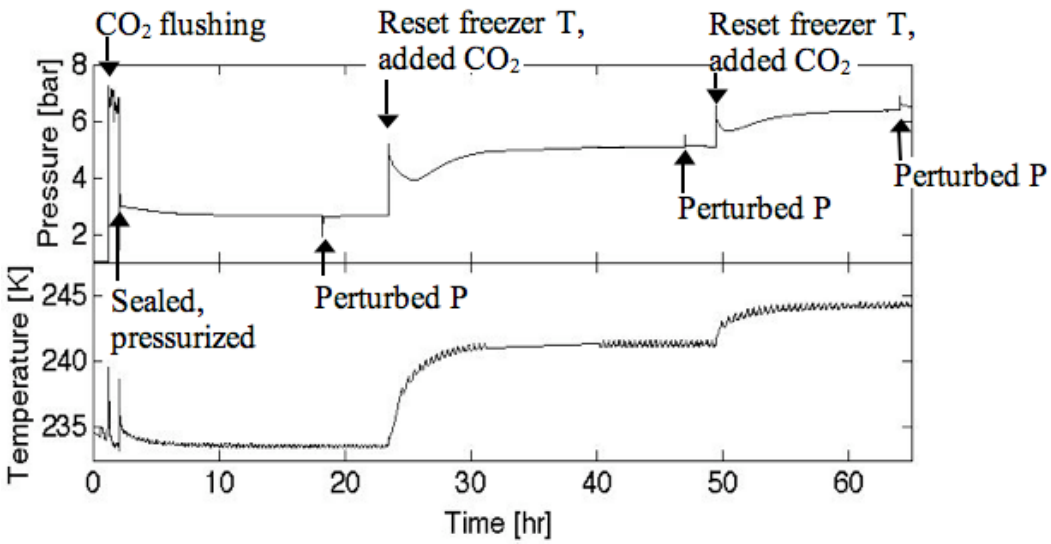

Figure 4-3 Sample I-H-G equilibrium measurement pressure (P) and temperature (T) profiles.

pressure transducer and the sample chamber (a schematic of the PTM is shown in Figure 1-5), but once the PTM is sealed and flow becomes negligible, the pressure is uniform throughout the PTM.

Figure 4-4 shows the measured equilibrium for several mixtures. The measured equilibrium pressures for both water and mixtures containing a variety of sugars and citric acid match the I-H-G equilibrium pressures.

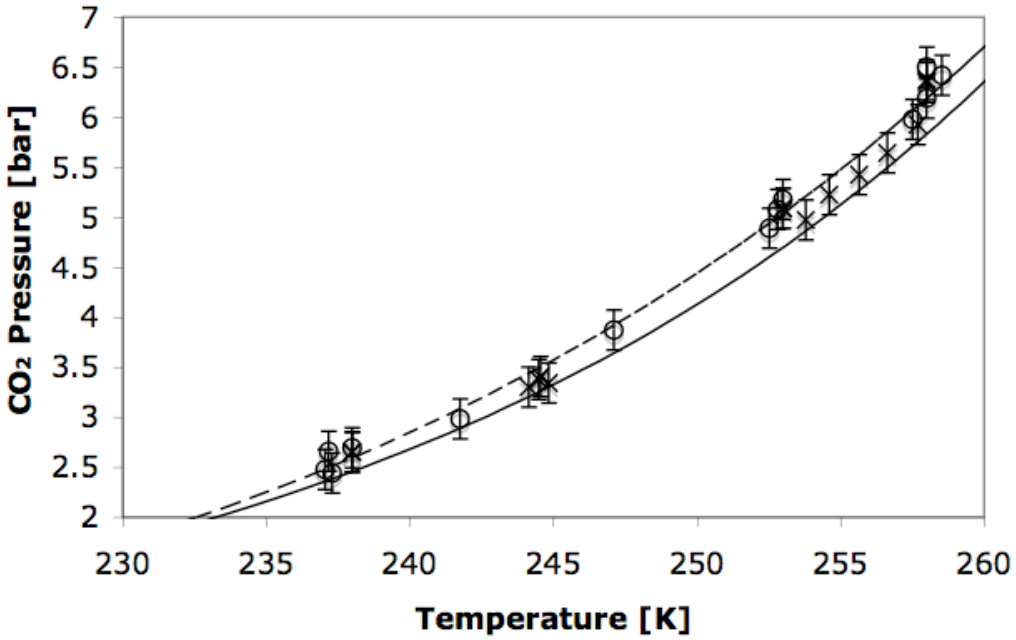

Figure 4-4 Measured I-H-G equilibrium pressures. Dashed curve - CSMGem model. Black curve - logarithmic fit to literature data. Circles - data for powder formed from water. X's - data for mixtures containing sucrose, corn syrup, CarboGain and or citric acid.

4.2 Product homogeneity

One aspect of developing a CO_2 hydrate confection that is packaged and distributed is ensuring that the initial product quality is not lost during its storage period. To test the storability of the CO_2 hydrate confection, the sponsors of this research formed flash-freezing powder into bite-size pellets, stored the pellets in sealed tubes for at least a week, and then tasted them. When the pellets were tasted, it was observed that among five pellets from the same tube, some were strongly carbonated, while others did not have any perceptible CO_2 despite all of the pellets coming from the same batch of powder, being stored at the same pressure, and being initially uniformly carbonated. This unintentional non-homogeneity in the CO_2 hydrate confection would be considered a defect.

It has been determined that in order to ensure a homogeneous product, there must be enough CO_2 in the storage vessel to practically eliminate the ice phase in addition to maintaining the minimum CO_2 pressure for CO_2 hydrate stability. If the CO_2 content of the package is not high enough, ice will be present, allowing the CO_2 to redistribute and form ice-rich regions and CO_2 hydrate-rich regions. The driving force for CO_2 redistribution can be surface energy minimization or a small temperature gradient. In the case of surface energy minimization, larger CO_2 hydrate and ice crystals grow at the expense of small CO_2 hydrate and ice crystals. In the case of a small temperature gradient, CO_2 hydrates in the warm area become unstable and dissociate, releasing CO_2 to the gas phase, while ice in the cold area becomes unstable and forms new CO_2 hydrates, capturing CO_2 from the gas phase. At the end of this section a formula for the CO_2 content required to avoid CO_2 redistribution is developed.

For basic tests of CO_2 hydrate confection storability, the flash-freezing powder is typically formed into 1-cm^3 pellets using initially a manually and then a pneumatically actuated piston-cylinder device. The cylinder is manually filled with fresh flash-freezing powder and then the piston compresses the powder and ejects the resulting pellet. The typical pressure applied to the powder is 15 bars, which results in a pellet with at least 50% porosity. The piston-cylinder device is stored and operated in a cold room or chest-style freezer at 253 K to avoid significantly warming the powder while it is formed into pellets. After storage, the pellets are considered defective if the CO_2 content of any pellet becomes too low to provide a strong sensation of carbonation when it is consumed (minimum levels are discussed further in section 6.3).

CO_2 redistribution due to surface energy minimization will lead to inhomogeneous bulk CO_2 concentration if the ice and CO_2 hydrate crystal sizes are unevenly distributed in the product. In section 5.1 it is argued that the solid-liquid and solid-vapor interfacial energies of CO_2 hydrate and ice with aqueous and gaseous phases are similar. This suggests that for similarly sized particles the driving forces to reduce CO_2 hydrate and ice interfacial areas are similar. As the ripening process continues, pellets will develop large CO_2 hydrate and ice crystals. The CO_2 content of each pellet will depend on the initial ice and CO_2 hydrate crystal size distribution, but it is unlikely that a pellet will contain only ice or only CO_2 hydrate because the typical pellet dimension, 0.01 m, is much larger than the dimension of the flash-freezing powder particles from which a pellet is made (on the order of 10^{-5} m).

CO_2 redistribution due to a temperature gradient will systematically form ice-rich regions in the warm area and CO_2-rich regions in the cold area. A simple model is developed below to show that even in a freezer at nearly uniform temperature, a pellet could become devoid of

CO_2 hydrates over just a couple weeks of storage if the warm area of the product remains in a fixed location. The rate of CO_2 redistribution is determined by the rate of heat flow through the product, which counters the heat loss (gain) due to the endothermic (exothermic) CO_2 hydrate dissociation (formation) reaction. The pressure in the container remains nearly constant during the redistribution because the CO_2 hydrate formation and dissociation reactions occur concurrently.

The storage time required for a pellet to become devoid of CO_2 hydrates can be estimated using the simple 1-D model shown in Figure 4-5. Initially, several pellets containing 50% CO_2 hydrate and 50% ice by mass are at temperature T_o and in equilibrium with gaseous carbon dioxide. At time t=0, a small temperature gradient develops in the surrounding environment such that the pellet at x=0 is exposed to a local temperature of $T_{env,l}$, which is greater than T_o. Heat flow into the pellet causes the CO_2 hydrate at this end of the stack to begin to dissociate and an interface develops in the pellet between the initial composition and a volume that is now 100% ice. This boundary will move along the stack with time. The energy balance at the interface for this process can be expressed as

$$\dot{m}'' h_{HI} + k_i \left.\frac{\partial T}{\partial x}\right|_{s,100\%\,ice} = k_{50} \left.\frac{\partial T}{\partial x}\right|_{s,50\%\,ice}, \qquad (4.2)$$

where $\dot{m}''$ is the rate of CO_2 release due to CO_2 hydrate dissociation per unit cross-sectional area, h_{HI} is the enthalpy of dissociation per kilogram CO_2, k_i is the thermal conductivity in pure ice, k_{50} is the thermal conductivity in the 50% mixture, T is temperature, x is the distance from the warm end of the pellet stack and s is the position of the 50% CO_2 hydrate-100% ice interface. The derivatives in Eq. 4.2 are evaluated on each side of the interface. The heat capacity of the pellet is neglected in this model because it is small relative to the enthalpy of dissociation of CO_2 hydrate. Note that in this model the warm end of the pellet stack is pinned to the origin of the x-axis. Because water is denser in ice than in CO_2 hydrate, the stack moves slowly toward the origin as the 50% mixture is converted to ice.

The right-hand side of equation 4.2 represents heat flow from the 100% ice interface to the remaining 50% mixture. It is assumed that the middle pellets remain isothermal because the CO_2 hydrate dissociation occurs at T_o and heat for the dissociation is supplied through the warm end of the pellet. Therefore the right-hand side of equation 4.2 is zero. On the left-

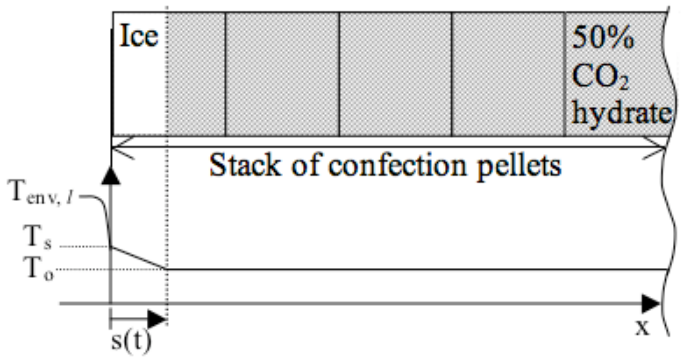

Figure 4-5 Simple 1-D CO_2 redistribution model showing moving 100% ice boundary at some time t. Vertical dotted line indicates interface between region that has been completely converted to ice and region with initial CO_2 hydrate concentration. Cold end where new CO_2 hydrate is forming is not shown.

hand side of equation 4.2, the second term is the heat flux from the environment, q_i $\left(= k_i \frac{\partial T}{\partial x}\bigg|_{s,100\%ice} \right)$. The heat flux can be determined by modeling the heat transfer from the environment to the ice-CO_2 hydrate interface as two resistors in series or:

$$k_i \frac{\partial T}{\partial x}\bigg|_{s,100\%ice} = q_i = \frac{T_{x=s} - T_{env,l}}{\frac{s}{k_i} + \frac{1}{h_{env}}},$$

where h_{env} is the convection coefficient between the environment and the surface of the pellet stack, $T_{x=s}$ is the temperature at the 100% ice interface, and $T_{env,l}$ is the temperature of the environment.

The rate of CO_2 release, $\dot{m}''$, is related to the velocity of the interface, ds/dt, by the ratio of water to CO_2 in the 50% mixture and the density of ice. The ratio of water to CO_2 in the 50% mixture (Θ) is

$$\Theta = \frac{2nM_{H_2O}}{M_{CO_2}} + 1,$$

where n is the water-CO_2 mole ratio in CO_2 hydrate, M_{H2O} is the molar mass of water and M_{CO2} is the molar mass of CO_2. With the density of ice, ρ_{ice}, the rate of CO_2 release is then

$$\dot{m}'' = -\frac{\rho_{ice}}{\Theta}\frac{ds}{dt}.$$

Solving equation 4.2 with the above substitutions for heat transfer through the ice and the rate of CO_2 release, it can be shown that the time, t, at which the moving interface reaches a position s is given by

$$t = \frac{\frac{\rho_{ice}}{\Theta} h_{HI}}{T_{x=s} - T_{env,l}} \left(\frac{s^2}{2k_i} + \frac{s}{h_{env}} \right). \tag{4.3}$$

Figure 4-6 shows the time required for the first pellet in a stack of 1 cm long pellets to be completely converted to ice for a range of temperature differences between the environment and the end of the pellet stack. In these models h_{env} is set to 3 W/m^2K, which is the approximate coefficient for radiation heat transfer between two surfaces near 253.15K. This should be a lower bound on the heat transfer rate to the product, so that the trend in Figure 4-6 represents the maximum time before detrimental CO_2 redistribution occurs. The position of the interface, s, is set to the length of one pellet after all of its CO_2 hydrates have dissociated, 0.0094 m. Note that the thermal conductivity of CO_2 hydrates is close to 75% lower than the thermal conductivity of ice, so the moving interface on the cold end where CO_2 hydrates are forming would progress more slowly, but for s=0.0094 m, the difference is negligible.

As shown in Figure 4-6, even in this simple 1-D model, which does not account for heat transfer at the circumference of the pellets, it is feasible for a pellet to lose all of its CO_2 after less than 10 days of storage with slow heat transfer across a 0.4 K temperature difference. Freezers often have temperature variations of several degrees. The greater the temperature stratification in the freezer, the more rapidly CO_2 redistribution will occur. The typical storage time of frozen dessert products is much longer than 10 days, therefore even in more general pellet storage geometries CO_2 redistribution is likely to occur unless ice is avoided in the storage container.

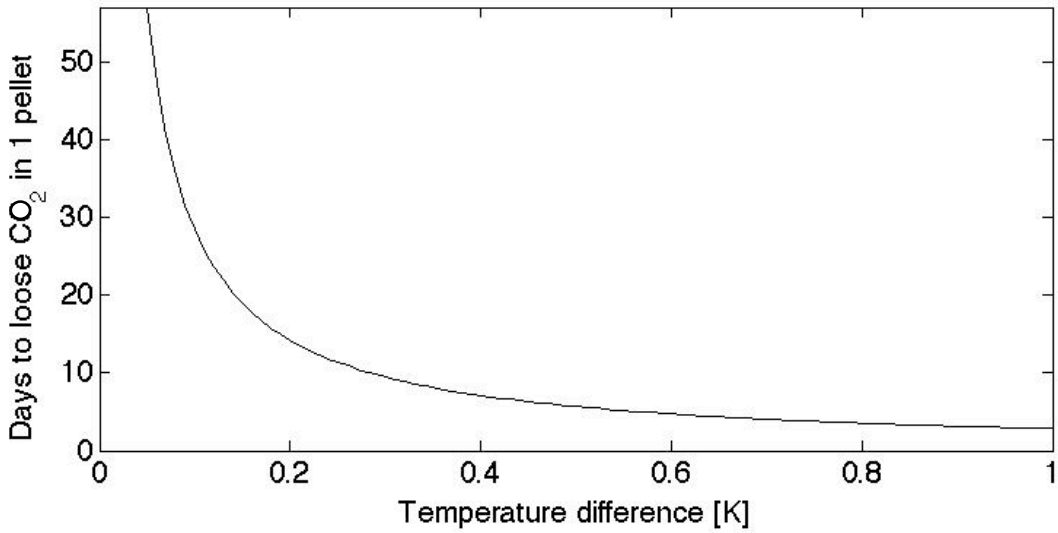

Figure 4-6 Time to develop 100% ice pellet as function of difference between environmental and initial pellet stack temperature using Eq. 4.3. In this model h_{env} is 3 W/m^2K, k_i is 2.2 W/mK, h_{HI} is 540 kJ/kg CO_2, ρ_{ice} is 920 kg/m^3, Θ is 6.38, n is 6.6, M_{H2O} is 0.018 kg/mol, M_{CO2} is 0.04401 kg/mol, and s is 0.0094 m.

The total CO_2 required in the package to avoid ice formation and therefore ensure a homogeneous product is the sum of the CO_2 needed to pressurize the volume of the storage container at the maximum storage temperature and the CO_2 needed to occupy the hydrate cages. The fraction of clathrate hydrate cages occupied by a guest gas molecule depends on the size of the molecule, the temperature and the pressure. The CO_2 hydrate structure consists of six large cages and two small cages per unit cell, which are formed by 46 water molecules. Typically, the fractional occupancy of the large cages is very high while the fractional occupancy of the small cages increases with increasing pressure (above the pressure for incipient CO_2 hydrate formation at a particular temperature). The software program CSMGem (Sloan & Koh, 2008), predicts the fractional occupancy of various gas hydrates, including CO_2 hydrates. At temperatures between 243 and 263 K the predicted incipient fractional cage occupancy for CO_2 hydrates is 97% in the large cages and 46% in the small cages (Sloan & Koh, 2008). Based on these fractional occupancy values there must be one CO_2 molecule for every 6.84 water molecules in order to fill the CO_2 hydrate cages.

Calculating the necessary CO_2 content requires knowing the volume of the container, V_c, the mass of mixture in the container, m_m, the density of the mixture, ρ_m, the water content of the mixture (1-TS) and the maximum storage temperature, T_{max}. The volume of vapor phase CO_2 in the storage container (also known as the headspace) is approximately

$$V_{vapor} = V_c - \frac{m_m}{\rho_m}.$$

The actual vapor volume is less because the density of water in hydrates is about 20% less than in aqueous solution. It is important not to determine the CO_2 vapor phase volume based on the nominal volume of the powder or compressed pellet because the frozen product has very high overrun (porosity). The mass of CO_2 required to avoid ice is

$$m_{CO_2,hyd} = \frac{f \cdot (1 - \mathrm{TS}) m_m}{M_{H_2O} \cdot n_{inc}} M_{CO_2}$$

where *f* represents the fraction of water in the dessert mixture solution that freezes (as discussed in section 3.1) and n_{inc} is the number of water molecules per CO_2 molecule at incipient CO_2 hydrate formation, 6.84. The total CO_2 required in the storage container is then $\rho_{CO2}*V_{vapor}+m_{CO2,hyd}$. The density of CO_2 vapor at T_{max} and the corresponding ice-CO_2 hydrate equilibrium pressure can be found using the NIST database (Lemmon, 2009). At 258 K the pressure required for CO_2 hydrates is 5.9 bars and the corresponding density of CO_2 vapor, ρ_{CO2}, is 12.65 kg/m^3. For a container packed to 100% overrun (50% bulk porosity) with a frozen confection made from 20% total solids mixture the total CO_2 requirement is 0.24 kg CO_2 per kg of mixture.

CO_2 redistribution has been successfully avoided in the previously described bite-size pellets by adding dry ice to the storage tubes at the time they are sealed. The dry ice ensures that there is sufficient CO_2 to pressurize the storage tube after it is sealed and convert any ice to CO_2 hydrate. When the pellets are packed with dry ice and tasted a week or two later every pellet is strongly carbonated. Adding dry ice is necessary because CO_2 is lost while the powder is compressed into pellets and transferred to the storage tubes. It should not be necessary to add dry ice in a continuous cycle implementation of the flash-freezing process that integrates powder production, forming and packaging. The measured CO_2 content of powder removed from the ICT is 0.12-0.25 kg CO_2 per kg of mixture. Theoretically, a 20% total solids powder could contain up to 0.27 kg CO_2 per kg of mixture (based on complete CO_2 hydrate formation). This would be more than sufficient to ensure a homogeneous CO_2 distribution in a confection packed to 100% overrun, so no dry ice would be needed.

4.3 Effect of powder compaction

The flash-freezing powder can be packed and compressed to reduce settling after packaging and to reduce the volume of the confection. Compaction may also slow CO_2 loss while the product is exposed to air or a CO_2 pressure lower than the ice-CO_2 hydrate equilibrium pressure, which could occur during filling of a package, if the package leaks, or when the consumer opens the package. Compaction may slow CO_2 loss by reducing the specific surface area, reducing mass transport through the void space, and by enabling a 'self-preservation' mechanism in which CO_2 hydrates at the surface of the pellet dissociate and leave an ice coating to stabilize CO_2 hydrates in the core. In this section the effectiveness of each of these mechanisms is discussed.

Currently the powder is compacted into bite-size pellets (approximately 1 cm^3), typically from an initial density of approximately 100 kg/m^3 to a density of 400-500 kg/m^3. A density of 400-500 kg/m^3 corresponds to an overrun close to 100%, which is similar to the overrun in conventional ice creams. This compaction is achieved by applying a pressure of 15 bar at a temperature near 253 K (Lopez, 2009). The texture of the compacted powder resembles tightly packed sand rather than a recrystallized or sintered continuous solid, even when the powder is compressed using an arbor press. However, some sintering must occur during pellet formation so that the pellets do not fall apart when released from the mold. In manual compression, it has been found that when pellets are made at temperatures below about 243 K, the pellets fall apart when they are removed from the mold.

The specific surface area of the CO_2 hydrate confection can be quite large even after compression, so CO_2 loss is typically not significantly slowed by the specific surface area

reduction associated with compression. The specific surface area of the uncompressed powder can be estimated based on the optical microscopy images of the powder in Figure 3-9. If the average sized particles in Figure 3-9 are modeled as 40 x 40 x 20 μm^3 rectangular prisms with a density of 1000 kg/m^3, the specific surface area of the uncompressed powder is 200 m^2/kg. (This value is comparable to the specific surface area of non-hollow snow particles that can have a typical value of 100 m^2/kg and can be as high as 350 m^2/kg (Kerbrat et al., 2008)). The compression process reduces the specific surface area from that of the free powder. For example, if in the compression process an average of two faces of each particle are brought into contact, the specific surface area of the compressed solid would be 25 to 50 percent smaller than that of the free powder. However, the resulting specific surface area is still 100 m^2/kg or greater (still comparable to the specific surface area of snow) and the mass flow rate from the particles is halved at most (because the surface area is halved at most). In comparison, the specific surface area of 44 ml of a carbonated beverage in a shot glass (4 cm diameter) would be around 0.03 m^2/kg, which is smaller by more than 3 orders of magnitude. Of course, CO_2 loss from a carbonated beverage and CO_2 loss from dissociating CO_2 hydrates involve different latent heats and surface concentration driving forces. Nevertheless the comparison indicates that even the compressed powder has much more surface area exposed for CO_2 loss than a carbonated beverage and hence the CO_2 mass flux from the powder is still high after compression because the surface area is so high.

The specific surface area of the compressed powder could be reduced more significantly if the compression process is done at a warmer temperature, for example 263 K, where the greater water mobility will increasingly enable sintering. With significant sintering, voids between the particles can be sealed off from the external environment, making a more significant impact on mass flux. The actual specific surface area of the compressed and uncompressed powder as a function of compression temperature could be measured using a technique such as methane absorption (see for example Kerbrat et al., 2008) in order to investigate sintering during compression and determine the optimum temperature for compression.

Transport of gaseous CO_2, H_2O and air through the pellet is slower than through the powder because the tight packing of the powder inhibits convection and diffusion through the void space. In analogy to a model for gas flux through porous catalysts (Mills, 1995) an effective diffusivity is estimated based on the porosity and tortuosity of the porous solid. For pore radii greater than 2 μm, the effective diffusivity is given by

$$D_{CO_2,eff} = \frac{\varepsilon_v}{\tau} D_{CO_2}$$

where ε_v represents the porosity (void volume divided by total volume), τ the tortuosity and D_{CO_2} the diffusivity of CO_2 in the gaseous phase outside of the porous material. Tortuosity is a measure of the path length a gas molecule travels to change position by unit distance. Several researchers have developed expressions for tortuosity as a function of the porosity, for example $\tau=1.25/\varepsilon_v^{1.1}$ (Meyer & Smith, 1985). Considering powder with $\varepsilon_v=0.9$, $\tau=1$ and pellet with $\varepsilon_v=0.5$, $\tau=3$, the ratio of effective CO_2 diffusivities is 5.4. Therefore the characteristic time for diffusion of CO_2 out of 50% porosity compressed powder should be 5.4 times greater than the characteristic time for diffusion of CO_2 out of an equivalent volume of uncompressed powder.

CO_2 hydrates sometimes exhibit a phenomenon called self-preservation, which significantly slows the rate of CO_2 loss, but it is unlikely that compressed powder pellets

exhibit this phenomenon. Self-preservation is the persistence of gas hydrates over extended periods of time at atmospheric pressure and 240-270 K (Sloan & Koh, 2008). Self-preservation occurs in CO_2 hydrates (Circone et al., 2003), but has more commonly been observed in methane hydrates (Stern et al., 2001; Giavarini et al., 2007). The gas hydrate persistence may be caused by formation of a coherent ice shell during dissociation of an outer layer of gas hydrate. Formation of this coherent ice shell depends on the structure of the original gas hydrate bulk. Zhang and Rogers (2008) showed that a careful hydrate formation process that minimized grain size, fractures, void space and entirely avoided ice in a methane hydrate sample led to self-preservation of greater than 99% of the initial methane hydrate. In the compressed pellets, significant dissociation would be required before self-preservation of the remaining fraction of CO_2 hydrates could occur because the porosity is high and stresses or fracturing due to internal aqueous and ice phases may hinder sealing of the ice shell. Indeed, a very low level of self-preservation is indicated by most of the PTM measurements of CO_2 loss from flash-freezing powder and pellets. It has been found that the mass of a sample typically decreases by 1-3% after it is melted, even though the sample mass was stable at atmospheric pressure in the freezer before it was melted and the melting was carried out in a sealed plastic bag. Even if this 1-3% mass retention until melting is due to self-preservation, it represents too little CO_2 to be perceived by the consumer.

The rate of mass decrease in compressed and uncompressed powder was compared in atmospheric pressure air at 253 K. The mass of each sample decreases as CO_2 hydrates dissociate and CO_2 vapor is transported away from the sample by diffusion and convection. In the test, a first sample can is filled with powder and then the powder is compressed manually using a pre-cooled plastic plunger. A second sample can is filled with powder from the same batch to the same height as the compressed powder in the first can, so that the bulk length scales in the two samples are matched. The porosity is 90% in the uncompressed sample and 70-80% in the compressed samples. The sample can diameter is 6.65 cm. Figure 4-7 shows the mass decrease rate for each sample at 253 K. The periodic spikes in the mass measurement coincide with the freezer compressor cycle. In all trials, half of the CO_2 content is lost in less than half an hour, regardless of compression. This indicates that the powder does not sinter significantly and compression of the powder does not significantly reduce the

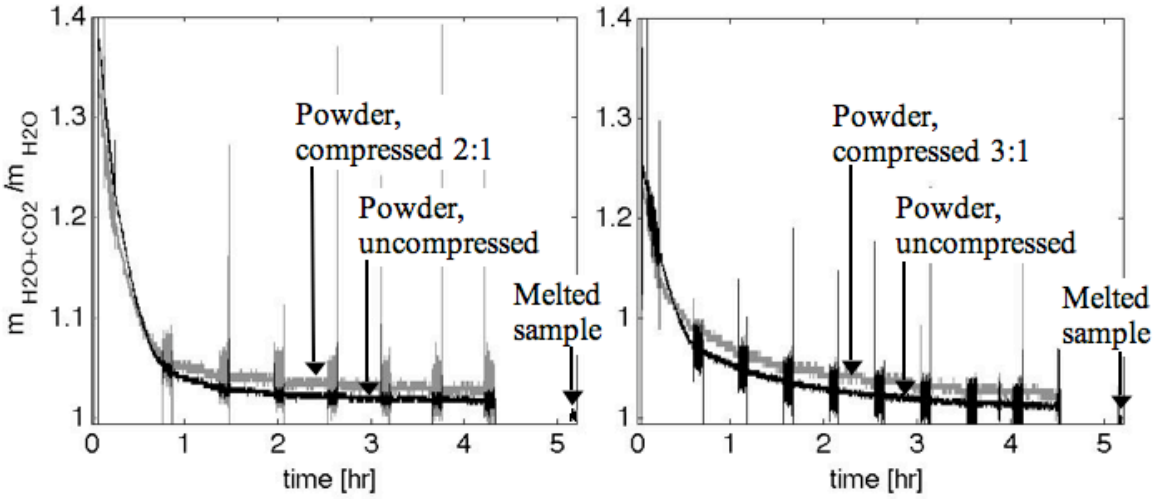

Figure 4-7 Mass decrease in compressed (black) and uncompressed (gray) powder made from water using the CO_2 flash freezer.

CO_2 loss rate. In both experiments the uncompressed powder seems to retain more CO_2. Perhaps the looser structure of the powder in the uncompressed sample allows it to settle in a favorable manner for achieving some self-preservation. However, the retained CO_2 content is much too small to be useful.

If the powder were compressed more than the samples in the tests above, the CO_2 loss rate would probably be mitigated more effectively. In the tests described above the extent of compression is constrained by the manual force that can be applied to the plastic plunger and the large cross-sectional area of the sample can. The actual 1-cm^3 pellets are compressed to 50% porosity. In a qualitative comparison using a water recipe, the 1-cm^3 pellets maintained nearly full CO_2 concentration while exposed to ambient pressure at 253 K for 20 minutes, whereas a bulk of powder from the same batch was mostly devoid of CO_2 after the same exposure. (The pellets were formed by a pneumatic piston-cylinder device that had been modified to attach directly to the ICT of the batch flash freezer and to eject the pellets into a holding tank for the duration of a batch, allowing the entire device to operate at ICT pressure. This piston-cylinder device is described in detail in Lopez (2009)). Further tests should be carried out with samples compressed to the typical pellet density and careful attention to matching length scales between compressed and uncompressed samples.

4.4 Coating options

It may be possible to stabilize CO_2 hydrates in the product by coating pellets with a material that provides low CO_2 permeability and can withstand a pressure differential without cracking, however an edible material with appropriate properties and a method of forming a sealed coating must be developed. Coating materials can be assessed by calculating the shell thickness required for mechanical stability and the shell thickness necessary to limit CO_2 loss from a spherical pellet. The shell thickness can be estimated from the maximum stress in a thick-walled, internally pressurized spherical shell,

$$r_o = r_i \left(\frac{\sigma_{mat} + P_i}{\sigma_{mat} + 1.5P_o - 0.5P_i} \right)^{1/3}, \tag{4.4}$$

where r_o is the outer shell thickness, r_i is the radius of the pellet before coating, P_i is the ice-CO_2 hydrate equilibrium pressure at the storage temperature, P_o is the pressure in the storage container and σ_{mat} is the maximum tensile stress of the material in question (Ragab & Bayoumi, 1999). The CO_2 loss rate from the shell can be estimated by considering the steady state flow rate of CO_2 through the shell from r_i to r_o (Crank, 1980),

$$\frac{dm_{CO_2}}{dt} = 4\pi D_{CO_2,mat} \frac{r_i r_o}{r_o - r_i} c_{CO_2,i} \tag{4.5}$$

where m_{CO2} is the mass of CO_2 in the pellet, $D_{CO2,mat}$ is the diffusivity of CO_2 through the shell material, and $c_{CO2,i}$ is the concentration of CO_2 in the shell material at the CO_2 hydrate-shell interface. The concentration of CO_2 at the interface is given by the solubility of CO_2 in the material at the ice-CO_2 hydrate equilibrium pressure. The concentration of CO_2 in the material at the outer radius is assumed to be zero.

An estimate of the time for complete CO_2 loss through an ice shell on a spherical pellet can be obtained using equations 4.4 and 4.5. The minimum shell thickness is calculated using

Eq. 4.4. For a pellet at 258 K, the internal pressure P_i should be 5.9 bar. The external pressure, P_o is assumed to be 1.01 bar. The maximum stress an ice shell can withstand without cracking depends on the grain size, temperature, strain rate and ice volume. The maximum tensile stress of ice is 0.7-3.1 MPa, at 253-263 K (Petrovic, 2003); the lowest value in the range is used to provide a conservative estimate of the minimum shell thickness (σ_{mat}=0.7 MPa). The CO_2 loss rate is calculated according to Eq. 4.5. The diffusivity of CO_2 in ice at 258 K is typically reported at 10^{-14} m^2/s (Rhode & Price, 2007), though Ikeda-Fukazawa et al. (2004) predict $4x10^{-10}$ m^2/s based on molecular dynamics simulations. The faster diffusivity is used in this calculation to give a conservative estimate of the time to lose all of the CO_2. The CO_2 concentration in ice, $c_{CO2,i}$, at 258 K and 5.9 bar is $5x10^{-9}$ mole per mole of ice (Rohde, 2007) or 0.0026 mol CO_2 per cubic meter of ice. The initial mass of CO_2 in the pellet is calculated by assuming 50% of the pellet volume is CO_2 hydrate with a CO_2 density of 296 kg/m^3. The time to lose CO_2 using these parameters is shown in the topmost traces in Figure 4-8, for a range of shell thicknesses and two pellet diameters. The CO_2 loss rate decreases with increasing shell thickness. CO_2 loss is faster with smaller pellets, due to the increased surface area to volume ratio, but the minimum shell thickness for mechanical stability increases with increasing pellet size. A 0.01m pellet with the minimum thickness shell for mechanical stability would lose less than 0.5% of its initial CO_2 content in one year.

While the predicted slow CO_2 loss through an ice shell seems promising, the topmost traces in Figure 4-8 do not account for grain boundaries in the ice shell. CO_2 diffusivity along grain boundaries may be several orders of magnitude faster than in the ice matrix and CO_2 solubility in a quasi-liquid boundary layer is much higher than CO_2 solubility in ice. As an upper bound, the time to lose CO_2 is also calculated assuming 1% of the shell surface is grain boundaries in which the CO_2 solubility and diffusivity are similar to that in water at 273 K. The CO_2 solubility in water at 273 K, 5.9 bar is $7.7x10^{-3}$ mol CO_2/mol water or 432 mol CO_2 per cubic meter (Diamond & Akinfiev, 2003). The diffusivity is 10^{-10} m^2/s. The results are shown in the lower traces of Figure 4-8. Using the above estimate for CO_2 loss through grain boundaries in the ice shell, the time to lose CO_2 in a 0.01 m pellet is on the order of 100 days, which is close to the typical shelf life of frozen confections. Therefore a pellet with the minimum thickness shell could lose a significant fraction of CO_2 while in storage. The

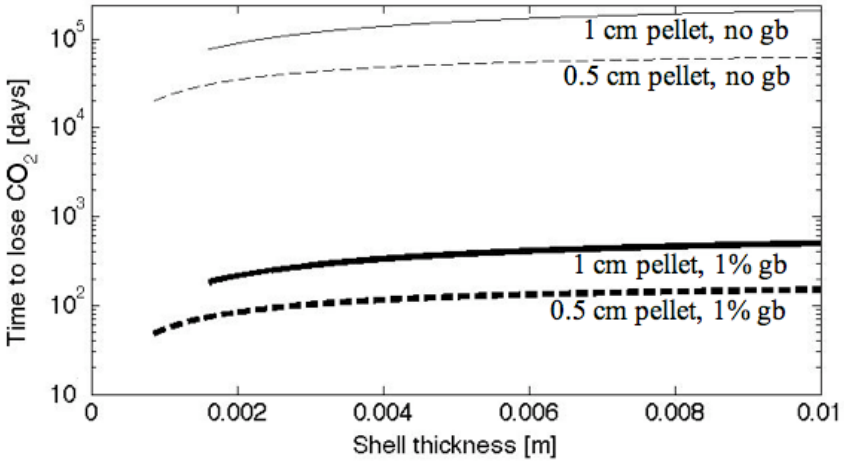

Figure 4-8 Time to lose CO_2 from a pellet with an ice shell as a function of shell thickness, pellet diameter, and grain boundary (gb) area of shell surface.

thickness of the shell is limited by the ice thickness that consumers can comfortably bite into. The cut-off chosen here is 1 cm, but this is surely unpleasantly thick.

In practice, formation of a sealed shell presents some challenges. If any part of the shell is formed from a liquid phase, CO_2 hydrates can dissociate while the shell material is freezing and form vent paths through the shell as it freezes. Additionally, the heat released due to the phase change in the shell may enhance CO_2 hydrate dissociation at the surface of the pellet. The pellet could be pre-cooled in a liquid N_2 bath before it is coated, but the coating material would need to withstand the volume changes associated with the severe temperature changes. Thus, an effective coating process is necessary in addition to finding a material that provides the required coating properties.

Based on the above discussion, coating a pellet of compressed powder to provide CO_2 hydrate stability is not easy. An edible material must be found or developed that has a high maximum tensile stress at typical freezer temperatures and a low CO_2 solubility and permeability. A process to seal the shell around the pellet despite CO_2 hydrate dissociation during sealing must also be developed. Of course, coatings that enhance the visual appearance of the pellets and or the textures in the CO_2 hydrate confection, but do not improve CO_2 hydrate stability could be developed more easily. The main concerns would be the coating application process and any interaction between the coating and CO_2 hydrates or CO_2 gas.

5 Shelf-life and heat shock

In packaged ice confections, isothermal recrystallization and temperature variations during storage change the structure of the ice confection, including the crystal size distribution and total crystalline mass fraction. In this chapter, recrystallization and heat shock in CO_2 hydrate confections are discussed in comparison to standard ice confections. CO_2 hydrates recrystallize in a manner similar to ice, but the transport processes are slower, which may reduce the total recrystallization during the shelf life of a CO_2 hydrate confection. Heat shock causes CO_2 hydrates to dissociate as well as causing ice to melt. This CO_2 hydrate dissociation can increase the pressure in a storage vessel significantly. In contrast to a standard ice confection where the mass fraction of crystalline water is essentially a function of temperature only, the mass fraction of crystalline water in a CO_2 hydrate confection increases both with increasing pressure and with decreasing temperature. This pressure effect can be used to mitigate heat shock damage by increasing the fraction of water that remains crystalline at higher temperature. The CO_2 hydrates that dissociate during heat shock can re-form when the product is subsequently cooled, but the extent of re-formation depends on the porosity of the heat-shocked confection and retention (by the container) of CO_2 while it is in the gas phase. Due to the different response to heat shock of CO_2 hydrate confections, compared to ice confections, packaging for a CO_2 hydrate confection must withstand elevated pressures or mitigate the pressure increase, for example by venting gas.

5.1 Recrystallization

A comparison of CO_2 hydrate and ice recrystallization under isothermal conditions requires knowledge of many parameters related to CO_2 hydrates that have not yet been measured. Recrystallization processes in gas hydrates and ice should be similar because both structures form by hydrogen bonding of water molecules and water can be transported to the growing crystal through the aqueous or vapor phase, which is similar in either system[1]. On the other hand, growth of CO_2 hydrate crystals may be slower than growth of ice crystals if:

1) the CO_2 hydrate surface reactions are slower than ice surface reactions and slower than the rate of transport of molecules to the growing crystal surface;
2) surface, bulk or grain boundary diffusion is slower in CO_2 hydrate than in ice and vapor or aqueous phase transport is inhibited; or
3) the surface energy of CO_2 hydrate is lower than the surface energy of ice.

Growth of CO_2 hydrate requires CO_2 molecules to associate with cage sites and water molecules to arrange around the CO_2 molecules. The kinetics of these steps may be slower than the kinetics of water molecules simply forming hydrogen bonds at the ice surface. Also, the enthalpy of dissociation of CO_2 hydrate per mole of water is larger than the enthalpy of fusion of ice, so a larger magnitude of heat transfer is involved in evaporation and

[1] Water transport through the vapor phase should be slightly slower at high CO_2 pressure. Diffusivity of a gas decreases with increasing pressure and the water vapor pressure in equilibrium with CO_2 hydrate decreases with increasing CO_2 pressure.

condensation reactions. Surface diffusivity and grain boundary diffusivity in CO_2 hydrates are not known, but bulk diffusivity of water in gas hydrate is two orders of magnitude slower than in ice (Sloan & Koh, 2008). The surface energy of CO_2 hydrate-vapor interfaces is not known. It may be similar to the surface energy of ice-vapor interfaces because the crystal-liquid interfacial energies are similar. The CO_2 hydrate-water and ice-water interfacial energies are both 30 mJ/m^2 (Anderson et al., 2003), and the ice-vapor interfacial energy is 109 mJ/m^2 (Blackford, 2007). Surface energy is related to the latent heat of fusion and the number of missing bonds at the surface of a crystal, but these differences between CO_2 hydrate and ice are present in the crystal-liquid interface without causing a difference in surface tension, so should be similarly matched in the crystal-vapor interface.

Recrystallization involves many processes to reduce the interfacial energy of the system. These processes include isomass rounding, accretion, and migration of molecules from smaller crystals to larger crystals due to differences in vapor pressure or solubility as a function of surface curvature. Information about recrystallization in frozen water systems is applicable to recrystallization with CO_2 hydrates. In snow with no aqueous phase, vapor transport between crystals typically exceeds other water transport mechanisms because the vapor pressure of ice is high (Blackford, 2007). In the presence of an aqueous phase, sintering of snow is significantly faster due to convective transport in the aqueous phase. In the presence of a temperature gradient, sintering of snow is even faster because water vapor concentration gradients are induced (Blackford, 2007). Increasing temperature increases the rate of sintering due to the Arrhenius-type temperature dependence of the surface reactions and molecular transport mechanisms. The rate-limiting step for crystal growth can change with temperature. Fernandez et al. (2008) suggested, based on experiments with a frozen salt solution, that at temperatures greater than 260 K recrystallization is limited by the surface reaction rate, whereas at temperatures between 253 and 260 K recrystallization is limited by migration of water molecules through the bulk. Recrystallization in frozen foods can be slowed by a high concentration of gelatin or soluble substances that significantly increase the viscosity (Fernandez et al., 2008) and modify water mobility.

Recrystallization in systems with CO_2 hydrate and ice is different from systems with only ice solid phase because: CO_2 hydrates and ice can exchange water, the CO_2 hydrate-ice interface affects to the total surface energy, and CO_2 gas bubbles can be removed by diffusion of CO_2 through ice to growing CO_2 hydrate grains. CO_2 hydrates and ice can exchange water because water dissolved from small ice crystals can be incorporated at the surface of larger CO_2 hydrate crystals. However, in order to maintain the ice-CO_2 hydrate equilibrium pressure ice crystals must grow at the expense of CO_2 hydrates at another location in the container. The CO_2 hydrate-ice interfacial energy is the same as the ice-ice grain boundary energy, 65 mJ/m^2 (Salamatin et al., 2003; Zhang et al., 2002; Blackford, 2007). Therefore ice can share a grain boundary with CO_2 hydrate as easily as with another ice crystal, but eventually as grains coarsen the phases will separate. Assuming the CO_2 hydrate-vapor interfacial energy is equal to the ice-vapor interfacial energy (109 mJ/m^2), the overall surface energy of the system can be reduced by ice and CO_2 hydrate forming one large particle compared to two separate particles in vapor. This is not, however, the case in a continuous aqueous phase, where the surface energy is reduced if the separate particles are surrounded by liquid. The surface energy associated with a CO_2 hydrate-water interface is the same as the surface energy associated with an ice-water interface (30 mJ/m^2), so the crystalline-aqueous interface does not contribute to differences in recrystallization.

Recrystallization of gas hydrates has been observed in several systems. Tohidi et al. (2001) observed agglomeration of CH_4 hydrate crystals in the presence of excess water and suggested the process was driven by surface energy minimization, similar to Ostwald ripening in ice. The recrystallization was observed over 2 days in storage at 269 K. Salamatin et al. (2003) and Uchida et al. (1994) observed coarsening of air clathrate-hydrates in polar ice-sheets. The crystal growth is controlled by oxygen and nitrogen diffusion through the ice sheet (Salamatin et al., 2003).

In contrast, in a dry system Kuhs et al. (2000) observed that the mesoporous microstructure of gas hydrate crystals formed by reaction of ice particles with hydrate forming gas was stable for several months. Kuhs et al. packed an ice powder with a typical grain size of a few hundred micrometers to 70% filling in a gas pressure cell. The pressure cell was equilibrated at a temperature between 243 and 273 K and pressurized with Ar, N_2, O_2, CH_4, or CO_2 to a pressure between the decomposition pressure and 100 MPa. The gas hydrate formation was allowed to proceed for several days to several weeks in order to reach greater than 90% transformation of ice to gas hydrate. Some of the samples were then stored at close to 273 K and a pressure slightly higher than the ice-gas hydrate equilibrium pressure for several months. At various stages of formation and storage the samples were observed using a field-emission scanning electron microscope with a cryo-stage and it was found that the bulk of the gas hydrate formed was porous on a submicron level and the porous structure was not altered over several months of storage at close to 273 K. While the results of Kuhs et al. are intriguing, they apply to a system with no aqueous phase, whereas there is always an aqueous phase in a frozen confection.

As a first approximation, recrystallization in confections containing CO_2 hydrates is similar to recrystallization in conventional ice confections. Crystals agglomerate and water molecules migrate from small crystals to large crystals to reduce the energy of the system. The rate of recrystallization increases with increasing temperature and increasing water mobility in the aqueous phase. It is possible that recrystallization in CO_2 hydrate systems is slower than in ice systems because the surface reaction is more complicated (more molecules are involved) and surface diffusion rates may be slower (water diffusion through the bulk is slower in CO_2 hydrates than in ice). The kinetics of water and CO_2 incorporation at a CO_2 hydrate surface are not well known, so studies of recrystallization in systems containing CO_2 hydrates are needed to determine the extent of reduction in recrystallization rate. Qualitatively, samples of CO_2 hydrate confections produced from flash-freezing powder did not recrystallize significantly after two weeks to one month of storage. Slower recrystallization would provide an advantage for the shelf life of CO_2 hydrate confections, but use of stabilizers is still likely to be necessary. Stabilizers that work in ice confections may be appropriate in CO_2 hydrate confections, but should be checked for interaction with CO_2 and response to pressure changes on a case-by-case basis.

5.2 Aqueous phase total solids concentration

The equilibrium concentration of total solids in the aqueous phase, or conversely the fraction of water that is crystallized, is a function of both pressure and temperature. The fraction of water that is crystallized in an ice confection at fixed temperature decreases with increasing pressure due to increasing CO_2 solubility in the aqueous phase (this will be discussed further

in the following paragraphs). Therefore the fraction of water crystallized in a CO_2 hydrate confection at ice-CO_2 hydrate equilibrium pressure is always lower than the fraction of water crystallized in the same ice confection at atmospheric pressure (for temperatures below the ice-CO_2 hydrate-aqueous phase-gas quadruple point). It will be shown that this effect is very small at typical freezer temperatures. In contrast, as pressure increases above the ice-CO_2 hydrate equilibrium pressure at a fixed temperature, the fraction of water that is crystallized increases until the aqueous phase becomes too viscous for further crystallization. It will be shown that the fraction of water crystallized can be increased above the fraction of water that is crystallized at atmospheric pressure. Therefore it is possible to cause a larger fraction of water in a CO_2 hydrate confection to crystallize than in an ice confection of the same recipe at the same temperature. This could be used to reduce the amount of melting of crystalline water during temperature cycling. Understanding the effect of temperature and pressure on the fraction of water that is crystalline in a CO_2 hydrate confection is also important for predicting the pressure evolution during heat shock, which will be discussed in the next section.

In an ice confection at a fixed temperature, the fraction of water that is crystallized decreases with increasing pressure. This occurs because at equilibrium, in both a conventional ice confection and an ice confection containing CO_2 hydrates, the chemical potential of water in the aqueous phase must be the same as the chemical potential of water in the solid phase. The chemical potential of water in the aqueous phase is given by

$$\mu_{w,aq} = \mu_{w,l}^{0} + RT\ln(\gamma_w x_w), \tag{5.1}$$

where T is the temperature, $\mu_{w,l}^{0}$ is the chemical potential of pure liquid water at T, R is the universal gas constant, γ_w is the activity coefficient of water, and x_w is the mole fraction of water in solution (Denbigh, 1981). Below 273 K, the chemical potential of pure liquid water is larger than the chemical potential of solid water, so the mole fraction of water in the aqueous phase must be less than one for the aqueous phase and ice to be in equilibrium.

In a conventional ice confection, the mole fraction of water in the aqueous phase is decreased by the dissolved solutes in the mixture. Under CO_2 pressure, the mole fraction of water in the aqueous phase is also decreased by dissolved CO_2. The recipe fixes the total solids content of the ice confection, but the amount of CO_2 dissolved in the aqueous phase increases with pressure. For any temperature and recipe, more water must be present in the aqueous phase at ice-CO_2 hydrate equilibrium pressure than at atmospheric pressure in order to achieve the same water mole fraction, and thus chemical equilibrium between water in the aqueous phase and ice. Therefore the total solids concentration in the aqueous phase in equilibrium with CO_2 hydrate and ice is lower than the total solids concentration at atmospheric pressure, and less water is crystallized for a particular recipe.

The decrease in total solids concentration in the aqueous phase at CO_2 hydrate equilibrium pressure is small. The change in crystallized water fraction can be estimated using the equation for the freezing point depression of an ideal solution. The freezing point of a solvent is related to the mole fraction of solvent in the solution by

$$\ln\left(\frac{1}{x_w}\right) = \frac{h_{sf} - \Delta c_p T_M}{R}\left(\frac{1}{T} - \frac{1}{T_M}\right) + \frac{\Delta c_p}{R}\ln\left(\frac{T_M}{T}\right), \tag{5.2}$$

where T_M is the melting temperature of the pure solvent, h_{sf} is the enthalpy of melting (on a molar basis) at T_M, Δc_p is the difference between the heat capacity of water in liquid and solid phase (on a molar basis), x_w is the mole fraction of water, and T is the freezing point of the

solution of concentration x_w (Denbigh, 1981). According to this ideal model, when the freezing point is 258 K the mole fraction of water in the aqueous phase is 0.86. The corresponding crystallized water fraction is 0.89 in a 25% sucrose recipe at atmospheric pressure. The crystallized water fraction in the same recipe at the equilibrium pressure for CO_2 hydrates is 0.87, assuming a CO_2 solubility of 0.015 mol CO_2/mol H_2O (Diamond & Akinfiev, 2003). The actual extent of crystallization both at atmospheric pressure and at CO_2 hydrate equilibrium pressure is probably smaller. The theoretical sucrose concentration at 258 K is 75%, but Blond et al. (1997) measured an actual concentration of 65% (x_w =0.91), indicating that more water remains in the aqueous phase than predicted. Regardless, at ice-CO_2 hydrate equilibrium pressure the fraction of water crystallized is slightly less than the fraction crystallized at atmospheric pressure.

In contrast, in a CO_2 hydrate confection, the (dissolved) total solids concentration in the aqueous phase increases with increasing CO_2 pressure at a fixed temperature. This can be seen by considering the chemical potential of water in equilibrium with CO_2 hydrates, which is given by the reaction equilibrium for CO_2 hydrates,

$$\mu_{CO_2} + n\mu_w = \mu_{hyd}, \tag{5.3}$$

where μ_{CO_2} is the chemical potential of gaseous CO_2, μ_w is the chemical potential of solid water, μ_{hyd} is the chemical potential of CO_2 hydrates, and n is the mole ratio of water to CO_2 in the CO_2 hydrates. When the pressure and or temperature of a CO_2 hydrate-aqueous phase-gas system is changed, the change in the chemical potential of water is related to the changes in chemical potential of CO_2 hydrate and CO_2 gas by

$$\Delta\mu_w = \frac{\Delta\mu_{hyd} - \Delta\mu_{CO_2}}{n}, \tag{5.4}$$

assuming that n is approximately constant. If the pressure is increased at constant temperature, the change in chemical potential of a pure substance can be calculated using a result of the Gibbs-Duhem equation,

$$\left.\frac{d\mu}{dp}\right|_T = v, \tag{5.5a}$$

where v is the molar volume of the substance (Denbigh, 1981). For an isothermal increase in pressure the change in chemical potential of a pure substance is then

$$\Delta\mu = v \times \Delta P. \tag{5.5b}$$

The molar volume of solids is much less than the molar volume of gases. Therefore, using Eq. 5.5b to estimate $\Delta\mu_{hyd}$ and $\Delta\mu_{CO_2}$, the right-hand side of equation 5.4 must be negative; the increase in chemical potential of CO_2 hydrate is much less than the increase in chemical potential of CO_2 gas. In this case, the left-hand side of equation 5.4 (the change in chemical potential of water) must also be negative. (Of course, the chemical potential of a hypothetical pure water phase increases with increasing pressure according to Eq. 5.5.) In order to lower the chemical potential of water in the aqueous phase sufficiently to achieve equilibrium as pressure increases, the aqueous phase solute concentration must increase. This is achieved by a combination of increased CO_2 concentration in the aqueous phase and removal of water from the aqueous phase to the CO_2 hydrate phase.

The fraction of water that is crystallized at a pressure greater than the CO_2 equilibrium pressure can be estimated using several idealizations. CO_2 is treated as an ideal gas, the molar volumes of water and CO_2 hydrate are treated as constant, the aqueous phase is treated as an ideal solution (γ_w=1), and the solubility of CO_2 in the aqueous phase is assumed to be equal to

the solubility of CO_2 in pure water. The water mole fraction in the aqueous phase at the desired pressure, $x_w(P)$, can be related to the water mole fraction in the aqueous phase at the ice-CO_2 hydrate equilibrium pressure, $x_w(P_{eq})$ and the change in chemical potential of water, $\Delta\mu_w$, by

$$\Delta\mu_w = \Delta\mu_w^o + RT\ln\left(\frac{x_w(P)}{x_w(P_{eq})}\right), \tag{5.6}$$

where $\Delta\mu_w^o$ is the change in chemical potential of hypothetical pure water and R is the universal gas constant. The terms $\Delta\mu_{hyd}$, $\Delta\mu_{CO_2}$ and $\Delta\mu_w^o$ in equations 5.4 and 5.6 are calculated according to Eq. 5.5. The fraction of water crystallized is found by determining the amount of water that must remain in the aqueous phase in order to achieve $x_w(P)$, accounting for both the mole fraction of solutes in the recipe and the mole fraction of dissolved CO_2. The resulting equation for the fraction of water crystallized, f_{xtal}, is

$$f_{xtal} = \frac{x_w}{1 - x_w - x_w\left(\frac{x_{CO_2}}{1 - x_{CO_2}}\right)}\left(1 - \frac{\mathrm{TS}/M_{suc}}{(1-\mathrm{TS})/M_w}\right), \tag{5.7}$$

where x_{CO_2} is the solubility of CO_2 in the water in the aqueous phase, TS is the mass fraction of solute in the recipe, M_{suc} is the molar mass of the solute (sucrose in this case), and M_w is the molar mass of water.

Using equations 5.1 through 5.7 the ideal fraction of water crystallized in a sucrose solution is calculated and plotted in Figure 5-1 at atmospheric pressure, ice-CO_2 hydrate equilibrium pressure, and two higher pressures. The plots show several important trends. As discussed above, the fraction of water crystallized at ice-CO_2 hydrate equilibrium pressure is lower than the fraction crystallized at atmospheric pressure, but the fraction of water crystallized increases with pressure above the ice-CO_2 hydrate equilibrium pressure. As expected, the fraction of water crystallized increases with decreasing temperature (as well as decreasing sucrose concentration). Thus in a system with CO_2 hydrates, freeze concentration occurs both with decrease in temperature and with increase in pressure.

Due to the idealizations used in equations 5.1-5.7, the curves in Figure 5-1 only show a theoretical fraction of water crystallized. In particular, the solubility of CO_2 in the aqueous phase is taken from Diamond and Akinfiev's (2003) data for CO_2 solubility in pure water. The actual CO_2 solubility is lower, both due to sucrose in the aqueous phase and due to the presence of CO_2 hydrates. The lower solubility would be expected to increase the predicted fraction of water crystallized. However, the effect of sucrose and CO_2 on the activity coefficient of water (γ_w) in the aqueous phase has been neglected. Including γ_w in the calculations would decrease the predicted fraction of water crystallized. As mentioned earlier in this section, the actual fraction of water crystallized in an ice confection is typically found to be lower than the theoretical fraction, especially at low temperatures where the sucrose concentration is high in the aqueous phase. Thus the actual fraction of water crystallized in the CO_2 hydrate confection is also likely to be lower than predicted.

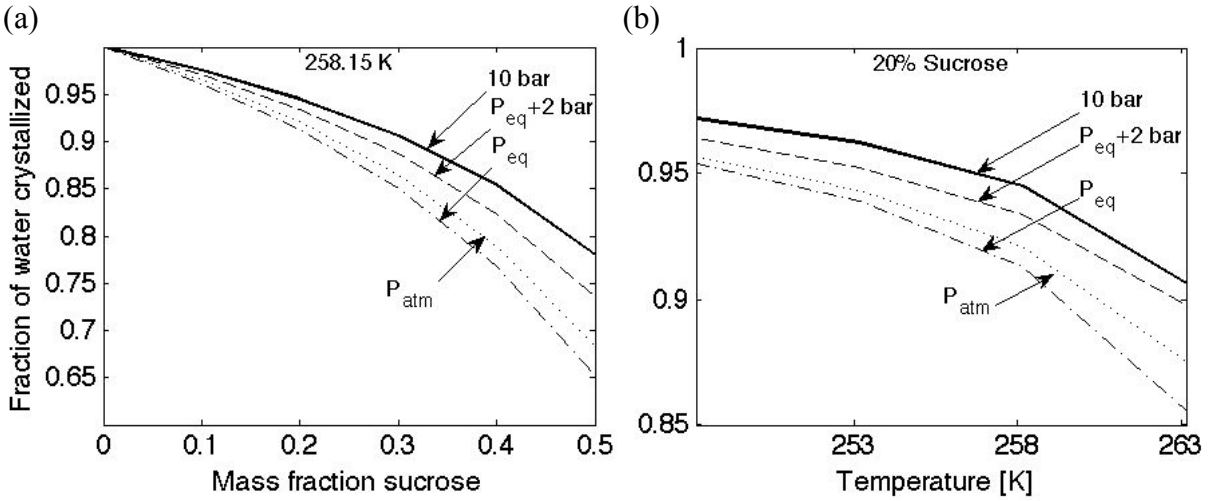

Figure 5-1 Ideal fraction of water crystallized (ice and or CO_2 hydrates) as a function of pressure and (a) sucrose mass fraction or (b) temperature. (Plots represent trends correctly, but not the actual crystallized fraction because the crystallized fractions here are calculated using several idealizations.)

5.3 Heat shock

In a product containing CO_2 hydrates, heat shock can cause both dissociation of CO_2 hydrates and melting of ice (if present). Dissociation of CO_2 hydrates can increase the storage vessel pressure significantly during heat shock, but this pressure increase can reduce the impact of heat shock on the microstructure of the product by increasing the fraction of water that remains crystallized, as explained in section 5.2. Typically, frozen desserts are stored in a warehouse and transported in freezers maintaining temperatures near 253 K, but retail cabinets and home freezers are at temperatures from 258 to 260 K and during transport in a consumer vehicle from the grocery store to home the ambient temperature is around 294 K (Marshall et al., 2003).

The pressure increase during heat shock depends on the recipe, the total CO_2 content in the package and the gas phase volume in the package (headspace). As the product warms, CO_2 hydrates will dissociate until the equilibrium pressure for CO_2 hydrates at the new temperature is reached and the chemical potential of the water in all phases matches the reaction equilibrium described in section 5.2. If the container volume is much greater than the product volume, the pressure will increase along the ice-CO_2 hydrate equilibrium curve until all of the CO_2 hydrates dissociate. After all of the CO_2 hydrates dissociate the pressure in the container will increase in proportion to temperature, similar to an ideal gas, although CO_2 solubility in the aqueous phase will slightly modify the pressure increase.

If no ice is present, CO_2 hydrates will dissociate as the product warms, even if the pressure is greater than the ice-CO_2 hydrate equilibrium pressure. In an ice confection, as the temperature increases ice melts to decrease the total solids concentration, following the freezing equilibrium curve of the mixture. Similarly, as temperature increases in a CO_2 hydrate confection, water must be provided from the crystalline phase to decrease the total solids concentration so that equilibrium is maintained between water in the aqueous phase and

water in the crystalline phase. If ice is not available to provide this water, CO_2 hydrates will dissociate, which can lead to a pressure in the storage vessel that is greater than the ice-CO_2 hydrate equilibrium pressure if there is little headspace.

Dissociation of CO_2 hydrates above ice-CO_2 hydrate equilibrium pressure has been confirmed by monitoring the change in mass and pressure as a powder sample is warmed from 251 to 262 K. In the experiment, a sample can containing flash-freezing powder is placed in the PTM, which was previously described in section 1.4, and the PTM is sealed. The CO_2 cylinder connected to the PTM is used to maintain the pressure at more than 8 bars until the mass of the sample stops increasing. This ensures that the powder is fully saturated with CO_2 hydrates before heat shock. Then the CO_2 supply line is closed and the freezer temperature is set to 261 K. Figure 5-2 shows the subsequent pressure, temperature and mass evolution as the CO_2 hydrate-saturated powder warms to 261 K. The mass of the sample decreases by more than 2 g, even though the pressure in the PTM is more than 2 bars in excess of the ice-CO_2 hydrate equilibrium pressure at all times. This mass decrease indicates that CO_2 hydrates dissociate until water in the aqueous phase is in equilibrium with water in the crystalline phase.

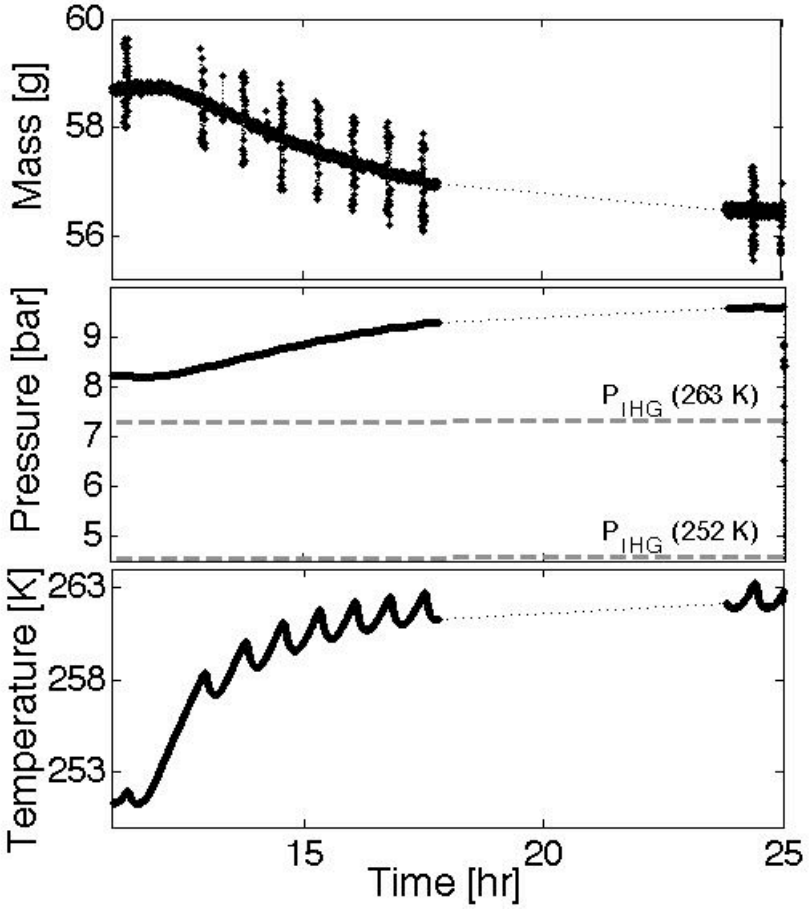

Figure 5-2 Heat shock of 25% sucrose powder at high CO_2 pressure. Gray dashed lines show Ice-CO_2 hydrate-Gas equilibrium pressure at coldest and warmest temperature of trial; sample pressure is always in excess of equilibrium pressure.

There are a few extraneous features in the data shown in Figure 5-2. The periodic spikes in the mass data show the vibrations caused by the freezer compressor, which cycles on and off. The small oscillation in temperature is due to warming between compressor cycles. There is no data between hour 18 and hour 23 because the data acquisition system quit and had to be restarted.

The pressure developed in the container during heat shock will affect the amount of water that leaves the crystalline phase (as described in section 5.2). In an ice confection with CO_2 hydrate it is possible to have water in a solid phase at temperatures up to 283 K if the pressure reaches 25 bars (see Figure 2-5). In a conventional ice confection, no solid phase would be present above the freezing point depression of the recipe, typically 271 K. The damage to the product structure during heat shock would be reduced when a larger solid water fraction persists. This reduction of heat shock damage is intriguing, but can only occur if the storage vessel is designed to safely handle pressures approaching 25 bar without leaking.

Short duration heat shock may also cause less damage in a product containing CO_2 hydrate compared to conventional ice confections because CO_2 hydrate dissociation to ice and gas is an endothermic process. This additional enthalpy sink should reduce the rate at which the product temperature increases.

Dissociation of CO_2 hydrates can cause the product to shrink. The volume of ice resulting from dissociation of CO_2 hydrate could be as little as 86% of the initial CO_2 hydrate volume because the density of water in CO_2 hydrates (800 kg/m^3) is smaller than the density of ice (920 kg/m^3). However, CO_2 hydrate can dissociate to a porous structure, so that the overall volume of the solid material does not change significantly until recrystallization processes have had time to proceed. This porous structure maintains surface area for re-formation of CO_2 hydrate when the temperature is reduced.

Changes in CO_2 pressure due to CO_2 hydrate equilibrium will also affect the aqueous phase. If the aqueous phase has glassy qualities and surrounds the CO_2 hydrates it may crack as the ice-CO_2 hydrate equilibrium pressure increases internally. If an aqueous phase with higher water mobility surrounds the CO_2 hydrate particle, CO_2 from the dissociating CO_2 hydrates will diffuse through the aqueous phase until the chemical potential of CO_2 is equal in the aqueous phase, the vapor phase, and the CO_2 hydrates. CO_2 solubility in the aqueous phase increases during heat shock due to increasing pressure and dilution of the aqueous phase. CO_2 diffusivity in the aqueous phase increases with increasing temperature both due to the lower aqueous phase viscosity (which is enhanced by dilution of the aqueous phase) and due to the increase in molecular kinetic energy. Thus CO_2 transport to the headspace of the storage vessel speeds up with increasing temperature. The aqueous phase does not protect CO_2 hydrates against heat shock.

CO_2 hydrates can re-form when the product is subsequently cooled. Heat shock can provide re-homogenization of CO_2 distribution because, for the majority of the re-formation process, the pressure is greater than the ice-CO_2 hydrate equilibrium pressure everywhere in container, even if there are small temperature gradients. If no CO_2 leaks from the storage vessel, it may be possible to re-form all of the CO_2 hydrates that were initially present in the storage vessel. However, CO_2 hydrate re-formation will be hindered if the surface area of the product is reduced due to shrinkage of the product and recrystallization processes that occurred during heat shock. Quiescent formation of CO_2 hydrate from large particles or liquid droplets is very slow because a CO_2 hydrate shell forms on the surface of the droplet and impedes CO_2 transport to the core of the droplet or ice particle.

Samples of flash-freezing powder and pellets formed from flash-freezing powder were subjected to thermal cycling to demonstrate CO_2 hydrate dissociation and re-formation. Powder or pellets were placed in the PTM sample can and the PTM was pressurized and sealed. After several hours, when the mass, temperature and pressure had stabilized, the freezer temperature was increased. After several more hours, when the system had stabilized at the warmer temperature, the freezer temperature was decreased to its original value. Figure 5-3 shows the mass, temperature and pressure during one test with powder and one test with pellets.

In Figure 5-3a the pressurization of the powder can be seen as the vertical line on the y-axis of the bottom graph. The sample mass initially decreases slightly and then increases to a stable value while the pressure initially increases slightly and then decreases to a stable value. This small oscillation may be due to dry ice sublimating from the fresh powder and then forming CO_2 hydrates. For the first temperature cycle, the freezer is warmed from 245 to 255 K. The pressure and mass increase and decrease, respectively, toward stable values as the sample warms. Due to the warming CO_2 hydrates dissociate until the pressure in the PTM is equal to the ice-CO_2 hydrate equilibrium pressure. At hour 50 the freezer temperature is re-set to 245 K. The mass decreases to its original value and the pressure increases to its original value. A second temperature cycle is initiated near hour 75 by increasing the freezer temperature to 261 K. The CO_2 hydrates again dissociate and the pressure concurrently increases. The stable pressure at 261 K does not reach the ice-CO_2 hydrate equilibrium pressure because there is not enough CO_2 in the PTM. Thus the mass at hour 100 indicates the mass of the sample without any CO_2 in it. Finally, the temperature is returned to 245 K and CO_2 hydrates re-form, causing the mass and pressure to return to their original values. In both temperature cycles, CO_2 hydrates are completely re-formed.

In Figure 5-3b the pressurization of the pellets is not shown because an initial temperature cycle was carried out with insufficient CO_2 and there were problems with the sealing of the PTM. At the start of the cycle shown in Figure 5-3b the mass, temperature and pressure are already stabilized at 254 K. The temperature in the freezer is then set to 267 K (erroneously) and reduced to 264 K around hour 25. Due to the warming, pressure in the PTM increases and the mass of the sample decreases. After the mass, temperature and pressure stabilize at 264 K the temperature is returned to 254 K. Mass and pressure increase and decrease respectively, as expected, but much more slowly than in the powder test. The final stable mass is lower than the initial mass, which suggests that not all of the initial CO_2 hydrates in the pellets re-formed. However, there was also a slight pressure leak during this experiment, which reduced the amount of CO_2 available in the PTM to form CO_2 hydrates and therefore contributes to the incomplete re-formation. The time constant for re-formation of CO_2 hydrates in the pellet geometry is much longer than for dissociation. This suggests that the pellet becomes less permeable due to recrystallization. In these heat shock tests, recrystallization is likely to be more significant in the pellet test than in the powder test because the pellet test temperatures are higher than the powder test temperatures.

Based on the above discussion, packaging for CO_2 hydrate confections must be designed with careful attention to the pressure evolved during heat shock. The highest pressure that could be evolved in a sealed package would occur if the CO_2 hydrate confection melted completely, releasing most of the CO_2 to the gas phase (a small fraction would dissolve in the melted mixture). The magnitude of this pressure depends on the total CO_2 content in the package and the headspace in the package. As discussed in section 4.2, for a homogeneous

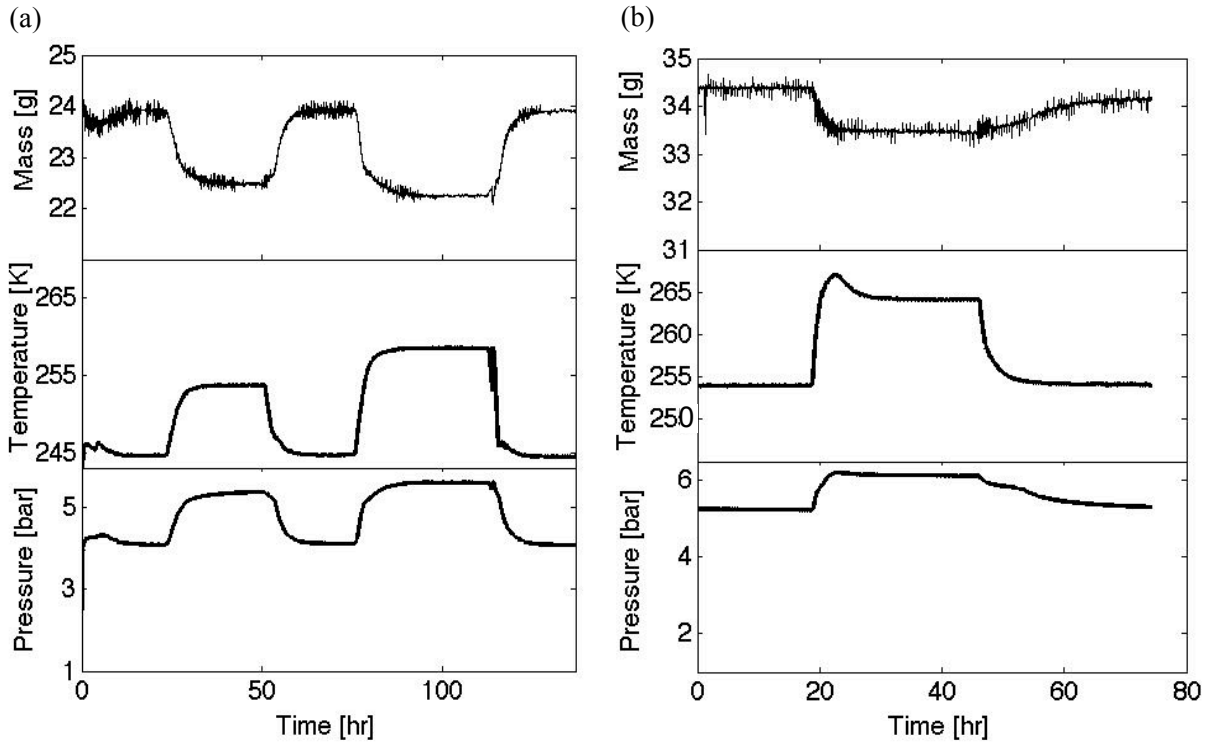

Figure 5-3 Pressure, temperature and mass of CO_2 hydrate confection sample during temperature cycling, demonstrating dissociation and reformation in (a) powder and (b) pellet.

product the total CO_2 content in the package must be enough to ensure that all crystallized water is CO_2 hydrate and to pressurize the package at the ice-CO_2 hydrate equilibrium pressure. This is a very large CO_2 content and for any reasonable package volume and filling level a pressure relief mechanism will be necessary to release CO_2 if the product is melted while sealed.

The maximum pressure attained in the package before CO_2 is vented can be chosen based on the temperature to which the confection should be able to be warmed without damage and the material properties of the package. The initial pressure in the package should be 5-6 bars, corresponding to stable CO_2 hydrates at 253 to 258 K. If the venting pressure is chosen to be low, for example 7 bars, then any small heat shock to the product, for example a temperature increase of 5 K, is likely to cause venting of CO_2. If CO_2 is released, there will not be enough CO_2 to re-form all CO_2 hydrates when the product is re-cooled. In contrast, if the venting pressure is high, for example 15 bars, the package can be designed with a small headspace, so that when heat shock occurs, a small amount of CO_2 hydrate dissociation increases the pressure in the package significantly, which decreases the amount of water that leaves the crystalline phase, and thus decreases the heat shock damage. All of the CO_2 released by dissociation would remain in the package and could be reabsorbed when the temperature is subsequently cooled. Design of an appropriate package for a CO_2 hydrate confection involves consideration of this trade-off.

(This page intentionally left blank.)

6 Eating CO_2 hydrate confections

Despite numerous patents describing addition of CO_2 hydrates to frozen foods (for example Bee, 1991; Gupta & Dimmel, 2003), there are no published studies of CO_2 hydrate dissociation in the mouth. Perception of CO_2 released from a gas hydrate structure is different from perception of CO_2 dissolved in carbonated beverages, fizzy yogurt or fizzy fruits. Due to the high concentration of CO_2 in CO_2 hydrate confections, CO_2 is detected both mechanically and chemically, whereas in carbonated beverages mechanical perception of CO_2 is of secondary importance (Green, 1992; Dessirier et al., 2000). Because the CO_2-water mole ratio of CO_2 hydrates is large compared to CO_2 solubility in water, a significant portion of the CO_2 in a CO_2 hydrate confection is likely to escape in the gas phase without being detected chemically. Based on preliminary sensory analysis, the CO_2 concentration in CO_2 hydrate confections must be higher than the concentration in soda to achieve the same perception of carbonation. However, the necessary CO_2 concentration for strong perception of carbonation (both chemical and mechanical) is significantly lower than the minimum CO_2 concentration to maintain a homogeneous product.

6.1 CO_2 perception

CO_2 in carbonated foods can be perceived through visual, audible, chemical and tactile stimulation. In the mouth, CO_2 in carbonated beverages is chiefly perceived by stimulation of cold-sensitive and chemical nociceptors (Green, 1992; Dessirier et al., 2000), rather than by tactile stimulation (i.e., bubbles bursting against the tongue). CO_2 stimulates cold-sensitive nociceptors (Green, 1992) and carbonic acid formed from CO_2 dissolved in water stimulates chemical nociceptors (Dessirier et al., 2000). Green (1992) showed that the perceived intensity of irritation increases with increasing CO_2 concentration up to at least 0.006 g CO_2/g solution. Green also showed that the perceived intensity increases with decreasing solution temperature in the range 297 to 277 K, at fixed CO_2 concentration.

Product temperature and mouth temperature influence nociceptor stimulation and enzyme activity related to CO_2 perception during consumption. Ice confections are typically 20 K cooler than refrigerated products. The tongue surface temperature is probably also colder during consumption of frozen foods compared to refrigerated foods because the frozen food is at a lower temperature and contains ice that must be melted. The instantaneous temperature at the interface between a piece of food and the tongue (or in a thin layer of saliva on the tongue) can be very roughly estimated by considering the interface temperature, T_m, upon contact between two semi-infinite solids initially at T_{food} and T_{tongue}. The interface temperature is given by

$$\frac{T_{food} - T_m}{T_m - T_{tongue}} = \sqrt{\frac{(k\rho c)_{tongue}}{(k\rho c)_{food}}}, \tag{6.1}$$

where k is thermal conductivity, ρ is density, and c is heat capacity (Mills, 1995). Modeling the tongue and the refrigerated food with the k, ρ, and c of water, the interface temperature while eating a refrigerated product would be 293.5 K for T_{food}=277 K and T_{tongue}=310 K

(normal body temperature). In contrast, with a frozen food melting of ice causes an extremely large effective heat capacity, so the temperature at the interface should approach the temperature of the phase change, a little less than 273 K. In reality, tongue motion and convection of saliva and food liquids will rapidly warm the food, but the above estimate gives an upper bound on the difference in mouth temperature between consumption of refrigerated and frozen foods. The temperature difference can be used to estimate the change in nociceptor stimulation between refrigerated and frozen foods.

Green (1992) made measurements of the intensity of irritation caused by CO_2 as a function of temperature and CO_2 concentration in water in the ranges 277-297 K and 0-6000 ppm CO_2 (by mass, 0.006 g CO_2/g solution). By considering the trends in Green's data, a rudimentary estimate can be made of the CO_2 concentration needed in a product at 258 K to match the perception of CO_2 in a refrigerated beverage. Figure 6-1 shows schematically Green's results for carbonated water at 297, 285 and 277 K. The intensity of irritation caused by CO_2 increases approximately linearly with CO_2 concentration and the rate of increase of intensity with CO_2 concentration is larger at cooler temperatures (in other words, the slope (ΔIntensity/ΔCO_2 concentration) increases with decreasing temperature). The dotted line in Figure 6-1 is an extrapolated (hypothetical) trend line for a carbonated product at 258 K. This line is based on assuming a linear relationship between the slope and temperature. In this case the CO_2 concentration necessary for the 258 K frozen confection to cause the same intensity of irritation as a refrigerated soda would be a little more than half the CO_2 concentration in soda. The trend at 258 K should be steeper than the trend at 277 K, but the actual slope is not known; in particular, it is possible that the stimulation of nociceptors by cold temperatures approaches a limit as the temperature drops below 273 K.

There are many differences between Green's experiments and the physical case where a frozen confection is consumed. For example Green's experiments involve carbonated liquids rather than partially solid products and, as discussed above, the tongue surface temperature during consumption of a frozen confection may be much colder than the tongue surface temperature in these experiments (i.e. T_m from Eq. 6.1 would be 293-303 K for Green's experiments, versus 273 K which was estimated for the frozen confection due to the melting of crystalline water). Thus it is not surprising that the CO_2 concentration necessary for

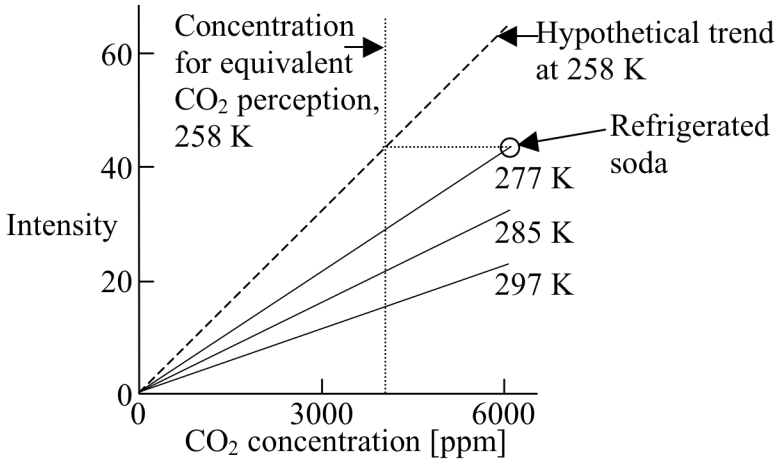

Figure 6-1 Schematic depiction of CO_2 irritation intensity as a function of CO_2 concentration and beverage temperature based on data from Green (1992). Solid lines represent trend of data from Green.

a CO_2 hydrate confection to match the perceived CO_2 intensity of a soda does not match this estimate. In fact, the necessary CO_2 concentration is much higher than half the CO_2 concentration in soda (this will be discussed further in section 6.3).

Chemical nociceptor stimulation requires carbonic acid. The reaction to form carbonic acid is catalyzed by carbonic anhydrase, an enzyme found in saliva (Murakami & Sly, 1987). Enzyme activity typically decreases with decreasing temperature, which should in turn decrease chemical stimulation that relies on enzyme catalyzation. Dessirier et al. (2000) showed that carbonic anhydrase is important for CO_2 perception on the tongue. In Dessirier's experiment, applying a carbonic anhydrase inhibitor, acetazolamide, to the tongue reduced the sensation caused by carbonated water. Carbonic anhydrase activity decreases exponentially with decreasing temperature and the activation energy is 4.69 kJ/mol in the temperature range 287-303 K (Sarraf et al., 2004). Using this activation energy it can be estimated that the specific activity of carbonic anhydrase at 273 K is 13% less than the specific activity at 293.5 K. The specific activity of an enzyme is the amount of product (in this case carbonic acid) the enzyme can make per unit time per mass of the enzyme (typical units are $\mu mol\ min^{-1}\ mg^{-1}$). A decrease in specific activity decreases the rate at which carbonic anhydrase can produce carbonic acid, so it could take longer for carbonic acid to be perceived in a frozen confection than in a beverage. Fortunately a frozen confection probably remains on the tongue longer than a beverage, which would allow all of the CO_2 that enters the saliva to be converted to carbonic acid while the confection is still in contact with the oral nociceptors. Possibly adding ingredients to the confection that increase salivation would improve chemical perception of CO_2 because the amount of carbonic anhydrase present in the mouth would be increased.

CO_2 can also be perceived in the mouth by bubble formation and bursting, which stimulates mechanoreceptors. In contrast to CO_2 perception in carbonated beverages, CO_2 perception in products containing CO_2 hydrates includes a strong element of bubble formation and bursting against the tongue and palate as the product melts in the mouth. Bubble formation and growth are controlled by the concentration of nucleation sites, the level of CO_2 supersaturation and surfactants in the recipe (Liger-Belair et al., 2008). There should be plenty of nucleation sites because bubbles can nucleate both on small gas pockets within the porosity of the confection and on surfaces in the mouth. The amount of CO_2 present when CO_2 hydrates dissociate in liquid is very high. If the CO_2 released by dissociation of CO_2 hydrates were trapped in the water released from the same CO_2 hydrates, the CO_2 concentration in that water would be 100 times the equilibrium solubility at atmospheric pressure and 273 K. Of course, CO_2 may also form bubbles in the freeze-concentrated aqueous phase and in saliva. The volume of gas at atmospheric pressure would be 149 times the volume of the original CO_2 hydrate. While bubbles cause a mechanical stimulation, Green (1992) suggested that bubbles could reduce the local chemical and thermal nociceptor stimulation by shielding the nociceptors from carbonated solution. In this case, the bubbles that are formed when a CO_2 hydrate confection is consumed would impede chemical perception of the CO_2 by the nociceptors. If it is the chemical stimulation that is required to match perception of carbonation in beverages, an increased CO_2 concentration may be needed.

6.2 CO_2 hydrate dissociation

CO_2 hydrate dissociation affects CO_2 perception. For CO_2 to be detected as carbonic acid it must be dissolved in water. When a carbonated beverage is consumed, CO_2 is already dissolved in the liquid. In contrast, when a CO_2 hydrate confection is consumed, most of the CO_2 is released from the crystal structure to the gas phase. The consumer will exhale the CO_2 that is released to the gas phase unless the gas dissolves in saliva or in the aqueous phase that forms as the crystalline phase of the confection melts. (Of course some CO_2 is already dissolved in the freeze-concentrated aqueous phase of the CO_2 hydrate confection, but it was shown in section 1.2 that this amount of CO_2 (0.75 g CO_2/kg solution) is small relative to the amount of CO_2 in a carbonated beverage (6 g CO_2/kg solution).) The amount of aqueous phase that is present as CO_2 hydrate dissociates depends on the details of the dissociation process. The typical model for gas hydrate dissociation is based on the assumption that the process is heat transfer limited. This model and the settings in which it has been successfully applied will be presented, as well as the implications of this model for CO_2 perception. However, experience with the flash-freezing powder suggests that the dissociation process is actually mass transfer limited. A new model will be described, which seems to be more appropriate for dissociation of CO_2 hydrates at atmospheric pressure. The implications of the mass-transfer limited model on CO_2 perception will also be discussed.

CO_2 hydrate dissociation at the time of consumption involves two steps. First, the confection is rapidly depressurized (by the consumer opening the packaging) and then the confection is heated (e.g. by contact with the consumer's tongue). For simplicity, the models are developed for a semi-infinite bulk of porous, pure CO_2 hydrate (the freeze concentrated aqueous phase is neglected). It is assumed that initially the CO_2 hydrate pellet is in a freezer at 253 K, in a storage vessel at 4.7 bars (the corresponding ice-CO_2 hydrate equilibrium pressure). After opening the storage vessel, the pellet is immediately placed on the tongue of the consumer, which is at 310 K. Only heat conduction from the tongue is considered.

In the heat-transfer limited model, as soon as the bulk is exposed to ambient pressure CO_2 hydrates begin to dissociate and continue to dissociate until the whole bulk is cooled to a temperature at which CO_2 hydrates are stable, namely the ice-CO_2 hydrate equilibrium temperature at one atmosphere, 218 K. (Note that CO_2 gas near the bulk will gradually mix with air, decreasing the CO_2 partial pressure and thus the equilibrium temperature. It is assumed that this effect can be neglected for this model because the dissociation occurs quickly and continuously; the associated flux of CO_2 gas away from the bulk should help maintain a local CO_2 atmosphere.) The fraction of CO_2 hydrate, f, that must dissociate to cool the bulk to the equilibrium temperature can be estimated according to

$$f = \frac{c_h(T_i - T_{eq})}{\Delta H_{ih}},$$

where c_h is the heat capacity of CO_2 hydrate, T_i is the initial temperature of the CO_2 hydrate, T_{eq} is the stable equilibrium temperature and ΔH_{ih} is the enthalpy of dissociation per kilogram CO_2 hydrate. CO_2 hydrates form a structure called sI (Sloan & Koh, 2008). The heat capacity of sI hydrates is typically 2080 J/kgK (Sloan & Koh, 2008). The enthalpy of dissociation of CO_2 hydrates is -23.8 kJ/mol hydrate (Anderson, 2003), which is -146 kJ/kg for CO_2 hydrates with a water to CO_2 molecular ratio of 6.6. Thus 50% of a CO_2 hydrate initially at 253 K must dissociate before the remaining material will reach 218 K. Because all

of the heat necessary for this dissociation comes internally from the bulk, the process should occur rapidly and spontaneously.

Following this spontaneous dissociation, the bulk remains 50% CO_2 hydrate, 50% ice (by water content) until heat transfer from the environment (and the consumer) causes further dissociation. Typically, the most significant heat flow should occur where the surface of the bulk comes into contact with the mouth of the consumer. Upon contact with the tongue, the temperature at the surface of the bulk will immediately warm to 310 K, causing the CO_2 hydrates and ice at the surface to dissociate and melt. An interface between the aqueous phase and the ice-CO_2 hydrate mixture will form. The temperature at this interface will be the melting temperature of ice, 273 K. Because the interior of the bulk is still at 218 K heat will flow from the aqueous phase interface into the bulk. This heat flow will cause CO_2 hydrate to begin to dissociate ahead of the aqueous interface. The CO_2 hydrate dissociation will occur at 218 K because that is the equilibrium temperature of CO_2 hydrates at atmospheric pressure. Therefore, two moving phase interfaces will develop in the bulk, one at which ice melts to water at 273 K and one at which the CO_2 hydrate remaining in the bulk dissociates to ice and gas at 218 K.

A simple 1-D model of heat transfer to the bulk from a 310 K surface can be developed to estimate the rate of ice melting and the rate of CO_2 hydrate dissociation. A schematic of this 1-D model is shown in Figure 6-2. The CO_2 hydrate and ice bulk is at 218 K. Heat is conducted to the 218 K CO_2 hydrate dissociation interface through the ice phase. Heat is conducted to the 273 K aqueous-ice interface through the aqueous phase. It is assumed that the aqueous phase remains stationary between the 273 K interface and the 310 K tongue. Of course, in reality the aqueous phase will flow out from under the crystalline bulk, but the stationary aqueous phase assumption has been used with reasonable results in similar models for gas hydrate plug dissociation in horizontal pipelines (Davies et al., 2006).

The rates of growth of the aqueous layer and the ice layer in this model can be estimated by considering a control volume at the aqueous-ice interface and another control volume at the ice-CO_2 hydrate interface. For this model, the heat capacities of the aqueous phase and the ice are neglected because they are small relative to the latent heat released at each interface. At the aqueous-ice interface, heat is conducted into the control volume through the

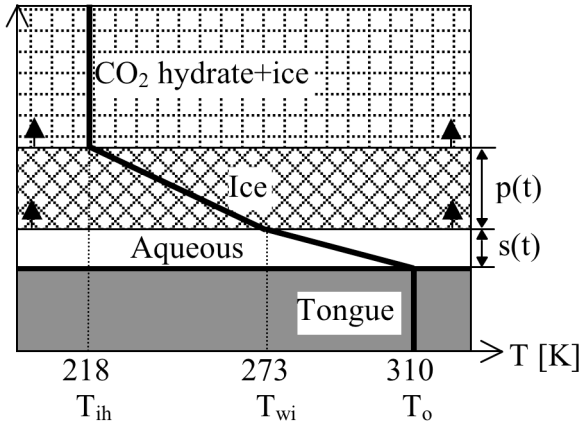

Figure 6-2 One-dimensional model for heat-transfer limited dissociation of CO_2 hydrate on the tongue

aqueous phase according to

$$\dot{q}_{conduction,aq} = -k_{aq}\frac{T_o - T_{wi}}{s},$$

where k_{aq} is the thermal conductivity in the aqueous phase, T_o is the temperature at the tongue interface, T_{wi} is the melting temperature of ice and s is the thickness of the aqueous layer at time t. Heat is conducted out of the control volume through the ice phase according to

$$\dot{q}_{conduction,i} = -k_i\frac{T_{wi} - T_{ih}}{p},$$

where k_i is the thermal conductivity in the ice, T_{ih} is the CO_2 hydrate dissociation temperature at one atmosphere CO_2 and p is the thickness of the ice layer at time t. Heat is absorbed due to the phase change at the aqueous-ice interface according to

$$\dot{q}_{phase\ change,wi} = \rho_i \Delta H_{wi}\frac{ds}{dt},$$

where ρ_i is the density of ice, ΔH_{wi} is the latent heat of ice melting, and ds/dt is the time derivative of the aqueous phase thickness. Similarly, at the ice-CO_2 hydrate interface, heat is conducted in through the ice layer according to $\dot{q}_{conduction,i}$ and heat is absorbed due to the phase change according to

$$\dot{q}_{phase\ change,ih} = \frac{1}{2}\rho_h \Delta H_{ih}\left(\frac{dp}{dt} + \frac{ds}{dt}\right),$$

where ρ_h is the density of CO_2 hydrate, ΔH_{ih} is the latent heat of CO_2 hydrate dissociation and dp/dt is the time derivative of the ice phase thickness. The factor ½ in the equation for heat absorbed by CO_2 hydrate dissociation accounts for the fact that half of the CO_2 hydrates dissociated spontaneously when the porous CO_2 hydrate was depressurized. There is no heat conduction through CO_2 hydrate phase because the temperature is uniformly 218 K.

Balancing the heat flows at each interface a coupled system of non-linear, first-order, ordinary differential equations is found

$$\begin{aligned}\frac{ds}{dt} &= \left(\frac{k_{aq}(T_o - T_{wi})}{\rho_i \Delta H_{wi}}\right)\frac{1}{s} + \left(\frac{-k_i(T_{wi} - T_{ih})}{\rho_i \Delta H_{wi}}\right)\frac{1}{p} \\ \frac{dp}{dt} &= \left(\frac{-k_{aq}(T_o - T_{wi})}{\rho_i \Delta H_{wi}}\right)\frac{1}{s} + \left[\left(\frac{k_i(T_{wi} - T_{ih})}{\tfrac{1}{2}\rho_h \Delta H_{ih}}\right) + \left(\frac{k_i(T_{wi} - T_{ih})}{\rho_i \Delta H_{wi}}\right)\right]\frac{1}{p}\end{aligned} \tag{6.2}$$

Typical values for the system are k_{aq} = 0.58 W/mK, k_i = 2 W/mK, ρ_i = 920 kg/m^3, ρ_h = 920 kg/m^3, ΔH_{wi}=-333 kJ/kg and ΔH_{ih}=-146 kJ/kg. After substituting these values into the differential equations it can be seen that there is a minimum ratio of the thickness of the ice layer to the thickness of the aqueous layer (p/s) below which ds/dt would be negative, which would be unphysical. This minimum ratio is 5.22. The system of equations (6.2) can be solved numerically, after picking an initial p to s ratio greater than 5.22. After several time steps the ratio of p to s stabilizes at a constant value (7.8 for the parameters used here) and s and p both grow with the square root of time.

A plot of the thickness of layers p and s as a function of time is shown in Figure 6-3. It can be seen that the ice-CO_2 hydrate interface moves quickly through the CO_2 hydrate pellet and the aqueous-ice interface lags behind. According to this model, after 30 s of heat flow from the 310 K tongue, CO_2 hydrate would be dissociated in the first 1 cm of the CO_2 hydrate bulk, but less than 2 mm of this layer would have melted.

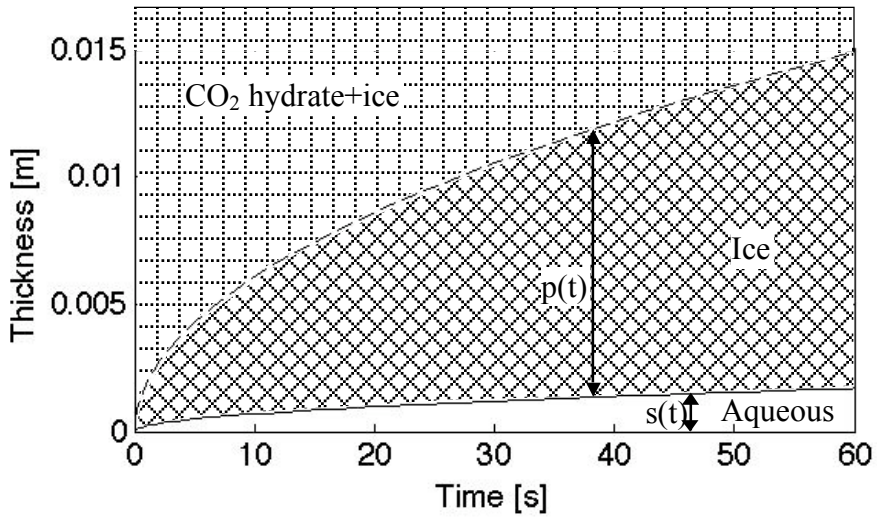

Figure 6-3 Evolution of aqueous and ice layer thicknesses according to Eq. 6.2

This heat-transfer limited model is based on a model that has been used successfully to predict dissociation of gas hydrate plugs in natural gas and oil pipelines. Davies et al. (2006) formed gas hydrate plugs by packing a 20 cm long, 4.8 cm internal diameter stainless steel cell with 250-850 μm ice grains, pressurizing the cell with methane or another gas hydrate former at 140 bars, and then warming the cell to 273 K and maintaining a high gas pressure until the water was completely converted to gas hydrate. The cell was then equilibrated in a glycol-water bath at 277 K (typical seafloor conditions) and depressurized to the desired pressure for the dissociation experiment. Davies modeled the dissociation as a heat-transfer limited process, with the gas hydrate plug dissociating radially at a rate determined by the heat equation. The surface temperature (the temperature at the inner diameter of the stainless steel cell) was fixed at 277 K. If the equilibrium temperature associated with the experimental dissociation pressure was less than 273 K, the model included two moving boundaries, a water-ice boundary and an ice-gas hydrate boundary. If the equilibrium temperature associated with the experimental pressure was greater than 273 K, then the model involved only one moving boundary, a water-gas hydrate interface. The temperature in the gas hydrate core was assumed to be uniform and close to the equilibrium dissociation temperature. Davies modified the density and thermal conductivity of the ice and gas hydrate phases by one minus the bulk porosity of the plug. This 1-D radial dissociation model predicted the total gas hydrate dissociation and ice melting time within 10%. In addition, in some of the experiments the cell was opened after 1, 2 or 3 hours of dissociation and it was confirmed visually that the plug was dissociating radially and that ice had formed around the shrinking gas hydrate core. However, in the reported data the model is only tested at dissociation temperatures 266.5 K and greater. Interestingly, Davies' model typically over predicts the gas hydrate dissociation and ice melting times, but switches to under-predicting the dissociation and melting time at the coldest dissociation temperature tested (266.5 K), which suggests that a different model may be more appropriate at colder dissociation temperatures.

Applying this heat transfer limited model to the dissociation of a CO_2 hydrate confection in the mouth, the major implication is that during the dissociation process only 11% of the water is melted. The remaining water melts after all of the CO_2 hydrates have dissociated.

This can be seen in Figure 6-3 where the thickness of the ice layer, p, is always 7.8 times the thickness of the aqueous layer, s, based on the numerical solution of Eq. 6.2. It is likely that CO_2 gas will dissolve in and saturate the water that is liquid while CO_2 hydrates are dissociating. However, the local CO_2 partial pressure will be significantly decreased by the time the remaining ice has melted, and thus the 89% of the water that melts after dissociation will not retain the same concentration of CO_2. In this case a CO_2 hydrate confection would initially seem strongly carbonated, but the perception of carbonation would cease before the pellet was completely melted.

According to the heat-transfer limited model, it would be expected that the flash-freezing powder would immediately cool to 218 K and lose 50% of its CO_2 content upon being exposed to atmospheric pressure. This spontaneous dissociation would occur when the ICT is vented after a batch is produced, when the PTM apparatus (which was described in section 1.4) is vented after a CO_2 hydrate formation experiment, and when a bottle of pellets is opened for tasting. However, this predicted rapid loss of CO_2 gas and decrease in temperature has not been observed. In fact, the CO_2 content of the powder at the time it is placed on the PTM load cell is typically 56 to 92% of the maximum CO_2 content despite the time delay (several minutes) and handling involved in transferring the powder from the ICT to the PTM sample can. In addition, in Figure 3-3 it was shown that it takes approximately 0.37 hours (22 minutes) for the measured CO_2 content to decrease by 50%. (Also, during taste tests there have been no comments about the powder or pellets being excessively cold, but this is not conclusive information because the temperature directly in the powder has not been measured and the low density of the powder and pellets could mitigate any perception of cooling.) Instead, experience with the flash-freezing powder suggests that the rate of CO_2 loss is slowed almost immediately by the kinetics of some step involved in the dissociation process, causing the CO_2 hydrate to remain at 253 K in a metastable state for a significant fraction of an hour.

The rate-limiting step in the dissociation process is probably CO_2 diffusion through the solid. When the pressure is rapidly decreased, CO_2 hydrate in the middle of a particle cannot dissociate if there is nowhere for the CO_2 to go (for example, in a solid crystal with no cracks or porosity). The CO_2 content of a CO_2 hydrate is so high that in order to fit all of the CO_2 and water molecules from a unit cell of CO_2 hydrate into the same unit cell volume after dissociation the CO_2 would have to be compressed to the density of liquid CO_2. Formation of liquid CO_2 would involve a pressure significantly higher than the minimum pressure for CO_2 hydrate stability. Thus the only CO_2 hydrate units that can dissociate immediately after the pressure is released are the ones that are close enough to the surface of the particle (or a crack running through the particle) for the gas to escape. These surface CO_2 hydrates dissociate to ice and gas, leaving behind a porous ice rind on the surface of the particle. The volume of this ice is 90% of the volume of the CO_2 hydrate that dissociated. Therefore close to 90% of the layer of CO_2 hydrate just inside the ice rind will be covered by ice and not directly exposed to the gas phase. Only a decreasing fraction of each subsequent layer will be able to immediately dissociate. In this case a thin surface layer of CO_2 hydrate will dissociate, after which further dissociation will be limited by the rate of CO_2 diffusion through ice and CO_2 hydrate. A gradient in the average CO_2 concentration will develop near the surface of the particle. This is shown schematically in Figure 6-4.

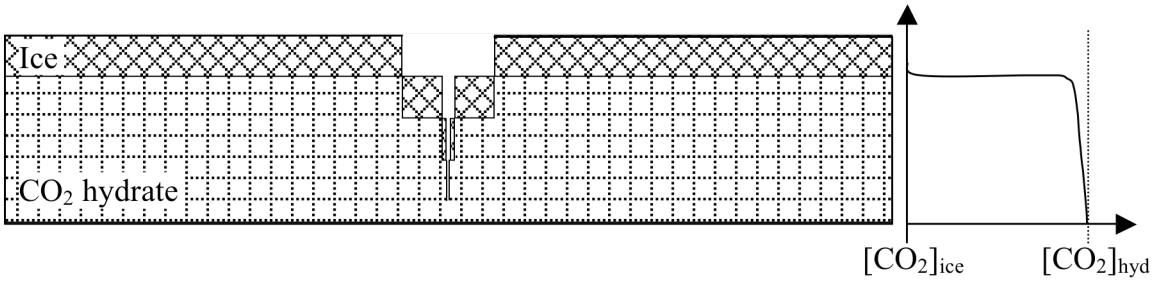

Figure 6-4 Schematic of ice surface layer remaining after spontaneous CO_2 hydrate dissociation. Average CO_2 concentration profile ($[CO_2]$) is shown to the right of the sketch.

The thickness of this initial surface layer is not known. It is probably less than the thickness of the initial open porosity CO_2 hydrate layer that Genov et al. (2004) observed during conversion of ice spheres to CO_2 hydrate, 1 to 4 μm. (It should be noted that in Genov's experiments this surface layer forms over several hours.) For reference, the diffusivity of CO_2 in CO_2 hydrate at 253 K is 9.4×10^{-15} m^2/s based on the model of Demurov et al. (2002), giving a characteristic CO_2 diffusion length in CO_2 hydrate of 0.19 μm in one second. This diffusion length also suggests that the thickness of the surface layer that dissociates spontaneously upon depressurization is on the order of or smaller than 1 μm. Thus even in the flash-freezing powder, which has a characteristic length of 20 to 40 μm (based on the microscopy images in Figure 3-9) only a small fraction of the particle would be able to dissociate spontaneously. The rest of the particle would dissociate at a rate limited by CO_2 diffusion through the solid.

The temperature distribution in the CO_2 hydrate bulk after the surface layer dissociates can be estimated by considering an impulse of heat removed from a semi-infinite body of CO_2 hydrate. The magnitude of the heat impulse is equal to the latent heat removed from the bulk by dissociation of the surface layer of CO_2 hydrates. This magnitude, per unit surface area, can be found according to

$$E = \rho_h \delta \Delta H_{ih},$$

where ρ_h is the density of CO_2 hydrate (1091 kg/m^3), δ is the thickness of the surface layer that dissociates, and ΔH_{ih} is the enthalpy of dissociation (-146 kJ/kg CO_2 hydrate). For a 1 μm thick layer the pulse of heat at the surface would be -159 J/m^2. The temperature profile in a semi-infinite body exposed to a pulse of heat, E, is

$$T(x,t) - T_i = \frac{E}{\rho_h c_h \sqrt{\pi \alpha_h t}} e^{-\frac{x^2}{4\alpha_h t}}, \qquad (6.3)$$

(Mills, 1995) where T(x,t) is the temperature at time t and distance x from the surface, T_i is the initial temperature of the body, c_h is the heat capacity of the body (2080 J/kg), and α_h is the thermal diffusivity of CO_2 hydrate (2.2×10^{-7} m^2/s). Equation 6.3 is non-physical at time t=0. The calculated surface temperature at t=0 is negative infinity because in deriving Eq. 6.3 all the energy is instantaneously removed from an infinitely thin layer at the surface of the solid. In reality this energy would be removed from a thin but finite thickness surface layer (~1 μm) over a finite time (~1 s) and the temperature would never decrease below 218 K, the CO_2 hydrate dissociation temperature at atmospheric pressure. However, Eq. 6.3 is expected to reflect the actual temperature distribution for times greater than the time it takes the surface

layer to dissociate. Accordingly, 1 second after the thermal pulse it can be predicted that the surface temperature is within 0.08 K of the initial bulk temperature.

It can be seen in Eq. 6.3 that the temperature change penetrates into the CO_2 hydrate bulk according to the term in the exponential, $x^2/4\alpha_h t$. A characteristic thermal diffusion length can be identified in this exponential; where the term in the exponential is equal to 1 the temperature change is only 37% of the change at the surface. Thus the characteristic thermal diffusion length is given by $x_{thermal}=\sqrt{4\alpha_h t}$. In a CO_2 hydrate bulk, the characteristic thermal diffusion length in 1 second is 938 μm. If the CO_2 hydrate body is smaller than this characteristic diffusion length, the change in temperature will propagate throughout the body and the cooling everywhere will be larger than predicted by Eq. 6.3 because the heat capacity of the body is finite. For example, particles on the scale of the flash-freezing powder (20 to 40 μm) will cool several degrees throughout the particle due to the surface dissociation. In a hypothetical 40 μm spherical particle, dissociation of a 1 μm shell of CO_2 hydrate would cause the entire particle to cool by 10 K. In either case (finite particle or CO_2 hydrate bulk much larger than the characteristic thermal diffusion length), all of the CO_2 hydrate in the surface layer can be expected to dissociate without achieving stability at 218 K. Dissociation only slows significantly because of mass transfer limitations.

Based on the above arguments, the particles or porous CO_2 hydrate bulk that come in contact with the tongue of the consumer should consist of CO_2 hydrate surrounded by a thin shell of ice and the temperature of the particles may be up to 10 K cooler than the temperature in storage. CO_2 hydrates have not stopped dissociating, but the dissociation rate is limited by the rate of diffusion of CO_2 to the surface of the particle. When the particle comes in contact with the tongue, the surface of the particle will melt instantaneously (as in the heat-transfer limited model) and a moving aqueous-CO_2 hydrate interface will develop. However, the heat conducted into the center of the particle cannot cause a CO_2 hydrate dissociation front to develop because the CO_2 hydrate dissociation continues to be controlled by diffusion of CO_2 through the solid surface layer. Similar to the characteristic thermal diffusion length identified in Eq. 6.3, the penetration depth of the decreased CO_2 concentration will increase according to the characteristic CO_2 diffusion length in CO_2 hydrate, $x_{diffusion}= \sqrt{4D_{CO2}t}$, where D_{CO2} is the diffusivity of CO_2 in CO_2 hydrate. The ratio of the characteristic CO_2 diffusion length to the characteristic thermal diffusion length is more than 4000. Therefore an ice-CO_2 hydrate interface would not be able to propagate ahead of the aqueous interface because the mass diffusion is so much slower than the thermal diffusion. Instead, the CO_2 hydrate dissociation front remains a "surface layer thickness" ahead of the aqueous interface. In this case, the heat conducted into the interior of a particle or bulk simply continues to warm the particle or bulk toward 273 K without causing CO_2 hydrate dissociation. CO_2 hydrate dissociation only occurs close to the aqueous-CO_2 hydrate interface where gas can escape.

This mass-transfer limited model of CO_2 hydrate dissociation is shown schematically in Figure 6-5. According to this model the un-dissociated CO_2 hydrate is essentially free of ice (because spontaneous dissociation only occurred at the particle surface) and there is not a significant ice layer separating the CO_2 hydrate and aqueous phases. Two temperature profiles are sketched in the figure to show that over time, heat conducted from the tongue through the aqueous phase causes the aqueous phase interface to propagate into the particle and also warms the CO_2 hydrate in the interior of the particle.

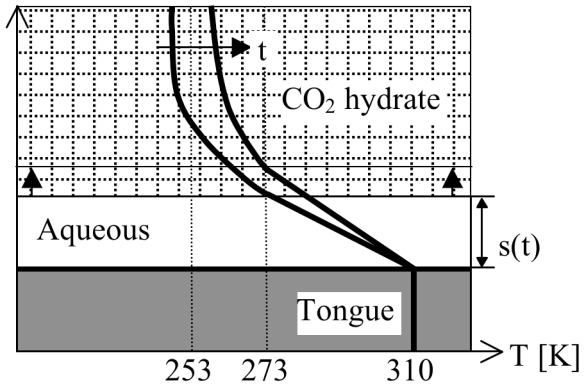

Figure 6-5 1-D model for dissociation of a CO_2 hydrate particle on the tongue with mass transfer-limited dissociation. Temperature profiles are sketched for two time steps.

In addition to our experience with delayed CO_2 loss from the flash-freezing powder, several researchers have observed persistence of CO_2 hydrates at metastable conditions below the ice point. In particular, Circone et al. (2004) measured gas evolution from CO_2 hydrates at atmospheric pressure with samples in isothermal baths at 240, 252 and 268 K. Circone et al. synthesized pure CO_2 hydrate by packing 180 to 250 μm ice particles in a 2.54 cm by 11 cm pressure vessel, pressurizing the vessel to greater than 50 bars with CO_2, and then ramping the temperature of the *D*-limonene bath surrounding the vessel to 281 K and allowing the water-to-CO_2 hydrate conversion process to complete over 50 hours. For the experiments in an isothermal bath at 240, 252 and 268 K, the temperature of the bath and pressure vessel were allowed to equilibrate at the experimental temperature, the pressure was slowly reduced to a few bars greater than the CO_2 hydrate equilibrium pressure, and then the pressure vessel was rapidly vented to 1.01 bar. After the rapid depressurization, the temperature in the pressure vessel immediately decreased by 5 to 8 K and then re-warmed to the isothermal bath temperature. Slow, steady CO_2 release was observed. After up to four hours less than 10% of the CO_2 in the sample had been released and the bath was heated to 282 K. As the sample temperature increased the CO_2 release rate increased and the majority of the CO_2 was released just before the sample temperature reached 273 K.

The mass transfer limited model presented here seems to contradict the heat transfer limited model used for dissociation of gas hydrate plugs in pipelines. It is possible that the two models are applicable at different dissociation pressures and temperatures. In particular, the heat transfer limited model should apply when a gas hydrate is depressurized to a pressure for which the associated equilibrium temperature is greater than 273 K. Above 273 K, gas hydrates dissociate to gas and water, rather than ice. Liquid water would not provide a barrier to further dissociation. The heat transfer limited model may work for depressurization of systems that dissociate at just below the ice point because the majority of the spontaneous dissociation would occur at a temperature greater than 273 K, which could lead to bubbling throughout the gas hydrate and subsequently provide conduits for CO_2 escape. In addition both water mobility and CO_2 diffusivity in ice at 273 K are higher than at 253 K, which would increase the rate at which ice agglomerates to minimize its surface energy and increase the rate of CO_2 transport through an ice covering.

Alternatively, the difference between experience with gas hydrate plug dissociation and CO_2 hydrate dissociation could be due to differences between the gases. Work on gas hydrate

plug dissociation involves methane and other natural gas constituents; CO_2 is a minor component at most. CO_2 molecules fit more tightly in the clathrate hydrate cages than methane molecules (Sloan & Koh, 2008), so there could be a difference in diffusion rate. Also, Kuhs et al. (2000) observed several different gas hydrates with a scanning-electron microscope on a cryostage and found that the bulk of the gas hydrates are porous on a micron scale. However, the pores in the CO_2 hydrate were typically 20-100 nm in diameter, with a porosity of 10-20% whereas the pores in CH_4, Ar, and N_2 hydrate were typically 100-400 nm with 25-40% porosity. The smaller pores and reduced bulk porosity of CO_2 hydrates in comparison to methane hydrates could make CO_2 hydrate dissociation more likely to be mass transfer limited than methane hydrate dissociation.

Assuming that the mass transfer limited model for CO_2 hydrate dissociation applies to consumption of CO_2 hydrate confections, the major implication is that the dissociation provides an immediate increase in the amount of aqueous phase available to dissolve CO_2. In addition, this aqueous phase is in close contact with the CO_2 gas released by dissociation. It seems reasonable to assume that the CO_2 partial pressure at the surface of the aqueous phase is 1 atmosphere due to the large amount of CO_2 stored in CO_2 hydrates (on the order of 100 times the volume of the pellet). The solubility of CO_2 in water at 273 K and 1 atm is 0.0034 kg CO_2/kg H_2O (Diamond & Akinfiev, 2003). This indicates that the water released by CO_2 hydrate dissociation should have a CO_2 concentration of close to 0.0034 kg CO_2/kg H_2O. However, even if the water released by CO_2 hydrate dissociation becomes saturated with dissolved CO_2, not all of the CO_2 from the CO_2 hydrate can be dissolved because the dissociation introduces 0.372 kg CO_2 per kg H_2O. This would correspond to a CO_2 capture efficiency of 1%, or in other words, for every gram of CO_2 in a confection, only 0.01 g is captured in the melted confection where it can be perceived chemically.

Some of the excess CO_2 gas may be dissolved in other water in the mouth, for example saliva or, if the CO_2 hydrate pellet initially contained ice, water from the melting ice. The amount of CO_2 dissolved in this other water will depend on the interaction between the water and escaping CO_2 gas. A sketch of a CO_2 hydrate pellet melting on a tongue is shown in Figure 6-6. The gas phase between the pellet and the tongue can reasonably be assumed to have a CO_2 partial pressure of 1 atm. Away from the pellet, CO_2 gas mixes with the air in the mouth so the CO_2 partial pressure is less than 1 atm. In addition, a consumer breathes periodically while the pellet melts, so the CO_2 partial pressure away from the pellet will be significantly less than 1 atm. Considering the partial pressure distribution of carbon dioxide in the gas phase, saliva and ice melt-water that are directly under the pellet can dissolve CO_2 up to the concentration that is in equilibrium with 1 atm CO_2 pressure. Saliva that is away from the pellet and ice melt-water that flows away from the pellet may dissolve some CO_2, but the CO_2 concentration will be significantly lower. Water that does not become saturated with dissolved CO_2 would dilute the overall perception of carbonation.

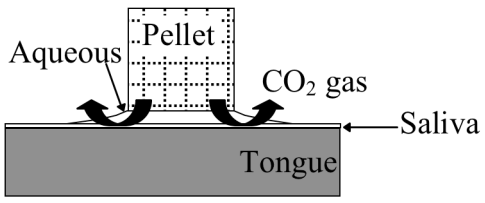

Figure 6-6 Schematic of CO_2 gas path during mass transfer limited dissociation of CO_2 hydrate pellet

The amount of saliva in the mouth just before swallowing is 1.07 mL and it is distributed over the surfaces of the mouth in a 0.07 to 0.1 mm layer (Collins & Dawes, 1987). If it is assumed that the average partial pressure of CO_2 in the mouth (away from the pellet) is 0.1 atm and the solubility of CO_2 in saliva is the same as the solubility of CO_2 in water, then at most 0.00032 kg CO_2 can be dissolved per kilogram of water (Diamond & Akinfiev, 2003). In this case the maximum mass of CO_2 dissolved by saliva would be $3.4x10^{-4}$ g each time the consumer swallows. Under a pellet with a cross-sectional area of 1 cm^2 the mass of CO_2 that could be dissolved in saliva (based on 1 atm CO_2 partial pressure) is $3.4x10^{-5}$ g. A 1 cm^3 100% overrun pellet contains 0.13 g CO_2, so CO_2 capture by saliva does not significantly increase the fraction of CO_2 that is captured during dissociation and melting of the confection. (Note that a CO_2 partial pressure of 0.1 atm is very high; the typical threshold limit value for short-term (15 minute) exposure (STEL-TLV) to CO_2 is 30,000 ppm, or approximately 0.03 atm.)

The CO_2 captured by ice melt-water could potentially increase the efficiency of CO_2 capture in the melted confection from the 1% value estimated above for a pure CO_2 hydrate. However, a significant increase in CO_2 perception between confections with 0.03 kg CO_2/kg mixture and with 0.13 kg CO_2/kg mixture is easily detected when eating the flash-freezing powder. This indicates that water from melting ice does not capture all of the CO_2 released from the confection. If 100% of the CO_2 in the frozen confection were captured in the melted confection, the chemical perception of carbonation would not change for any initial CO_2 concentration in the confection that is greater than 0.0034 kg CO_2/kg H_2O. The observed increase in perception with increasing concentration indicates that water melted from ice does not improve the efficiency of CO_2 capture significantly (especially because this change in perception is observed at concentrations an order of magnitude greater than the solubility of CO_2 in water). Regardless of the efficiency of CO_2 capture, the mass transfer limited dissociation model presented here implies that the CO_2 concentration in the melted confection will never exceed the atmospheric pressure solubility of CO_2 in the confection. The consumer will always exhale a significant fraction of the CO_2 in the confection.

Due to the rapid release of CO_2 gas as a CO_2 hydrate confection is eaten higher concentrations of flavor compounds can be necessary. CO_2 gas released by dissociation of CO_2 hydrates that is not subsequently dissolved in an aqueous phase is most likely to leave the mouth with the next breath of the consumer. This flow of exhaled gas could entrain some of the volatile flavor ingredients, reducing the concentration of flavor in the melted confection.

6.3 Necessary CO_2 concentration

Two initial sensory analysis tests were carried out on cola flavored CO_2 flash-freezing powder to determine the threshold of fizziness perception as a function of CO_2 concentration and compare the intensity of the sensation to fresh, cold soda (A. Pizzagalli 2007, pers. comm. September 28). In the first test, ten panelists ranked fizziness ("bubbles perceived and gas released") and tingling ("small needles on the tongue") of powders with several CO_2 concentrations on a 0 to 100 scale in comparison to a reference powder containing 0.13 g CO_2/g mixture. Below 0.03 g CO_2/g mixture, more than 20% of the panelists ranked the powder samples as not fizzy, and the ranking of intensity averaged over all of the panelists

was less than half of the reference intensity. In the second test, panelists stated whether fresh powder was fizzier than fresh, cold soda. All panelists considered the reference powder fizzier than the soda, but by 0.03 g CO_2/g mixture, only 30% of the panelists considered the powder fizzier than the soda. In addition to the sensory analysis tests, an unofficial tasting of pellets made from flash-freezing powder identified a minimum CO_2 content of 0.05 g CO_2/g mixture for significant fizziness (A. Pizzagalli 2008. pers. comm. January 18). These tests indicate that the CO_2 content of the CO_2 hydrate confection should be at least 0.03 g CO_2/g mixture for sensory purposes.

It is possible that the minimum CO_2 content in the CO_2 hydrate confection depends on the form of the frozen confection (powder versus pellet). In a fine powder, small particles can spread across the tongue and significant surface area will be in direct contact with saliva. CO_2 diffusion into the saliva is proportional to the surface area of the CO_2 source, so more CO_2 may go into saliva from the powder than from the pellets, improving CO_2 capture from the gas phase. In addition, the particles melt more rapidly than the pellet, which could lead to more circulation of the carbonated, melted mixture and saliva in the mouth before swallowing than in the case of a pellet. An increase in circulation would increase contact between the carbonated solution and nociceptors.

The CO_2 content necessary for sensory perception in CO_2 hydrate confections is much higher than the typical CO_2 content of other food products. The CO_2 concentration in most carbonated beverages is 0.0014 to 0.006 g CO_2/g beverage (Green, 1992). This range is similar to the solubility of CO_2 in water at 277 K and 1 to 3 atmospheres (see Figure 2-1). Champagne wines and other highly carbonated sparkling wines can reach 12 g/L of CO_2 or 0.012g CO_2/g solution (Descoins et al., 2006; Green, 1992). The limit for sensory detection of carbonation in a carbonated Swiss-style yogurt at 278 K is 263 ppm or 0.00026 g CO_2/g yogurt for college-age students (Wright et al., 2003), but typically the product is carbonated to 0.0013 g CO_2/g yogurt (Taylor & Ogden, 2002). These carbonation levels are a third to a twentieth of the carbonation level necessary in the CO_2 hydrate confection for sensory purposes.

The large CO_2 concentration necessary in a CO_2 hydrate confection compared to other carbonated foods is probably due to the large fraction of CO_2 that escapes in the gas phase. A similar high CO_2 concentration may not be necessary in a carbonated frozen food with a different mechanism to supply CO_2 (such as bubbles or an acid-carbonate chemical reaction) because the CO_2 concentration would be closer to the concentration that could be retained in the melted mixture.

The model for CO_2 hydrate dissociation presented in section 6.2 suggests that the dissolved CO_2 concentration in the melted confection and in the saliva could not exceed 0.0034 g CO_2/ g H_2O, the solubility of CO_2 in 273 K water at atmospheric pressure. This concentration is only a little more than half the concentration in typical carbonated beverages, but the CO_2 hydrate powder and pellets are still perceived as more carbonated than a fresh soda when the CO_2 concentration is greater than 0.13 g CO_2/g mixture. This is surprising because Green (1992) showed that water with a CO_2 concentration of 0.003 g CO_2/g H_2O was perceived as less carbonated than water with a CO_2 concentration of 0.006 g CO_2/g H_2O. One possible explanation is that the increase in nociceptor activity due to the cold temperature of the confection (described in section 6.1) does in fact reduce the amount of CO_2 required to match the irritation caused by a carbonated beverage by approximately 50%. An alternative explanation is that what really matters for chemical CO_2 perception is the concentration of

CO_2 induced in saliva, because that is where the enzyme carbonic anhydrase catalyzes the reaction to form carbonic acid. Dessirier et al. (2000) showed that inhibiting carbonic anhydrase decreases the intensity of CO_2 perception. In this case, 0.13 g CO_2/g mixture happens to be the concentration at which the amount of CO_2 that dissolves in saliva is the same as the amount that dissolves in saliva during consumption of a fresh soda. A third possible explanation is that in the consumer's interpretation of the amount of CO_2 in the confection the enhanced perception of CO_2 through bubble formation compensates for decreased chemical perception.

Despite the above preliminary results for sensory perception of fizziness in CO_2 hydrate confections, the minimum CO_2 concentration in the CO_2 hydrate confection is actually constrained by the CO_2 necessary to maintain a homogeneous product, as described in section 4.2. The minimum CO_2 concentration required for homogeneity in storage is 0.2 g CO_2/g mixture, 4-6 times the minimum concentration for CO_2 perception. Because so much excess CO_2 is required to maintain homogeneity, it may be advantageous that CO_2 escapes the mouth in the gas phase during consumption, because the amount of CO_2 consumed is reduced. CO_2 can lead to burping and other reactions in the rest of the digestive system, which are not desirable.

Finally, ingredients in the recipe can change CO_2 release. For example, the perceived CO_2 release rate and bubble size are reduced in CO_2 hydrate confections made from recipes with higher total solids content (J. Saikali 2009, pers. comm. March 24). The total solids may dilute the concentration of CO_2 at nociceptor sites. In addition, high total solids mixtures are generally more viscous, which can increase resistance to CO_2 diffusion and bubble growth. Addition of surfactants that stabilize bubbles can increase the size of bubbles that develop in the mouth, causing a smooth, creamy, foaming sensation (J. Saikali 2009, pers. comm. March 24). Some ingredients, such as lecithin, can increase the intensity of CO_2 stimulation, even leading to the sensation of pain (J. Saikali 2009, pers. comm. March 24), possibly by improving dissolution of CO_2 in saliva. Based on these observations, CO_2 perception in CO_2 hydrate confections should be tested in parallel to tests on the effect of mixture properties and added emulsifiers and surfactants.

(This page intentionally left blank.)

7 Summary and conclusions

This thesis provides a scientific basis for producing and distributing carbonated frozen confections involving CO_2 hydrates. CO_2 hydrates are an attractive method of carbonating ice confections because the crystalline CO_2-H_2O structure can take the place of ice, providing a very high CO_2 concentration without limiting the confection recipe or product texture. CO_2 hydrate confections can be rapidly formed using the CO_2 flash-freezing process. The process involves emulsifying the ingredients mixture in liquid CO_2 and then flashing the combined fluids to a pressure that induces evaporation of CO_2 and concurrent freezing of the mixture. In this thesis, the impact of process parameters on CO_2 hydrate formation, the impact of CO_2 hydrates on storage and distribution parameters, and the effects of CO_2 hydrates on perception of carbonation have been addressed.

When the mixture-liquid CO_2 emulsion is formed, the important considerations are breakup of the mixture in the liquid CO_2 and the temperature and pressure of the fluids. The effect of the recipe on CO_2 solubility is unimportant because the solubility of CO_2 in water is much less than the concentration of CO_2 in CO_2 hydrates. CO_2 may cause precipitation of proteins or solubilize a small fraction of fats from the recipe, which can affect the microstructure of the frozen product, but does not change the flashing process significantly. In the emulsion chamber it is only important that the mixture is broken up into droplets smaller than the orifice of the flash-freezing nozzle, which ensures that mixture and CO_2 are in intimate contact during flash freezing. In the current apparatus the estimated droplet size is 150-200 μm, which is less than half the diameter of the flash-freezing nozzle orifice. This droplet size is probably too large for a viscous mixture to be saturated with CO_2 during residence of the droplet in the emulsion chamber. It has been argued that it is not necessary to saturate the mixture with CO_2 in the emulsion chamber because the atomization of the mixture during flash freezing generates sufficient surface area for CO_2 absorption during crystallization. CO_2 hydrate formation in the emulsion chamber is avoided by keeping the temperature in the emulsion chamber greater than 283 K because CO_2 hydrates can block the flash-freezing nozzle and reduce breakup of the mixture during flash freezing. The pressure in the emulsion chamber is chosen to ensure that CO_2 is a slightly sub-cooled liquid.

When mixture-liquid CO_2 emulsion is flashed into the ice confection tank (ICT), the important parameters are the CO_2:mixture flow ratio and the ICT pressure. The ideal mass flow ratio is calculated by balancing the heat released by crystallization of water and the heat absorbed by evaporation of CO_2. The ratio is typically close to 2.5, but varies with the water content of the mixture due to both the latent heat of crystallization and the CO_2 concentration in CO_2 hydrates. The ICT pressure influences atomization of the mixture and nucleation of CO_2 hydrate. Decreasing the pressure drop across the flash-freezing nozzle decreases atomization of the mixture. Atomization of the mixture is necessary due to the competition between ice and CO_2 hydrate growth. Evaporating CO_2 removes heat from the mixture rapidly, such that any portion of the mixture without sufficient exposure to CO_2 will form ice instead of CO_2 hydrate. If the ICT pressure is lower than 4.7 bars, it is likely that ice will nucleate before CO_2 hydrates and the entire crystallization process will occur outside of CO_2 hydrate formation range. It has been shown that conversion of ice to CO_2 hydrate is a slow process, even in the fine powder geometry produced by the CO_2 flash-freezing process.

Because ice to CO_2 hydrate conversion is such a slow process, CO_2 hydrate formation from ice cannot occur during the residence of the powder in the ICT.

CO_2 hydrates determine the minimum long-term storage pressure of a CO_2 hydrate confection and the amount of CO_2 necessary in a storage vessel. The minimum pressure is given by the ice-CO_2 hydrate-gas equilibrium curve regardless of the solutes in the aqueous phase. In a typical home freezer the CO_2 hydrate confection must be stored at 5.9 bars, which is higher than the pressure of soda, but within the operating range of current commercial carbonated beverage bottles. CO_2 hydrates additionally dictate the minimum CO_2 content of the storage vessel. In order to ensure a homogeneous CO_2 distribution in the confection there must be enough CO_2 to pressurize the vessel and convert any ice to CO_2 hydrate. If there is any ice present, the confection will develop ice-rich regions and CO_2 hydrate-rich regions because redistribution of CO_2 hydrates with a very small temperature gradient is fast relative to the typical shelf life of frozen confections. The CO_2 hydrate confection can be stored as a powder or compressed, but compression at 253 K from 90% porosity to less than 50% porosity does not induce significant sintering. This compression is only expected to reduce the rate of CO_2 loss at ambient pressure by about a factor of 10. It would be desirable to find an edible coating for compressed CO_2 hydrate confection powder that would provide low CO_2 permeability and withstand the CO_2 hydrate equilibrium pressure, but none has been found thus far. An ice shell is likely to be ineffective because CO_2 diffusion along ice grain boundaries is too fast. In addition, application of a coating material that is at a higher temperature than the pellet can cause CO_2 hydrates to dissociate while the material solidifies, which would allow the escaping gas to form channels in the frozen shell and continue to escape through the shell during storage. Thus compressing and coating the powder does not change the minimum storage pressure or the necessary CO_2 content in the storage vessel.

CO_2 hydrates impact the evolution of the confection during its shelf life, in particular during heat shock. Gas hydrates recrystallize in a similar manner to ice, but the processes may be slower due to reduced diffusion rates and more complicated surface reactions. Further investigation is required, but it is likely that stabilizers used in conventional ice confections will also be useful in CO_2 hydrate confections. CO_2 hydrate confections are different from ice confections because CO_2 is released during heat shock and the fraction of water crystallized varies with both temperature and pressure. In a system with a freeze-concentrated aqueous phase, heat shock leads to dissociation of CO_2 hydrates even if the container pressure is higher than the ice-CO_2 hydrate equilibrium pressure. For packaging with a small gas-phase volume this can result in significant pressure increases. CO_2 hydrates re-form when the temperature is reduced, but the rate of re-formation can be much slower than the rate of dissociation if the specific surface area of the confection is decreased during heat shock. Design of packaging for a CO_2 hydrate confection requires careful consideration because the pressure evolved in the container during heat shock must be controlled, but if CO_2 is vented from the package, ice will be present in the re-cooled product, leading to inhomogeneities in the product.

CO_2 hydrates enable perception of carbonation both by stimulation of nociceptors in the mouth and by tactile detection of bubbles. Nociceptors are stimulated by carbonic acid formed from CO_2 dissolved in water. The CO_2 release can be modulated to produce a range of sensations, from slow bubble growth to rapid foaming to strong tingling. Based on preliminary sensory analysis, the minimum concentration for fizziness is three to ten times greater than the concentration found in other refrigerated, carbonated products (i.e. 0.03 g

CO_2/g frozen confection versus 0.006 g CO_2/g carbonated beverage). A significant fraction of the gas released from dissociating CO_2 hydrates escapes the product without being dissolved because the concentration of CO_2 in CO_2 hydrates is more than 100 times the solubility of CO_2 in water at 273 K and atmospheric pressure. Further work is required to determine consumer preferences and understand CO_2 hydrate dissociation in the mouth. The minimum CO_2 concentration in CO_2 hydrate confections is actually determined by the concentration required to ensure a homogeneous product. This concentration is 4-6 times the minimum concentration for perception of fizziness, so it may not be bad to have some CO_2 escape during consumption.

Overall, this thesis makes several contributions to understanding CO_2 hydrates in systems involving an aqueous phase at 218-273 K. These contributions are important for development of CO_2 hydrate confections and may be of interest as production of gas from methane hydrates in permafrost regions is developed (an initial proof-of-concept of energy recovery from gas hydrates in permafrost was demonstrated in 2002 (Sloan & Koh, 2008)). CO_2 hydrate formation by CO_2 flash freezing can be useful for carbonating confections as well as producing fine gas hydrate particles with a high specific surface area for research purposes. The key parameters for CO_2 hydrate formation by CO_2 flash freezing have been identified. In particular, it is not essential to saturate a solution with CO_2 before flash freezing and the pressure at the exit of the flash-freezing nozzle must be greater than 4.7 bars to cause CO_2 hydrate formation rather than ice formation. It has also been shown that the rate of conversion of ice to CO_2 hydrate is not increased by an intermingled high-viscosity aqueous phase. The key parameters for storage of CO_2 hydrates have been identified. Solutes in the aqueous phase do not affect the CO_2 hydrate equilibrium pressure with ice, whereas solutes in the aqueous phase act as thermodynamic inhibitors above 273 K. The aqueous phase can be freeze-concentrated both with decreasing temperature and with increasing pressure, so the extent of water crystallized in a CO_2 hydrate confection can be higher or lower than in an ice confection of the same recipe at the same temperature. A small temperature gradient will cause redistribution of CO_2 in the presence of ice, so the minimum CO_2 concentration in a storage vessel to ensure homogeneity is fixed by the amount of CO_2 necessary to avoid ice. Finally, when CO_2 hydrate confections are eaten, CO_2 must dissolve in the melted confection or in saliva subsequent to dissociation and the CO_2 concentration in these aqueous fluids in the mouth will not exceed the concentration of CO_2 in water at 273 K and 1 atmosphere. A significant fraction of CO_2 in a CO_2 hydrate is always released to the gas phase and exhaled because the water in a kilogram of CO_2 hydrate can only dissolve a small fraction of the CO_2 in a kilogram of CO_2 hydrate. With these contributions it is now possible to optimize CO_2 use during flash freezing and in a CO_2 hydrate product as well as to design appropriate packaging for CO_2 hydrate confections.

(This page intentionally left blank.)

8 Recommendations

Based on the conclusions of this thesis, further work is recommended both to develop a commercially viable packaged carbonated frozen confection and to improve understanding of CO_2 hydrates in frozen confections. Before detailing this future work, it is important to point out that relatively little development would be necessary to use a batch implementation of the CO_2 flash-freezing process to make a CO_2 hydrate confection that is eaten at the site of production. This batch implementation could be similar to the current apparatus, but careful attention should be paid to ease of cleaning, operation and ability to produce CO_2 hydrate confections quickly on demand and with little down time between batches. This would involve carefully designing the ICT for fast temperature stabilization and recovery of the powder.

8.1 Next steps for a commercially viable packaged CO_2 hydrate confection

For a CO_2 hydrate confection that is packaged and distributed, significant work is needed to develop a continuous process and appropriate packaging. A schematic diagram of a possible continuous cycle is shown in Figure 8-1. In a continuous process, vented CO_2 would be filtered, recompressed, cooled, and metered with the correct amount of make-up CO_2 to maintain the optimum flow ratio. The powder would be extracted through a device such as an airlock or screw conveyor without depressurizing the ICT. This device must convey the powder without crushing or melting it and prevent the powder from bridging. It may be necessary to agitate the powder in the ICT because the irregularly shaped particles bridge easily. In addition to conveying the powder, the extraction device may pack or shape it. After any processes to coat or stir in add-ins, the CO_2 hydrate confection must be packaged. It is probably possible to develop the CO_2 recovery and metering system using filters, compressors and metering devices currently available, provided they are designed for food applications. The powder extraction device requires significant development and is discussed further in Lopez (2009). The packaging requires significant development due to the high CO_2 content of the confection and the pressure evolution with heat shock.

Work to enable development of the CO_2 recovery system and confection packaging should begin with understanding and controlling the CO_2 concentration in the powder. The CO_2 concentration of the powder affects the amount of CO_2 in the packaging as well as metering of makeup CO_2. A CO_2 flash-freezing apparatus should be implemented that includes flow meters for the mixture, liquid CO_2 and vented CO_2, and a method for extracting powder samples from the ICT continuously and measuring the CO_2 concentration automatically. This instrumentation will remove current uncertainties about CO_2 content related to variations during a batch production and manual transfer of powder samples to the PTM apparatus. The automated method of measuring CO_2 concentration should first be used to determine whether the currently observed variability in flash-freezing powder CO_2 concentration is due to the manual process of measuring the concentration or due to competition between ice and CO_2 hydrate nucleation during flash freezing. This test will

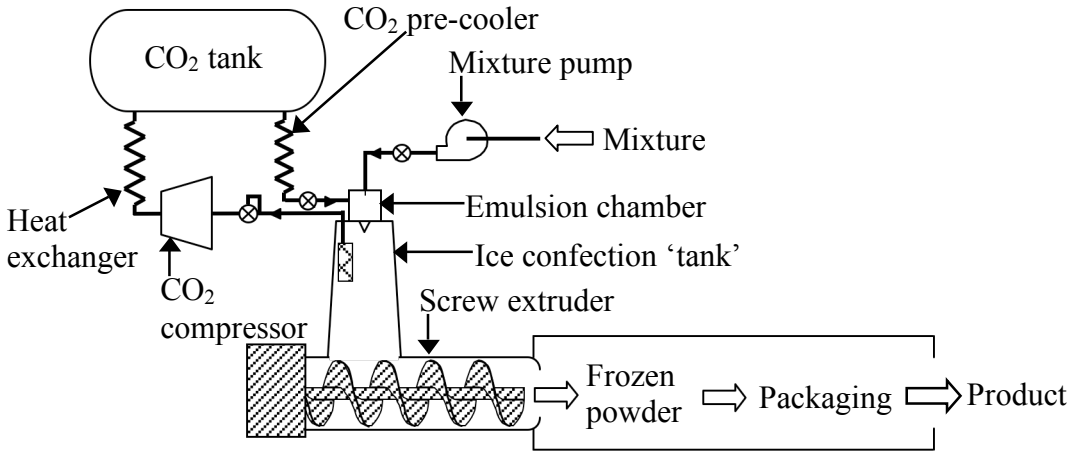

Figure 8-1 Schematic diagram of possible implementation of continuous cycle CO_2 flash freezing.

involve measuring the initial flash-freezing powder CO_2 concentration multiple times with the ICT operating at 10 bars and all parameters fixed. This test can be carried out using pure water in the place of mixture in order to determine whether complete CO_2 hydrate formation is consistently possible with the ICT operating at 10 bars. After these initial tests, the CO_2 content of the powder as a function of ICT pressure should be determined. It is likely that increasing the ICT pressure will improve CO_2 hydrate formation and the consistency of the results. If results are favorable at higher ICT pressure this will additionally reduce the work required for recompression of the CO_2. Finally, the CO_2 content of the powder as a function of recipe, in particular viscosity, should be determined.

After controlling the initial CO_2 concentration of the powder, appropriate packaging must be designed. The packaging will change significantly depending on the final product design, so research on consumer preferences for the CO_2 hydrate confection is needed prior to or at least concurrently with packaging development. For example, it has been demonstrated that ingredients in the recipe can modify the CO_2 release in the mouth to be smooth with slowly growing bubbles or rapid with intense tingling, but it is not known what sensation a consumer would prefer. The water content of the recipe will vary depending on the desired sensation. Also, the CO_2 hydrate confection could be packaged in a low- or high-density bulk or as pellets, which would affect the headspace of the packaging and the style/geometry of the package. It may be possible to distribute a product that contains both ice and CO_2 hydrates by planning for inhomogeneity. In this case the package would be labeled "Shake well before opening," and the product would be designed so that a typical bite of the carbonated confection is made up of multiple pellets or granules. This would enable a decrease in the CO_2 content of the package. The product may be developed to include add-ins or coatings, such as nuts or chocolate, which have a low water content and do not absorb CO_2. Add-ins or coatings can reduce the headspace in the packaging without increasing the necessary CO_2 content. In addition to carrying out consumer testing to determine the preferred type of product, development of coatings may be needed.

With a clear idea of the type of product desired, the packaging process and package itself must be developed. The packaging process must ensure that the CO_2 content of each package is consistent and correct for maintaining stable CO_2 hydrates that are homogeneously distributed. This is likely to require extracting the powder and packaging the CO_2 hydrate

confection without ever reducing the pressure below CO_2 hydrate equilibrium pressure at operating temperature. At the very least, achieving a consistent CO_2 content will require automation of the extraction and packaging processes and pressurization of the package or addition of dry ice at the time of sealing; however the effect of this pressure cycling on the product should be investigated. The package must be developed to operate at CO_2 hydrate equilibrium pressure, provide easy access to the confection, handle the pressure evolution during heat shock, and safely vent CO_2 if the product is melted while the package is sealed. A model must be developed for pressure evolution in a sealed package containing CO_2 hydrate confection as a function of recipe, add-ins, headspace and CO_2 content. This model would be extremely important for predicting the CO_2 released during heat shock. It could be based on the aqueous phase total solids concentration discussion in section 5.2, but should be supported by experimental measurements. Hopefully, the packaging can be designed so that it is not necessary to vent CO_2 during normal heat shock, otherwise a homogeneous CO_2 distribution cannot be maintained after heat shock. The package must be designed to include pressure relief devices, such a burst discs, which release CO_2 if pressure in the packaging becomes too high, particularly if the product is allowed to melt.

In addition to processing and packaging development, work is needed to understand CO_2 hydrate evolution while the product is in the distribution chain. Conventional ice confection stabilizers should be tested to see if they are effective in the presence of CO_2 hydrates and are located at the desired phase interfaces after flash freezing. The temperature cycling procedure developed to mimic the deterioration of conventional ice confections between production and consumption should be reviewed for its appropriateness to CO_2 hydrate confections. This temperature cycling is used to produce the textural changes that would occur in a confection during distribution over a shortened time period (e.g. 11 days) by subjecting the confection to multiple temperature cycles and temperature fluctuations greater than would be expected in a standard cold chain. It may be necessary to increase the exposure time of a CO_2 hydrate confection to a warm temperature during temperature cycling if CO_2 hydrates mitigate short-term product degradation due to their enthalpy of dissociation. In addition, tests of product evolution during temperature cycling should be adapted to mimic the in-package pressure conditions because the pressure during heat shock tests can have a significant impact on the extent of melting of water, and hence the deterioration of the product.

8.2 Further work to improve understanding of CO_2 hydrates in frozen foods

Work to improve understanding of CO_2 hydrates in frozen food systems based on this thesis can be divided into: experiments to confirm theories presented in this thesis, fundamental measurements, and experiments that would extend knowledge of CO_2 hydrate behavior.

Several theories presented in this thesis have not yet been demonstrated experimentally. An emulsion chamber with a view window and image capture capability could be used to confirm that in the emulsion chamber mixture is dispersed as droplets in liquid CO_2 and that the droplet size is 150-200 μm. It could also be confirmed that substitution of a capillary tube in place of the pressure-swirl type mixture nozzle provides the same spray mode breakup of the mixture and approximate droplet size. Finally, the effect of mixture droplet size in the emulsion chamber on CO_2 hydrate formation during flash freezing can be tested by varying

the diameter of the capillary tube to achieve a variety of mixture jet breakup modes. It is predicted that droplet size will only have a significant effect when the droplets are larger than the flash-freezing nozzle orifice diameter.

It may also be possible to use a visual pH indicator (such as bromocresol green or bromophenol blue) to estimate the extent of saturation of the mixture droplets in the emulsion chamber and look for evidence of internal circulation. If it is possible to differentiate between saturated and unsaturated mixture droplets, this could confirm that CO_2 hydrate formation does not require saturation of the mixture with CO_2 in the emulsion chamber. If it is possible to identify internal circulation, the predicted reduction in circulation with increasing mixture viscosity could be confirmed. The visual pH indicator will not provide new information if the mixture droplet surface becomes opaque when it is saturated with CO_2, because the droplet surface should be saturated almost immediately in the emulsion chamber.

Many of the theories in this thesis could also be supported by careful, consistent measurement of CO_2 concentration in the fresh powder and study of the fresh powder microstructure. This would require development of apparatus to extract powder during a trial and transfer that powder to the measurement or microscopy apparatus without any opportunity for CO_2 hydrate dissociation. With such systems, it could be confirmed that CO_2 solubility in the mixture does not affect the initial CO_2 concentration of the powder. Additionally, the minimal effect of CO_2 saturation of the mixture on CO_2 hydrate formation during flash freezing could be confirmed. This would be done by measuring the CO_2 content of the powder when 1) the mixture is pre-saturated with CO_2 at 50 bar before entering the emulsion chamber or 2) the volume of the emulsion chamber is decreased to reduce the residence time. The effect of CO_2 hydrate formation in the emulsion chamber could be studied by observing the initial CO_2 content and the microstructure of the flash-frozen powder. It would be necessary to use a heated flash-freezing nozzle. With a well-instrumented CO_2 flash-freezing apparatus it should also be possible to demonstrate the change in product temperature with a small decrease in CO_2 flow ratio and that significant CO_2 hydrate formation does not occur for ICT pressure less than 4.7 bars.

The importance of the pressure-swirl type flash-freezing nozzle could be tested by substituting a capillary tube. This would require some effort to ensure a constant flow ratio regardless of the type of flash-freezing nozzle. If both flashing of CO_2 and acceleration of the emulsion through the pressure-swirl nozzle are important for atomizing the mixture, microscopy will show larger mixture particles when the capillary tube is used. In addition, the CO_2 content of the powder may be decreased. Cryogenic scanning electron microscopy could be used to identify the microstructure of the powder. In particular, very small crystals at the surface of larger particles could indicate fat dissolution in liquid CO_2 or protein precipitation in the emulsion chamber. Understanding the distribution of protein and fat in the frozen product is relevant to predicting the functionality of these ingredients in flash-frozen confections.

There are also theories in this thesis that would be supported by studying the flash-freezing powder in storage. The decrease in rate of CO_2 evolution from compressed powder relative to low-density powder could be measured at higher levels of compression than achieved for this thesis. In section 4.3 it is argued that compression to 50% bulk porosity should reduce the rate of CO_2 loss by approximately a factor of ten. The specific surface area of compressed and uncompressed powder could also be measured to confirm that the powder is compressed with minimal sintering. Specific surface area measurements would be made as

a function of the powder temperature during compression and the extent of compression. It has been suggested in this thesis, based on experience forming pellets manually with flash-freezing powder, that the optimum temperature for compression is around 253 K because the powder would sinter too much at higher temperatures and not enough at lower temperatures.

The rate of redistribution of CO_2 to form an ice-rich and a CO_2 hydrate-rich region in the presence of a fixed temperature gradient could be measured. Perhaps this could be done using Raman or infrared spectroscopy. In addition, the increase in concentration of solutes in the aqueous phase of the confection with increasing pressure could be confirmed. It has been argued in this thesis that the extent of crystallization is a function of both pressure and temperature. This could be tested using differential scanning calorimetry, as the heat release during melting should increase with the fraction of water crystallized.

Several tests are needed to confirm theories related to sensory perception of CO_2 hydrates during consumption. First, the mouth temperature during consumption of a CO_2 hydrate confection could be measured. In this thesis it has been suggested that the mouth is colder while eating a CO_2 hydrate confection than during consumption of other carbonated foods and also colder than during consumption of conventional ice confections. Using a trained sensory analysis panel the difference in CO_2 perception with powder and pellet form products should be tested. Measurements could be made of the CO_2 concentration and volatile concentration in the exhaled breath of a person eating the CO_2 hydrate confection. It has been suggested that a fraction of the CO_2 and volatiles in the confection can escape detection by the consumer because they are lost in the exhaled breath.

In this thesis several parameters were estimated, but not measured directly. Measurement of these fundamental parameters would fill gaps in general knowledge about systems involving gas hydrates, CO_2 and aqueous solutions. First, the solubility of CO_2 in aqueous solutions at emulsion chamber temperature and pressure could be measured as a function of the type and concentration of solutes. Measurements of CO_2 solubility in various sugar solutions are currently only available in the literature at low pressures corresponding to gaseous CO_2 and at supercritical CO_2 conditions. Conflicting measurements of the effect of proteins on CO_2 solubility were found in the literature and while it is known that CO_2 is more soluble in liquid than solid phase fat, the overall solubility of CO_2 in mixtures containing solid fat is not known. Second, diffusivity of CO_2 in aqueous sugar solutions, as a function of viscosity, could be measured. In this thesis, the decrease in CO_2 diffusivity with increasing viscosity is estimated based on results for amine solutions. Knowing the diffusivity of CO_2 in the mixture would improve estimation of how well the mixture is saturated with CO_2 in the emulsion chamber. Third, the ice-gas hydrate-gas equilibrium pressure below 273 K for mixed gas hydrates containing air and CO_2 could be measured. Currently, the effect of air on gas hydrate stability is estimated based on the CSMGem model from Sloan and Koh (2008), but there are no experimental results in this temperature range that can be used for validation. This equilibrium curve is important for any packaging that contains a significant air fraction.

There are also several fundamental measurements that would provide insight into recrystallization of CO_2 hydrate systems relative to ice systems. First, CO_2 hydrate-vapor interfacial energy could be measured. Currently it is simply estimated as equal to ice-vapor interfacial energy. Second, water diffusivity and CO_2 surface and grain boundary diffusivity in CO_2 hydrates could be measured. Third, the surface reaction rate at a growing CO_2 hydrate surface compared to the rate of incorporation of water at a growing ice surface could be measured. Fourth, the rate of recrystallization of CO_2 hydrates with and without the presence

of an aqueous phase could be measured. The relative importance of vapor phase transport for recrystallization can be studied by submerging the powder in kerosene or silicon oil to cut off vapor phase transport. Similar methods to those described in the review of ice recrystallization by Blackford (2007) should be used to allow easy comparison. The results of these measurements could be used to develop strategies to reduce CO_2 hydrate recrystallization that capitalize on any properties of CO_2 hydrates that offer an advantage.

Finally, there are research directions that would extend our knowledge of CO_2 hydrates in frozen food systems. First, it may be possible to change the powder texture by using a fat that is liquid at emulsion chamber temperature. If the fat is saturated with CO_2 it may be possible to skip the homogenization step in mixture preparation or increase the surface area of the fat as it crystallizes. Second, the rate of CO_2 hydrate formation in a quiescent system containing ethanol should be measured. It is possible that the concentrated ethanol liquid phase improves CO_2 transport for formation of CO_2 hydrates throughout frozen grains. This could enable fast formation of alcoholic frozen confections without use of the CO_2 flash-freezing process. Third, coating materials that would allow use of CO_2 hydrate pellets as inclusions in a bulk could be investigated. For example, if a water-ice bulk is aerated with CO_2 and stored at CO_2 hydrate equilibrium pressure it may be possible to have CO_2 hydrate inclusions with a coating that significantly slows CO_2 redistribution. This coating would not experience a pressure differential and the CO_2 concentration gradient across the coating should significantly reduce the driving force for CO_2 transport, avoiding the problem of inhomogeneity in the confection.

In conclusion, the most important next step for CO_2 hydrate confections produced by CO_2 flash freezing is development of a consistent and reliable system for measurement of the initial CO_2 content. With this apparatus in place, the effects of a wide range of parameters would be discernable. For CO_2 hydrate confections, an understanding of consumer preferences is needed. Different types of products need different development. For example, a ‘planned inhomogeneity’ product would not require investigation of coating materials and add-ins, but consumer perception of CO_2 would be important. In a ‘planned inhomogeneity’ product, pressure evolution during heat shock would be mitigated, simplifying the package design, though a pressure relief mechanism is likely to still be needed. A ‘planned inhomogeneity’ product is likely to be a desirable option for packaged and distributed CO_2 hydrate confections.

9 References

Anderson, G. (2003). Enthalpy of dissociation and hydration number of carbon dioxide hydrate from the Clapeyron equation. *J. Chem. Thermodynamics*, 35. 1171-1183.

Anderson, R., Llamedo, M., Tohidi, B., & Burgass, R. (2003). Experimental measurement of methane and carbon dioxide clathrate hydrate equilibria in mesoporous silica. *J. Phys. Chem. B*, 107. 3507-3514.

Bee, R.D. (1991). Frozen product and method of making it. U.S. Patent No. 5,055,315. Washington, D.C.: U.S. Patent and Trademark Office.

Blackford, J. (2007). Topical review: sintering and microstructure of ice: a review. *J. Phys. D: Appl. Phys*., 40. R355–R385.

Blond, G., Simatos, D., Catte, M., Dussap, C.G., & Gros, J.B. (1997). Modeling of the water-sucrose state diagram below 0°C. *Carbohydrate Research,* 298. 139-145.

Bobev, S. & Tait, K. (2004). Methanol-inhibitor or promoter of the formation of gas hydrates from deuterated ice? *American Mineralogist*, 89. 1208-1214.

Botelho, G. (2007, June 1). Getting fizzy with it: Carbonated foods bubble up. *CNN.* Retrieved from http://www.cnn.com/2007/US/05/22/carbonated.food/index.html

Calix, T. Ferrentino, G. & Balaban, M. (2008). Measurement of high-pressure carbon dioxide solubility in orange juice, apple juice, and model liquid foods. *Journal of Food Science*, 73(9). E439-E445.

Chang, D. & Lee, C. (2005). Development of a simplified bubble growth model for flash boiling sprays in direct injection spark ignition engines. *Proceedings of the Combustion Institute*, 30. 2737-2744.

Circone, S., Stern, L., Kirby, S., Durham, W., Chakoumakos, B. Rawn, C., Rondinone, A., & Ishii, Y. (2003). CO_2 hydrate: synthesis, composition, structure, dissociation behavior, and a comparison to structure I CH_4 hydrate. *J. Phys. Chem. B*, 107. 5529-5539.

Circone, S.,Stern, L., & Kirby, S. (2004). The role of water in gas hydrate dissociation. *J. Phys. Chem.*, 108. 5747-5755.

Chun, M. & Lee, H. (1999). Phase equilibria of carbon dioxide hydrate system in the presence of sucrose, glucose and fructose. *J. Chem. Eng. Data*, 44. 1081-1084.

Clarke, C. (2004). *The Science of Ice Cream*. Cambridge, UK: Royal Society of Chemistry.

Collins, L. & Dawes, C. (1987) The surface area of the adult human mout hand thickness of the salivary film covering the teeth and oral mucosa. *J. of Dental Research*, 66. 1300-1302.

Crank, J. (1980). *The Mathematics of Diffusion, 2nd ed.* New York, NY: Oxford University Press.

Davies, S., Selim, M., Sloan, E., Bollavaram, P. & Peters, D. (2006). Hydrate plug dissociation. *AIChE Journal*, 52(12). 4016-4027.

Davies, S., Hester, K., Lachance, J., Koh, C., & Sloan, E. (2009). Studies of hydrate nucleation with high pressure differential scanning calorimetry. *Chemical Engineering Science.* 64. 370-375.

Demurov, A., Radhakrishnan, R., & Trout, B. (2002). Computations of diffusivities in ice and CO_2 clathrate hydrates via molecular dynamics and Monte Carlo simulations. *J. Chemical Physics*. 116(2). 702-709.

Denbigh, K. (1981). *The Principles of Chemical Equilibrium, 4th edition.* Cambrige, UK: Cambridge University Press.

Descoins, C., Mathlouthi, M., Moual, M., & Hennequin, J. (2006). Carbonation monitoring of beverage in a laboratory scale unit with on-line measurement of dissolved CO_2. *Food Chemistry*, 95. 541-553.

Dessirier, J. Simons, C., Carstens, M., O'Mahony, M., & Carstens, E. (2000). Psychophysical and neurobiological evidence that the oral sensation elicited by carbonated water is of chemogenic origin. *Chemical Senses*, 25. 277-284.

Diamond, L.W. & Akinfiev, N.N. (2003). Solubility of CO_2 in water from -1.5 to 100°C and from 0.1 to 100 MPa: evaluation of literature data and thermodynamic modeling. *Fluid Phase Equilibria*, 208. 265-290.

Fernandez, P., Otero, L., Martina, M., Molina-Garcia, A., & Sanz, P. (2008). High-pressure shift freezing: recrystallization during storage. *Eur Food Res Technol.*, 227. 1367-1377.

Fritsching, U. (2006). Spray systems. In C. Crowe (Ed.), *Multiphase Flow Handbook.* Boca Raton, FL: CRC Press Taylor and Francis Group.

Genov, G., Kuhs, W., Staykova, D., Goreshnik, E., & Salamatin, A. (2004). Experimental studies on the formation of porous gas hydrates. *American Mineralogist*, 89. 1228-1239.

Giavarini C, Maccioni F, Politi M, & Santarelli, M. (2007). CO_2 hydrate: Formation and dissociation compared to methane hydrate. *Energy and Fuels*, 21(6). 3284-3291.

Glasner, J. (2005, October 3). All That Fizzes Is Not Soda. *Wired News. Tech Biz. Media*. Retrieved from http://www.wired.com/techbiz/media/news/2005/10/69017

Green, B. (1992). The effects of temperature and concentration on the perceived intensity and quality of carbonation. *Chemical Senses*. 17(4). 435-450.

Gupta, A. & Dimmel, B. (2003). CO_2-hydrate product and method of manufacture thereof. U.S. Patent No. 6,576,276. Washington, D.C.: U.S. Patent and Trademark Office.

Henning, R., Schultz, A., Thieu, V. & Halpern, Y. (2000). Neutron diffraction studies of CO_2 clathrate hydrate: formation from deuterated ice. *J. Phys. Chem. A*, 104. 5066-5071.

Hindmarsh, J., Russell, A. & Chen, X. (2003). Experimental and numerical analysis of the temperature transition of a suspended freezing water droplet. *International Journal of Heat and Mass Transfer*. 46. 1199-1213.

Hindmarsh, J., Russell, A. & Chen, X. (2004). Experimental and numerical analysis of the temperature transition of a freezing food solution droplet. *Chemical Engineering Science*. 59. 2503-2515.

Hindmarsh, J., Russell, A. & Chen, X. (2007). Fundamentals of the spray freezing of foods – microstructure of frozen droplets. *J. Food Engineering*, 78(1). 136-150.

Hofland, G., van Es, M., van der Wielen, L. & Witkamp, G. (1999). Isoelectric precipitation of casein using high-pressure CO_2. *Ind. Eng. Chem. Res*. 38. 4919-4927.

Hofland, G., Rijke, A., Thiering, R., van der Wielen, L. & Witkamp, G. (2000). Isoelectric precipitation of soybean protein using carbon dioxide as a volatile acid. *Journal of Chromatography B*. 743. 357-368.

Huang, E., Chang, H., Lian, C. & Sievers, R. (2003). Fine particle pharmaceutical manufacturing using dense carbon dioxide mixed with aqueous or alcoholic solutions. In A. Gopalan, C. Wai & H. Jacobs (Eds.) *Supercritical Carbon Dioxide Separations and Processes* (324-338). Washington, DC: American Chemical Society, Oxford University Press.

Ibrahim, A. & Jog, M. (2007). Nonlinear breakup model for a liquid sheet emanating from a pressure-swirl atomizer. *J. of Engineering for Gas Turbines and Power*, 129. 945-953.

Ikeda-Fukazawa, T., Kawamura, K. & Hondoh, T. (2004). Mechanism of molecular diffusion in ice crystals. *Molecular Simulation*. 30(13-15). 973-979.

Incropera, F. & DeWitt, D. (2002). *Fundamentals of heat and mass transfer* (5^{th} ed.) New York:John Wiley & Sons, Inc.

Jho, C., Nealon, D., Shogbola, S. & King Jr., A. (1978). Effect of pressure on the surface tension of water: adsorption of hydrocarbon gases and carbon dioxide on water at temperatures between 0 and 50°C. *J. of Colloid and Interface Science*, 65(1). 141-154.

Kashchiev, D. & Firoozabadi, A. (2002). Driving force for crystallization of gas hydrates. *J. Crystal Growth*, 21. 220-230.

Kerbrat, M., Pinzer, B., Huthwelker, T., Gäggeler, H., Ammann, M. & Schneebeli, M. (2008). Measuring the specific surface area of snow with X-ray tomography and gas adsorption: comparison and implications for surface smoothness. *Atmospheric Chemistry and Physics*. 8. 1261-1275.

King, M. & Bott, T. (1993). Introduction. In M. King & T. Bott (Eds.), *Extraction of Natural Products Using Near-Critical Solvents* (pp. 1-33). Bishopbriggs, Glasgow, UK: Blackie Academic & Professional, an imprint of Chapman & Hall.

Kitamura, Y., Morimitsu, H. & Takahashi, T. (1986). Critical superheat for flashing of superheated liquid jets. *Ind. Eng. Chem. Fundam*., 25. 206-211.

Kolev, N. I. (2007). *Multiphase Flow Dynamics 2: Thermal and mechanical interactions (3rd ed.)* Berlin, Germany: Springer.

Kuhs, W., Klapproth, A., Gotthardt, F., Techmer, K. & Heinrichs, T. (2000). The formation of meso- and macroporous gas hydrates. *Geophysical Research Letters*, 27(18). 2929-2932.

Kuhs, W., Genov, G., Goreshnik, E., Zeller, A., Techmer, K. & Bohrmann, G. The impact of porous microstructures of gas hydrates on their macroscopic properties. *International Journal of Offshore and Polar Engineering*, 14(4). 305-309.

Kuhs, W., Staykova, D. & Salamatin, A. (2006). Formation of methane hydrate from polydisperse ice powders. *J. Phys. Chem. B*, 110. 13283-13295.

Lee, S., Liang, L., Riestenberg, D., West, O., Tsouris, C. & Adams, E. (2003). CO_2 hydrate composite for ocean carbon sequestration. *Environ. Sci. Technol*. 37. 3701-3708.

Lefebvre, A. (1989). *Atomization and Sprays.* USA: Taylor and Francis.

Lemmon, E.W., McLinden, M.O. & Friend, D.G., (2009). Thermophysical properties of fluid systems. In P.J. Linstrom & W.G. Mallard (Eds.), *NIST Chemistry WebBook, NIST Standard Reference Database Number 69*. Gaithersburg, MD: National Institute of Standards and Technology. http://webbook.nist.gov, (retrieved May 25, 2009).

Li, J., Rodrigues, M., Paiva, A., Matos, H. & Gomes de Azevedo, E. (2005). Modeling of the PGSS process by crystallization and atomization. *AIChE Journal*, 51(8). 2343-2357.

Liger-Belair, G., Polidori, G. & Jeandet, P. (2008). Recent advances in the science of champagne bubbles. *Chemical Society Reviews*. 37(11). 2490-2511.

Lopez, D. (2009). Development of a pressurized low-temperature tablet press for a carbon dioxide flash frozen ice confection. Masters Thesis in Mechanical Engineering. Massachusetts Institute of Technology.

Ma, Y. & Barbano, D.M. (2003). Effect of temperature of CO_2 injection on the pH and freezing point of milks and creams. *J. Dairy Sci*, 86(5). 1578-1589.

Marshall, R., Goff, D., Hartel, R. (2003). *Ice Cream, 6th ed.* New York, NY: Kluwer Academic/Plenum Publishers.

Meraj, S. (2000). Pressure in a can of soda. In G. Elert (Ed.) *The Physics Factbook*. Retrieved June 20, 2009 from http://hypertextbook.com/facts/2000/SeemaMeraj.shtml

Meyssami, B., Balaban, M. & Teixeira, A. (1992). Prediction of pH in model systems pressurized with carbon dioxide. *Biotechnol. Prog*. 8. 149-154.

Meyer, B. & Smith, D. (1985). Flow through porous media: comparison of consolidated and unconsolidated materials. *Indust. Eng. Chem. Fundamentals*, 24(3). 360–368.

Migliori, M., Gabriele, D., Di Sanzo, R., de Cindio, B. & Correra, S. (2007). Viscosity of multicomponent solutions of simple and complex sugars in water. *J. Chem. Eng. Data*. 52. 1347-1353.

Mills, A. (1995). *Heat and Mass Transfer*. Chicago, IL: Irwin.

Moon, S., Bai, C., Abo-Serie, E. & Choi, J. (2007). Internal and near-nozzle flow of a pressure-swirl atomizer under varied fuel temperature. *Atomization and Sprays*, 17. 529-550.

Moudrakovski, I., McLaurin, G., Ratcliffe, C. & Ripmeester, J. (2004). Methane and carbon dioxide hydrate formation in water droplets: spatially resolved measurements from magnetic resonance microimaging. *J. Phys. Chem. B*, 108. 17591-17595.

Murakami, H. & Sly, W. (1987). Purification and characterization of human salivary carbonic-anhydrase. *Journal of Biological Chemistry*, 262(3). 1382-1388.

Nitchman, H. & Cunningham, Jr., W. (1985). System, apparatus and method of dispensing a liquid from disposable container and a container therefor[sic]. US Patent No. 4,531,656. Washington D.C.: U.S. Patent and Trademark Office

Ogasawara, K., Yamasaki, A. & Teng, H. (2001). Mass transfer from CO_2 drops traveling in high-pressure and low-temperature water. *Energy & Fuels*, 15. 147-150.

Olson, E. (1999). Fuel nozzles for oil burners: Technical aspects of applications. *Delavan, Inc. Technical Publications*. Retrieved June 20, 2009 from http://www.delavaninc.com/pdf/Fuel_Nozzles_for_Burners.PDF

Petrovic, J. (2003). Review - Mechanical properties of ice and snow. *Journal of Materials Science*, 38. 1-6.

Pruppacher, H. & Klett, J. (1997). *Microphysics of Clouds and Precipitation: Second Revised and Enlarged Edition with an Introduction to Cloud Chemistry and Cloud Electricity*. Dordrecht, The Netherlands: Kluwer Academic Publishers.

Radhakrishnan, R., Demurov, A., Herzog, H. & Trout, B. (2003). A consistent and verifiable macroscopic model for the dissolution of liquid CO_2 in water under hydrate forming conditions. *Energy Conversion and Management*, 44. 771-780.

Radhakrishnan, R. & Trout, B. (2002). A new approach for studying nucleation phenomena using molecular simulations: Application to CO_2 hydrate clathrates. *Journal of Chemical Physics*. 17(4). 1786-1796.

Ragab, A. & Bayoumi, S. (1999). *Engineering Solid Mechanics: Fundamentals and Applications*. New York, NY: John Wiley.

Rhode, R. & Price, P. (2007). Diffusion-controlled metabolism for long-term survival of single isolated microorganisms trapped within ice crystals. *Proceedings of the National Academy of Sciences of the United States of America (PNAS)*, 104(42). 16592-16597.

Riestenberg, D., Chiu, E., Gborigi, M., Liang, L., West, O. & Tsouris, C. (2004). Investigation of jet breakup and droplet size distribution of liquid CO_2 and water systems-implications for CO_2 hydrate formation for ocean carbon sequestration. *American Mineralogist*. 89. 1240-1246.

Roos, Y. & Karel, M. (1991). Water and molecular-weight effects on glass transitions in amorphous carbohydrates and carbohydrate solutions. *Journal of Food Science*. 56(6). 1676-1681.

Saboni, A., Alexandrova, S., Spasic, A. & Gourdon, C. (2007). Effect of the viscosity ratio on mass transfer from a fluid sphere at low to very high Peclet numbers. *Chemical Engineering Science*, 62. 4742-4750.

Salamatin, A., Lipenkov, V., & Hondoh, T. (2003). Air-hydrate crystal growth in polar ice. *Journal of Crystal Growth*, 257. 412–426.

Sarraf, N., Saboury, A., Ranjbar, B. & Moosavi-Movahedi, A. (2004). Structural and functional changes of bovine carbonic anhydrase as a consequence of temperature. *Acta Biochimica Polonica*. 51(3). 665-671.

Sloan, E. & Koh, C. (2008). *Clathrate hydrates of natural gases* (3rd ed.). Boca Raton, FL: CRC Press.

Stern L., Circone S., Kirby S. & Durham, W. (2001). Anomalous preservation of pure methane hydrate at 1 atm. *Journal of Physical Chemistry B*, 105(9). 1756-1762.

Takaizumi, K. & Wakabayashi, T. (1997). The freezing process in methanol-, ethanol-, and propanol-water systems as revealed by differential scanning calorimetry. *J. Solution Chemistry*. 26(10).

Takeya S., Hondoh, T. & Uchida, T. (2000). In-situ observations of CO_2 hydrate by X-ray diffraction. *Annals of the New York Academy of Sciences*, 912. 973-982.

Takeya S., Uchida T., Nagao J, Ohmura, R. Shimada, W., Kamata, Y., Ebinuma, T. & Narita, H. (2005). Particle size effect of CH4 hydrate for self-preservation. *Chemical Engineering Science*, 60(5). 1383-1387.

Taylor, D. & Ogden, L. (2002). Carbonation of viscous fluids: carbon dioxide holding capacity and rate to saturation of simulated yogurt. *Journal of Food Science*. 67(3). 1032-1035.

Teng, H., Yamasaki, A. & Shindo, Y. (1996). Stability of the hydrate layer formed on the surface of a CO_2 droplet in high-pressure, low-temperature water. *Chemical Engineering Science*, 51(22). 4979-4986.

Tester, J. & Modell, M. (1996). *Thermodynamics and its Applications.* Upper Saddle River, NJ: Prentice Hall.

Tohidi, B., Anderson, R., Clennell, M., Burgass, R., & Biderkab, A. (2001). Visual observation of gas-hydrate formation and dissociation in synthetic porous media by means of glass micromodels. *Geology*, 29(9). 867-870.

Tomasula, P., Craig Jr, J., Boswell, R., Cook, R., Kurantz, M. & Maxwell, M. (1995). Preparation of casein using carbon dioxide. *Journal of Dairy Science*, 78(3). 506-514.

Tomasula, P. & Boswell, P. (1999). Measurement of the solubility of carbon dioxide in milk at high pressures. *Journal of Supercritical Fluids*, 16. 21-26.

Uchida, T. & Dawabata, J. (1997). Measurements of mechanical properties of the liquid CO_2-water-CO_2-hydrate system. *Energy*. 22(2/3). 357-361.

Uchida, T., Ebinuma, T., & Narita, H. (2000). Observations of CO_2-hydrate decomposition and reformation processes. *Journal of Crystal Growth*, 217. 189-200.

Uchida, T., Hondoh, T., Mae, S., Lipenkov V., & Duval, P. (1994). Air-hydrate crystals in deep ice-core samples from Vostok station, Antarctica. *Journal of Glaciology*, 40(134). 79-86.

Vanderwege, B. & Hochgreb, S. (1998). The effect of fuel volatility on sprays from high-pressure swirl injectors. *27th Symposium (International) on Combustion/The Combustion Institute*. 1865-1871.

Versteeg, G. & van Swaall, W. (1988). Solubility and diffusivity of acid gases (CO_2, N_2O) in aqueous alkanolamine solutions. *J. Chem. Eng. Data*. 33. 29-34.

Vieira, M. & Simões-Moreira, J. (2007). Low-pressure flashing mechanisms in iso-octane liquid jets. *J. Fluid Mech*. 572. 121-144.

Vu, H., García-Valladares, O. & Aguilar, G. (2008). Vapor/liquid phase interaction in flare flashing sprays used in dermatologic cooling. *International Journal of Heat and Mass Transfer*. 51. 5721-5731.

White, F. (1999). *Fluid Mechanics* (4th ed.). Boston, MA:WCB/McGraw-Hill.

Wright, A., Ogden, L. & Eggett, D. (2003). Determination of carbonation threshold in yogurt. *Journal of Food Science*, 68(1). 378-381.

Yamasaki, A., Teng, H., Wakatsuki, M., Yanagisawa, Y. & Yamada, K. (2000). CO_2 hydrate formation in various hydrodynamic conditions. In Gas Hydrates: Challenges for the Future. *Annals of the New York Academy of Sciences*. 912. 235-245.

Zhang, G. & Rogers, R. (2008). Ultra-stability of gas hydrates at 1 atm and 268.2 K. *Chemical Engineering Science*. 63. 2066-2074.

Zhang, W., Wilder, J., & Smith, D. (2002). Interpretation of ethane hydrate equilibrium data for porous media involving hydrate-ice equilibria. *AIChE Journal*, 40(10). 2324-2331.